

# MODELLING THE INFLUENCE OF VARYING SEDIMENT SOURCES ON COASTLINES



**Vibhav Atish Deoraj**

Supervisor: Prof. D.D. Stretch

Dr. J.J. Pringle

University of KwaZulu-Natal

Submitted in fulfilment of the academic requirements for the degree of  
*Master of Science in Civil Engineering, College of Agriculture,  
Engineering and Science, University of KwaZulu-Natal, Durban*

March 2019



## Declaration

I, Vibhav Atish Deoraj (Student Number: 213503072), hereby declare that all work contained herein is original and my own intellectual property and has in no way been submitted partially, or in whole to any other university. Where the work of others has been included to any extent within this dissertation, all necessary acknowledgements, references and credit have been given. All research relevant to this dissertation was carried out at the University of KwaZulu-Natal, Howard College Campus, more specifically within the Centre for Research in Environmental, Coastal and Hydrological Engineering at the School of Civil Engineering, Surveying and Construction. This dissertation was supervised by Professor Derek D. Stretch and Dr. Justin J. Pringle.

---

Vibhav Atish Deoraj

---

Date

As the candidate's supervisor I agree to the submission of this dissertation.

---

Prof. Derek D. Stretch

---

Date

---

Dr. Justin J. Pringle

---

Date



## Acknowledgements

To the following individuals, I would like to extend my deepest appreciation:

My supervisor, Professor Derek D. Stretch, for his invaluable guidance and assistance throughout the course of this dissertation, and for constantly believing in my abilities and instilling confidence in the face of adversity. Your belief made me strive for constant self-improvement, and for that I am exceedingly grateful.

My co-supervisor, Dr. Justin J. Pringle for dealing with my constant questions and visits on the regular and for always having your door open regardless of your workload. You are a constant source of inspiration and your guidance, assistance and advice are greatly appreciated.

Dr. Katrin Tirok for always being available for a quick or lengthy consult on any possible topic. Your work ethic and drive is a constant source of inspiration.

Mum, Dad and Didi, my wonderful family for their unrelenting support and companionship throughout the entire period as well as my academic career, without whom I would not be where I am today.

My friends and the people at the Civil Engineering Department for their support. A special thank you goes out to Ooma Chetty who was always willing to go the extra mile.



## Abstract

Coastal erosion is of concern to developed shorelines worldwide and has largely intensified due to anthropogenic influences. Sea-level rise, reductions in sediment supply and changes to wave behaviour due to changes in climate were identified as potential causes of chronic erosion. With climate change expected to increase the frequency and intensity of storms, coastline management and planning will require greater attention. A major obstacle of coastal planning is the lack of available models for predicting long-term changes. Furthermore, reliable long-term wave data are often unavailable or unreliable. Predicting long-term changes is essential for effective management of coastal defence schemes. One-line models present a reduced-physics and reduced dimension approach and provide an efficient and viable alternative to 2D and 3D models while being less computationally intensive.

The long-term impacts of varying sediment inputs on the stretch of coastline between uMhlanga and the uMngeni River mouth in Durban are explored using a one-line model. Site selection was based on ongoing erosion and known operations of sand-mining, damming and a sand-bypass scheme. Existing models are used as a framework to develop a coastline model that uses statistically modelled wave climates as the input source of wave data.

Results indicated that a minimum longshore sediment supply ( $460,961 \text{ m}^3/\text{year}$ ) required to maintain beach volume in the study region exceeds the estimate by Corbella & Stretch (2012) of  $418,333 \text{ m}^3/\text{year}$ . Observed beach erosion by eThekweni Municipality indicated a current longshore sediment supply of  $410,276 \text{ m}^3/\text{year}$ . Furthermore, volume conservation did not ensure beach width conservation along the entire coastline, with a minimum sediment influx of  $596,183 \text{ m}^3/\text{year}$  required for beach width and beach plan area conservation.

Shore nourishment behaviour were analysed in the form of alongshore sand waves with results showing that multiple, smaller nourishments results in more realistic sand wave amplitudes that are required for diffusion dominant waves. Smaller nourishments allow for more diffusive effects while maintaining a diffusive state whereas larger nourishments tend to become advection dominant following rapid diffusion.

---

An investigation of the advection-diffusion relationship of river sediment discharges inferred that sand waves along the Durban coastline are advection dominated. A critical aspect ratio of between 0.037 and 0.041 represented the equilibrium point between advection and diffusion. River sediment discharges of this aspect ratio are potentially significant in preventing erosion given the relatively high diffusive rate and slow advection speed associated with the value. Furthermore, extreme river discharges exceeding  $200,000 m^3$  remained in coastal systems for between 3 and 4 years and are potentially important mechanisms behind coastline recovery after storms.

# Table of contents

<b>List of figures</b>	<b>xiii</b>
<b>List of tables</b>	<b>xvii</b>
<b>1 Introduction</b>	<b>1</b>
1.1 Coastal Erosion . . . . .	1
1.1.1 Impacts of Urbanisation . . . . .	2
1.1.2 Coastal Management . . . . .	2
1.1.3 Coastal Planning . . . . .	3
1.2 Problem Definiton . . . . .	4
1.2.1 Research Question . . . . .	4
1.3 Motivation . . . . .	5
1.4 Aims & Objectives . . . . .	6
1.5 Approach . . . . .	7
1.5.1 Case Study: Durban . . . . .	7
1.6 Outline of Dissertation . . . . .	9
<b>2 Literature Review</b>	<b>11</b>
2.1 Introduction . . . . .	11
2.2 Coastal Erosion . . . . .	12
2.3 Coastal Sediment Sources . . . . .	13
2.4 Impacts on Sediment Supplies . . . . .	14
2.4.1 Coastal Structures . . . . .	14
2.4.2 Fluvial Sediment Yields . . . . .	15
2.5 Coastal Management & Planning . . . . .	17
2.5.1 Shore Nourishments . . . . .	18
2.5.2 Sand-bypassing . . . . .	20
2.5.3 Set-back Lines . . . . .	20

## Table of contents

---

2.5.4	Dune Management . . . . .	21
2.5.5	Restricted Beach Access . . . . .	21
2.6	Coastline Behaviour . . . . .	22
2.6.1	Sand Wave Formation . . . . .	22
2.6.2	Sand Wave Advection . . . . .	23
2.7	Numerical Modelling . . . . .	25
2.7.1	Overview of Coastal Models . . . . .	25
2.7.2	Examples of One-line Models . . . . .	26
2.7.3	Long-term Modelling . . . . .	27
2.8	Coastal Hydrodynamics . . . . .	28
2.8.1	One-line Theory . . . . .	28
2.8.2	Wave Transformation: Refraction . . . . .	29
2.8.3	Wave Transformation: Shoaling . . . . .	30
2.8.4	Wave Transformation: Wave Breaking . . . . .	31
2.8.5	Longshore Sediment Transport . . . . .	32
2.8.6	Boundary Conditions . . . . .	33
2.8.7	Equilibrium Beach Profile . . . . .	35
2.9	Statistically Modelled Wave Climates . . . . .	36
2.9.1	Stochastically Simulated Regional Wave Climates . . . . .	37
2.10	Potential Inclusion of Climate Change Phenomena . . . . .	39
2.11	Summary . . . . .	40
<b>3</b>	<b>Case Study: Durban</b>	<b>43</b>
3.1	Site Location . . . . .	43
3.2	Selection Criteria . . . . .	43
3.3	Data For Study . . . . .	44
3.3.1	Coastline Coordinates . . . . .	44
3.3.2	Wave Climate: Simulated Data . . . . .	45
3.3.3	Wave Climate: Observed Data . . . . .	46
3.3.4	River Sediment Discharges . . . . .	47
3.3.5	Longshore Transport Volumes . . . . .	48
<b>4</b>	<b>Model Development</b>	<b>49</b>
4.1	Model Overview . . . . .	49
4.2	General Model Structure . . . . .	50
4.3	Internal Model Structure . . . . .	51
4.4	Initialisation Process . . . . .	52

## Table of contents

---

4.4.1	Grid Resolution . . . . .	52
4.4.2	Data Import & Handling . . . . .	53
4.4.3	River Flooding Sequence . . . . .	53
4.4.4	Base Coastline Generation . . . . .	54
4.5	Model Numerics . . . . .	55
4.5.1	Grid Orientation . . . . .	55
4.5.2	Wave Transformation . . . . .	56
4.5.3	Longshore Sediment Transport . . . . .	59
4.5.4	Lateral Boundary Conditions . . . . .	60
4.5.5	Coastline Changes . . . . .	61
4.6	Beach Nourishments . . . . .	62
4.6.1	Nourishment Shape . . . . .	63
4.6.2	River Discharges . . . . .	63
4.6.3	Longshore Sediment Supply . . . . .	63
4.7	Nourishment Diffusion & Advection . . . . .	64
4.7.1	Vertical Boundary Conditions . . . . .	66
4.8	Model Checks . . . . .	68
4.8.1	Wave Transformation Limits . . . . .	68
4.8.2	Conservation of Mass . . . . .	68
4.9	Model Calibration . . . . .	69
4.10	Sensitivity Analysis . . . . .	71
4.10.1	Input Error Effects . . . . .	71
4.10.2	Model Stability and Accuracy . . . . .	72
<b>5</b>	<b>Results &amp; Discussion</b>	<b>73</b>
5.1	Wave Climate Comparison . . . . .	73
5.2	Model Calibration . . . . .	76
5.2.1	Longshore Sediment Transport Coefficient . . . . .	76
5.2.2	Data Correlation . . . . .	78
5.2.3	Residual Values . . . . .	79
5.3	Sensitivity Analysis . . . . .	80
5.3.1	Input Errors . . . . .	80
5.3.2	Accuracy and Stability of Solution Scheme . . . . .	82
5.4	Continuous Sediment Supply . . . . .	84
5.4.1	Sediment Demand . . . . .	84
5.4.2	Coastline Evolution . . . . .	86
5.4.3	Area Conservation . . . . .	87

## Table of contents

---

5.4.4	Erosion & Accretion Rates . . . . .	89
5.5	Longshore Sand Wave Migration . . . . .	90
5.5.1	Advection Rate Calibration . . . . .	90
5.5.2	Sand Wave Advection . . . . .	92
5.5.3	Sand Wave Diffusion . . . . .	94
5.5.4	Advection-Diffusion Relationship . . . . .	95
5.5.5	River Discharge Behaviour . . . . .	98
5.5.6	Extreme Event Occurrence . . . . .	99
5.6	Nourishment Sand Waves . . . . .	101
5.6.1	Nourishment Frequency Effects . . . . .	102
5.6.2	Coastline Position Influence . . . . .	104
<b>6</b>	<b>Summary &amp; Conclusions</b>	<b>107</b>
6.1	One-line Model . . . . .	107
6.2	Simulated Wave Data . . . . .	108
6.3	Long-term Coastline Change . . . . .	109
6.4	Summary . . . . .	111
6.5	Recommendations for Further Research . . . . .	112
	<b>References</b>	<b>115</b>
	<b>Appendix A Beach Data</b>	<b>127</b>
	<b>Appendix B Wave Data Statistics</b>	<b>131</b>
	B.1 Observed Wave Data . . . . .	131
	B.2 Simulated Wave Data . . . . .	132
	<b>Appendix C Model Calibration</b>	<b>133</b>
	<b>Appendix D Model Pseudocode</b>	<b>135</b>

# List of figures

1.1	Locality plot of the study region in national and local context. . . . .	7
1.2	Locations of observation buoys at Durban and Richards Bay along the KwaZulu-Natal coastline (Pringle, 2015). . . . .	8
2.1	Sediment sources of active coastal systems (Rosati, 2005) . . . . .	13
2.2	Sediment transport around a harbour mouth (Bosboom and Stive, 2015)	15
2.3	Graphic representations of river-dominated and wave-dominated estuaries (Cooper, 1993) . . . . .	17
2.4	The Sand Engine at the initial stage of deposition (Stive et al., 2013) .	18
2.5	Propagation of perturbations with cross-shore variations in longshore transport (Roelvink and Reniers, 2011). . . . .	24
2.6	Obliquely incident waves propagating on uniform depth contours (Bosboom and Stive, 2015) . . . . .	30
2.7	Maximum crest angle governing wave breaking (Bosboom and Stive, 2015)	31
2.8	Observed ( <i>left</i> ) and simulated ( <i>right</i> ) wave roses for the given circulation pattern ( <i>middle</i> ). Line widths indicate relative magnitudes of wind velocity. Significant wave heights are given in the colour legend below (Pringle, 2015). . . . .	38
3.1	Locality plot of study region in national and local context. . . . .	44
3.2	Surveyed cross-shore profile from study region. Dashed line and red text indicate measurements from previous survey. Solid line and black text refer to current surveyed data. Beach heights are measured from LLD (eThekweni Municipality, 2017) . . . . .	44
3.3	Simulated data wave roses for summer ( <i>left</i> ) and winter ( <i>right</i> ). The legend indicates significant wave heights (Pringle, 2015) . . . . .	45

## List of figures

---

3.4	Observed summer ( <i>upper left</i> ), autumn ( <i>upper right</i> ), winter ( <i>lower left</i> ) and spring ( <i>lower right</i> ) wave roses for the East Coast. The legend indicates significant wave heights (Pringle, 2015) . . . . .	46
3.5	Map of the uMngeni River catchment (der Zel, 1975) . . . . .	47
3.6	Annual sediment losses for the Durban Bight accounting for sediment volumes contributed by the bypass scheme (Corbella and Stretch, 2012 <i>b</i> )	48
4.1	Schematic of general coastline model structure. . . . .	50
4.2	Flow chart detailing the internal model structure. . . . .	51
4.3	Coastline grid setup used in GENESIS (Hanson, 1989) . . . . .	52
4.4	Stored wave data for a randomly selected wave climate . . . . .	53
4.5	Transformation of a coastline section from quadrant 1 to 2. N indicates north and theta indicates the relative coastline orientation. Grey arrows perpendicular to the coast indicate coastal normals. . . . .	55
4.6	Relative orientations of breaking and deepwater waves (Ashton and Murray, 2006) . . . . .	56
4.7	Shoreline extension used for the uMhlanga boundary. . . . .	60
4.8	Model domain setup showing grid and longshore transport points . . .	61
4.9	Visualisation of tangent method used for diffusing and advecting sand waves. . . . .	64
4.10	Coastline orientations used for calculating $S_{x,0}$ . . . . .	65
4.11	Example of an advected and diffused sand wave. . . . .	65
4.12	Conceptual diagram showing cell classifications for minus and plus area ( <i>a</i> ) and regular ( <i>b</i> ) cells (Hanson and Kraus, 1986). . . . .	67
4.13	Conceptual diagram showing shoreline and transport corrections for minus ( <i>a</i> ) and regular ( <i>b</i> ) (Hanson and Kraus, 1986). . . . .	67
4.14	Distributions of various datasets used for model calibration. . . . .	69
5.1	Probability distribution of wave heights based on direction. . . . .	74
5.2	Cumulative frequency distribution for observed and simulated wave heights. . . . .	75
5.3	Linear regression plots of calibration ( <i>a</i> ) and validation ( <i>b</i> ) data sets showing annual longshore transport (LST). . . . .	76
5.4	Time series of observed ( <i>black</i> ) and predicted ( <i>grey</i> ) longshore transport rates. . . . .	77

5.5	Normalised probability distributions for datasets used in model calibration. Vertical lines correspond to one standard deviation from the mean. . . . .	78
5.6	Residual values for calculated and observed longshore transport rates. .	79
5.7	An unstable simulation ( <i>a</i> ) and a stable simulation ( <i>b</i> ). . . . .	83
5.8	Sediment influx versus net sediment change in model domain with the associated trend line. Labelled markers indicate measured rates by the respective studies and bars indicate value ranges. . . . .	85
5.9	Randomly selected 50 year simulation result with 10 year intervals shown in red ( <i>a</i> ) and average final beach positions for the labelled supply rates ( <i>b</i> ). . . . .	86
5.10	Coastline plan evolution for a sediment supply rate of 600,000 $m^3/year$ . 88	88
5.11	Sediment influx versus change in area for the aforementioned 2.4 km stretch of coastline with the trend line. . . . .	88
5.12	Observed sand waves used for model calibration ( <i>a</i> ) and validation ( <i>b</i> ). Arrows indicate crest positions at monthly intervals (eThekwini Municipality, 2017). . . . .	91
5.13	Linear regression analysis results for calibration ( <i>a</i> ) and validation ( <i>b</i> ) datasets. . . . .	92
5.14	Advection velocities for various aspect ratios with min-max ranges. . .	94
5.15	Percentage reduction in sand wave amplitude after 1 year. . . . .	95
5.16	Dimensionless diffusion-advection relationship for varying river discharge volumes ( <i>b</i> ) with discharge positions ( <i>a</i> ). . . . .	96
5.17	Simulated sand wave behaviour over 1 year for a 30,000 $m^3$ ( <i>a</i> ), 60,000 $m^3$ ( <i>b</i> ) and 100,000 $m^3$ ( <i>c</i> ) river sediment discharge. Figure titles indicate amplitude of initial sand wave together with the aspect ratio. . . . .	98
5.18	Simulation of a 200,000 $m^3$ sand wave with a width of 2000 metres. The plotted lines denote initial and final positions of the sand wave. . . .	101
5.19	Advection-diffusion relationship for varying aspect ratios correlating to various nourishment volumes. . . . .	102
A.1	Surveyed coastline coordinates in UTM format showing regions above ( <i>green</i> ) and below ( <i>red</i> ) MSL (eThekwini Municipality, 2017). . . . .	127
A.2	Profile localities from uMngeni to uMhlanga (eThekwini Municipality, 2017) . . . . .	128
A.3	Technical notes for eThekwini Municipalities Beach Survey - January 2017	129

## List of figures

---

- B.1 Wave roses for a single simulated wave sequence at different intervals. . 132

# List of tables

2.1	Notable process inclusions/exclusions of various one-line models (Thomas and Frey, 2013) . . . . .	27
3.1	Annual seasonal occurrences in South Africa (After Pringle, 2015) . . .	45
3.2	Annual sand yields in the uMngeni River (Theron et al., 2008) . . . . .	47
4.1	Mean seasonal rainfall and probability distributions (DWAF, 2011) . . .	54
4.2	Allocation of observed longshore transport rates for model calibration. .	70
4.3	Wave characteristic values for sensitivity analysis. . . . .	71
5.1	Statistical properties of observed and simulated wave climates. . . . .	73
5.2	Summarised model calibration results. Slope is the correlation between validation and calibration datasets. Mean is an average annual longshore transport rate for the respective datasets with the associated standard deviation. . . . .	78
5.3	Relative error in longshore sediment transport (Q) due to combined input errors. . . . .	81
5.4	Stability and accuracy of explicit numerical scheme for labelled schemes.	82
5.5	Input data for model simulations with descriptions and the associated value. . . . .	84
5.6	Annual erosion and accretion rates for various sediment inputs. The sum row represents the resultant annual erosion rate for the given supply rate. . . . .	89
5.7	Summarised advection rate calibration results. Advection rates are presented in <i>km/year</i> . . . . .	91
5.8	River discharge physical parameters. . . . .	93
5.9	River discharge physical parameters. Volumes in the first row are $\times 10^3$ .	97
5.10	Extreme event discharge results. Retention time refers to the time taken for the sand wave crest to reach the left end of the model domain. . . .	100

## List of tables

---

5.11	Nourishment sand wave parameters used for analysis in figure 5.19. . . . .	103
5.12	Travel times for a 209,167 $m^3$ nourishment of varying aspect ratios between multiple points along the Durban coastline. Point of application of the nourishment is position 3. . . . .	104
5.13	Travel times for a 209,167 $m^3$ nourishment of varying aspect ratios between multiple points along the Durban coastline. Point of application of the nourishment is position 2 while column 5 assumes nourishment application at position 3. . . . .	105
B.1	Annual wave characteristics for observed wave data. . . . .	131
B.2	Statistics for randomly selected 100 year wave sequences. . . . .	132
C.1	Results of model calibration using first half of observed wave data. . . . .	133
C.2	Results of model validation using second half of observed wave data. . . . .	133

# Chapter 1

## Introduction

### 1.1 Coastal Erosion

Coastlines are complex environments, characterised by the constant interaction between fluid and solid media (Carter, 1988). Coastal erosion occurs as a result of various natural processes such as waves, currents and wind which in turn affects the sediment budget and disturbs the equilibrium state (Mallik et al., 1987). Chronic coastal erosion has largely intensified and is of international concern (Van Rijn, 2011) with overdevelopment and global sea-level rise attracting widespread attention from researchers (Feagin et al., 2005).

While beach erosion is a natural process, excessive loss of beach width and frontal dune instability reduce the coastlines ability to protect against coastal flooding during storms (Saye et al., 2005). Beaches act as buffer zones and protect the hinterland against attacking waves (Ruggiero et al., 2001). Chronic erosion may be a result of anthropogenic factors or natural cycles, with Corbella and Stretch (2012*c*) suggesting changes in wave characteristics as another potential contributor.

Corbella and Stretch (2012*b*) identify three major causes of long-term erosion: sea-level rise, meteorological changes that directly alter wave climates and reductions in sediment supply. Zhang et al. (2004) identified a strong relationship between sea-level rise and coastal erosion however it was found to be a secondary cause of erosion in regions where coastal engineering projects masked this effect. Sediment supply reductions due to anthropogenic activities are of increasing concern with a strong correlation found between rates of shoreline change and relative human development due to influences on coastal sediment sources (Hapke et al., 2009). The resulting impacts of urbanisation are likely to intensify given current settlement trends.

### 1.1.1 Impacts of Urbanisation

Coastlines are some of the most biologically diverse and densely populated regions on the planet. Beaches are under increased pressure due to population growth, demographic shifts and economic development. Coastlines contribute greatly towards the tourism industry worldwide, hence loss of beach width has severe implications physically, environmentally and economically (Phillips and Jones, 2006). Crossland et al. (2005) estimates that the average population density along coastlines by 2050 will be 134 people per square kilometre, nearly double that of 1990.

Increased population densities combined with large seasonal fluxes of people due to tourism has placed increased demand on natural resources such as sand. Rapid urbanisation has seen a rise in the construction sector, exacerbating the demand on these resources (Adger, 2003). Expansion of coastal cities has led to the construction of numerous coastal structures such as groynes and artificial marinas which inhibit a major sediment source in littoral drift. These structures alter wave conditions and act as a sink for sediment, limiting sediment supply and causing down-drift coastal regions to become vulnerable (Haslett, 2016). Other sediment sources such as rivers are greatly compromised due to prevalence of damming and sand mining. Sand mining has increased in accordance with an increased construction and transportation sector, with sand being a major component of aggregate materials (Padmalal and Maya, 2014). Dams have been found to reduce sediment content produced within a catchment area by around 40%, with this number increasing depending on the number of dams along the river course (Kondolf, 1997). The combined effect of coastal development together with sand extraction from rivers severely alters natural transactional processes between major sediment sources and the coastline, causing the beach to adapt to a new, reduced sediment budget. Human intervention is thereafter required to rectify the result of reduced sediment budgets, causing a new phenomenon of varying sediment supplies.

### 1.1.2 Coastal Management

Chronic erosion along coastlines has prompted the implementation of various hard and soft engineering solutions to preserve and maintain profiles. Hard engineering solutions include permanent fixtures such as groins and breakwaters whereas soft engineering solutions include sand-nourishments and bypassing schemes (Phillips and Jones, 2006). Major cities around the world have adopted either or both of these solutions to safeguard infrastructural assets (Yuan and Cox, 2013). Hard solutions are primarily aimed at resisting natural processes however these structures are associated

with significant local changes to the coastline due to the inhibition of littoral drift processes (Airoldi et al., 2005). Soft engineering schemes such as nourishments and sand-bypassing are implemented to imitate natural processes such as littoral drift however these schemes are operated intermittently. Fluvial deposits are commonly introduced in flood-driven pulses, with closed river mouths only contributing sediment during breach events (Theron et al., 2008). Coastline evolution is therefore variable and somewhat dependent on the operation of these schemes. The collective result is severe alteration and damage to the coastal landscape, with minimal indications of coastal development being restricted (Nordstrom, 2000). Coastal planning therefore becomes significant in understanding how coastlines respond to different sediment supply scenarios.

### 1.1.3 Coastal Planning

With climate change and sea-level rise increasing coastal vulnerability, coastal planning is becoming increasingly important. Landward retreat of the coastal profile is expected due to changes in sea-level rise (Ranasinghe et al., 2012) while the frequency of high-intensity storms is also expected to increase (Mendelsohn et al., 2012). Long-term planning often relies on the availability of reliable wave data and an efficient numerical tool for prediction, usually in the form of a model. Lengthy records of wave data are often unavailable or unreliable, hence the use of stochastically simulated wave climates offers an alternative. This provides potential for simulating long-term coastline changes.

Numerous numerical models are currently available which differ in complexity and application. Simpler models include one-line and two-line shoreline models with more complex examples being 2D process-based beach profile and 3D process-based beach profile models (Gravois et al., 2016). Numerical models serve as useful tools in predicting short to medium term changes in bathymetry associated with coastal features such as groins and breakwaters (Nicholson et al., 1997). Coastal area models include a higher level of detail however these ‘process based’ models are computationally intensive, and require for a reduction of forcing conditions (Tonnon et al., 2018). Coastline models offer benefits of faster running times and application of the full wave climate (Tonnon et al., 2018). Stive et al. (2011) proposed a coastal evolution concept which predicted shoreline position changes for varying sea-level rise scenarios. This study uses existing coastline models as a framework to develop a coastline response model capable of predicting long term responses to varying sediment supply schemes. Simulated wave data using statistical methods serve as the data source for the study. Focus is placed

on sediment supply shortages as the primary cause of erosion along the stretch fo coastline between uMhlanga and the uMngeni River mouth.

## 1.2 Problem Definiton

Chronic beach erosion due to anthropogenic influences on coastal and fluvial sediment reserves has had a significant impact on coastline evolution. Construction along coastlines along with resource exploitation along major sediment sources such as rivers have negatively impacted sediment budgets, altering the equilibrium state of beaches. Successful coastal management and planning is made difficult due to the dependance on reliable wave records and the availability of numerical models. Statistical methods for modelling wave climates provide an alternative to observed wave records. The advent of an efficient numerical tool for simulating coastline changes over long periods for various sediment supply scenarios will assist in improving coastal management. This could prevent severe or permanent damage to coastlines and settlements.

### 1.2.1 Research Question

*Can varying sediment supplies be identified as a primary cause of coastal erosion along anthropogenically impacted beaches?*

This study focuses on the KwaZulu-Natal coastline and wave climate where the research question is investigated in the context of a case study within the Durban area. It may be posed more specifically below:

**What are the long-term impacts of varying sediment supplies along the Durban coastline?**

1. What is the most effective way to simulate long term coastline evolution within reasonable timeframes?
2. Are statistically modelled wave climates appropriate for this study?
3. How does the coastline respond to a varying sediment supplies in the long-term?
4. How do nourishment schemes behave along the coastline?
5. How do river discharges behave and are they potentially significant in preventing erosion?

## 1.3 Motivation

The east coast of South Africa is linked to a high energy wave climate in regions such as KwaZulu-Natal (Pringle et al., 2015). The city of Durban is the country's third most populated city with strong historical reliance on tourism as a major financial income source (Maharaj et al., 2008). Although highly important for tourism, Durban's coastline has experienced severe erosion in recent years.

An annual beach survey programme by the eThekweni Municipality (2017) yielded sediment losses in the region of 270,000 cubic metres between 2011 and 2017 within a certain stretch of coastline. This may be attributed to the increased influence of humans on coastal sediment sources and processes. Construction and lengthening of the harbour breakwaters resulted in the eventual inhibition of longshore transport (Laubscher et al., 1990), requiring for the re-evaluation of the sand-bypassing scheme to account for the changes. Additionally, construction of dams and sand mining along numerous rivers in the province resulted in almost complete depletion of sand discharges to the ocean (Theron et al., 2008). River sediment yields were reduced by around 66% which proves significant given that rivers constitute 80% of the overall sediment supply (Theron et al., 2008). The cumulative result of these changes is the loss of beach width.

Sandy beaches act as natural buffers by absorbing wave energy and adapting to changes in seasonal and long term wave climates (Scott et al., 2016). Loss of beach width causes lowland coastal regions to become vulnerable to storm surges and high energy wave events (Morton and Sallenger, 2003). Morton and Sallenger (2003) adds that high energy wave events result in almost instantaneous erosion of beaches, exacerbating the effects felt by beach width loss. Climate change effects are expected to result in more severe storm events (Webster et al., 2005). Furthermore, Leatherman et al. (2000) identified a strong relationship between sea level rise and sandy beach erosion, estimating beach erosion of 15 metres for a sustained 10 cm rise in sea levels. With high population densities and the development of valuable infrastructure, the risk of coastal cities to storm damage continues to increase.

The transport sector has strong influences regarding economic development with ports serving as an important connection between sea and land transport (Dwarakish and Salim, 2015). This has resulted in major industries being located along coastal belts in close proximity to ports (Dwarakish and Salim, 2015). Long-term coastal planning is increasingly important given population and development trends along with observed losses of coastal protection. Schoonees (2000) estimated longshore transport volumes at the harbour to be between 300,000 and 500,000  $m^3/year$ . Corbella and Stretch (2012c) studied erosion trends using process based models, estimating a longshore

## Introduction

---

sediment supply of 418,333  $m^3/year$  which falls within the estimate by Schoonees (2000). Corbella and Stretch (2012c) did conclude that Durban's beaches are eroding, indicating that increased erosion is potentially significant to long term planning. eThekweni Municipality's annual beach surveys for the stretch of coastline between uMngeni and uMhlanga have indicated erosion as well. This data may not necessarily be useful for long term planning as predicted coastline changes are limited to the period of observed wave data which does not account for future events outside this period.

A model for simulating long term changes in coastline shape will aid in improving the operation of bypassing schemes. Furthermore, identifying the contribution of rivers will improve regulation of river activities. The use of simulated wave climates negates the need for long periods of observed wave data. Simulated wave data is advantageous in the sense that they are based on observed data and may be used to replace periods of observed records where data acquisition was interrupted. Additionally, they may be used to extend existing wave records and have demonstrated the ability to be downscaled from regional to site specific locations (Pringle et al., 2015).

## 1.4 Aims & Objectives

*Develop a numerical model to simulate long-term changes along the Durban coastline under varying sediment input schemes.*

Objectives:

1. Identify the necessary processes and numerics to develop a coastline model.
2. Assess the viability of using simulated wave climates to represent observed data.
3. Calibrate and validate the coastal model using relevant observed regional data.
4. Evaluate the model sensitivity.
5. Identify relative contributions and variability of sediment into the selected region from primary and secondary sediment sources.
6. Use the coastline model to run a number of simulations incorporating various sediment input schemes.
7. Use the model to assess the behaviour of sand waves and nourishments.

## 1.5 Approach

The KwaZulu-Natal coastline along the East coast of South Africa is used as a case study, more specifically the stretch of coastline between the uMhlanga Lighthouse and the uMngeni River mouth within the Durban area, shown on figure 1.1.

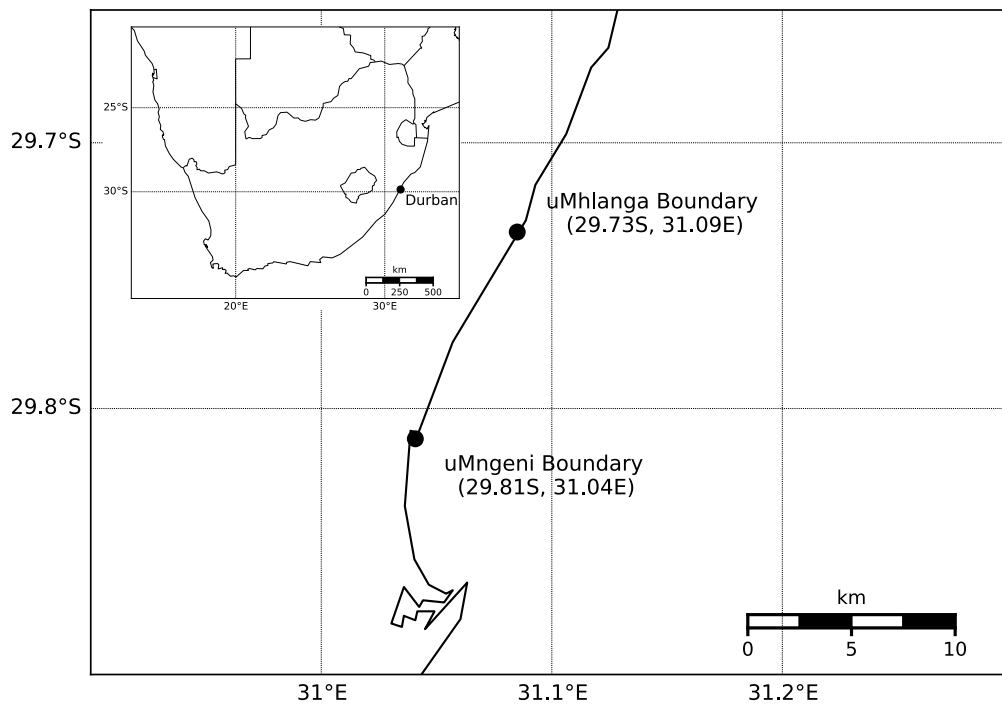


Fig. 1.1 Locality plot of the study region in national and local context.

### 1.5.1 Case Study: Durban

Durban has a lengthy history of beach protection, primarily centred around the effective operation of a port (Corbella and Stretch, 2012a). Following construction in 1857, various extensions of the breakwaters and further dredging of the inlet were carried out. A sand-bypassing scheme was initiated in 1935 to account for the approximate sand loss of  $650,000 \text{ m}^3$  due to dredging (Corbella and Stretch, 2012a). Site selection was based on the presence of a major fluvial sediment source in the uMngeni River together with the aforementioned sand-bypassing scheme south of the study region. Additionally, the uMngeni River has experienced severe reductions in sediment yields due to sand mining and damming, potentially affecting coastline evolution. According to beach survey data from the eThekweni Municipality, this annotated region experienced annual sand

## Introduction

---

losses of around  $40,000 \text{ m}^3$  between 2011 and 2017 which is assumed to be a result of reduced fluvial yields and inadequate littoral drift volumes.

Schoonees (2000) carried out a study along the Durban coastline which approximated annual longshore transport rates at a number of points. Corbella and Stretch (2012*b*) carried out a similar study, analysing records of beach profiles to estimate annual longshore transport rates along the coastline. This data was used in model calibration and also served as the current estimate of longshore sediment supply for the study region. Modelled values were compared against these values.

Wave data over an 18 year observation period are available for the Durban coastline from 2 wave rider buoys and an acoustic doppler current profiler (ADCP) (see fig. 1.2). This data was supplemented by an 18 year wave record observed at Richards Bay using a waverider buoy, which was used to verify the Durban data. Wave records were reduced to 13 years due to lack of directional wave data. This data was used to calibrate and verify the longshore sediment transport formula in the numerical model.

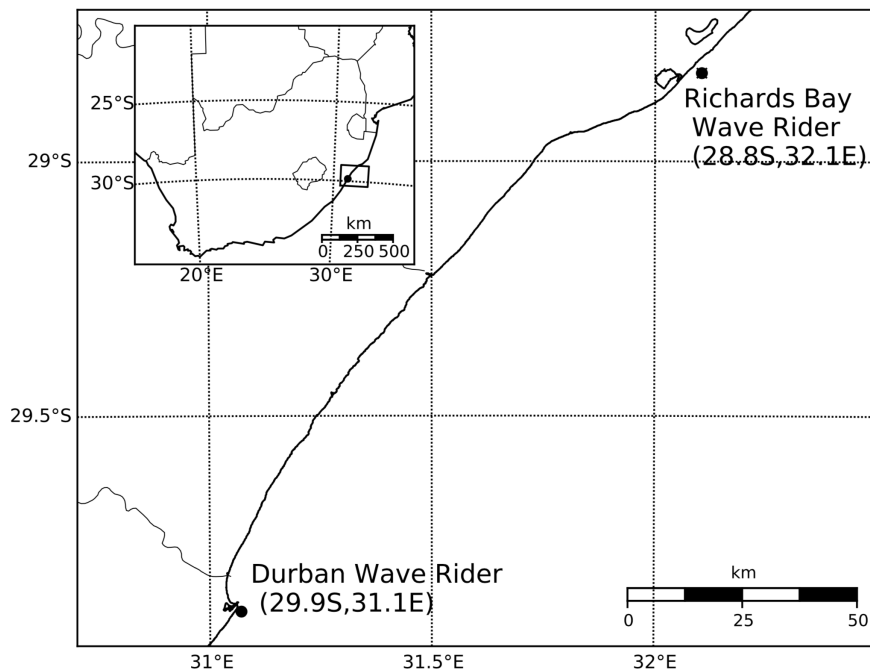


Fig. 1.2 Locations of observation buoys at Durban and Richards Bay along the KwaZulu-Natal coastline (Pringle, 2015).

The eThekweni Municipality carries out annual beach survey programmes within the study region, providing beach volumes and profile shapes at regular intervals. This data was used to compare modelled beach changes and observed changes to identify possible trends in longshore transport.

Using previous coastline models as a framework, a numerical model was developed to simulate long term changes along coastlines. Wave data for these simulations were stochastically simulated regional wave climates conditioned on synoptic scale meteorology. The model incorporated the necessary coastal hydrodynamics whilst simulating varying storm frequencies and intensities to replicate the episodic nature of river flooding events. Observed wave data for the region was used to calibrate and verify the model. A sensitivity analysis was carried out to understand the effects of input errors in variables on the results obtained. Finally, numerous simulations were carried out under different schemes in an attempt to explain observed coastline behaviour.

## 1.6 Outline of Dissertation

A literature review examining the major subject areas relevant to this study follows on from this chapter. The two chapters that follow the literature review detail the methods used in this investigation, followed by the results and discussion. Conclusions are presented in the final chapter with important data from this study displayed in the appendices that conclude the document.

The dissertation is composed of the following chapters, outlined below:

**Chapter 2** examines key areas relevant to this study through a literature review.

**Chapter 3** presents a description of the case study used in this dissertation, detailing site selection criteria and data sources used.

**Chapter 4** details the structure and numerics of the coastline model.

**Chapter 5** presents the findings of the study together with the appropriate discussions. This chapter includes results of model calibration, data verification and long term simulations.

**Chapter 6** summarises the work presented in the previous chapter and provides conclusions. This includes a discussion regarding the future applications of this study.

## Introduction

---

**Appendix A** contains beach data used for this study such as coastline coordinates, profile dimensions and sediment information.

**Appendix B** displays statistical information relating to observed and simulated wave data used for model calibration in this study.

**Appendix C** shows summarised results of model calibration.

**Appendix D** shows the numerical model pseudocode.

# Chapter 2

## Literature Review

### 2.1 Introduction

This chapter reviews literature relevant to achieving the aims and objectives of this dissertation. Initially, coastal erosion is discussed in both a global and local context (Sect. 2.2) together with potential causes. This next section (Sect. 2.4) relates to sediment supply reductions, discussing various sources of sediment and the impacts of urbanisation on coastal sediment sources. These sections serve to highlight the significance of reduced sediment supplies as a major cause of coastal erosion.

Coastal management is thereafter discussed (Sect. 2.5) in terms of hard and soft engineering solutions used to preserve beach profiles. This includes a discussion of how solutions often exacerbate problems due to poor understanding, implementation and operation where applicable.

Section 2.7 relates to coastal planning and highlights the importance of long-term planning in ensuring optimal performance of coastal management schemes such as sand-bypassing and shore nourishments. Challenges relating to long-term planning are highlighted followed an overview of numerical coastal models. Various types of numerical models are reviewed within this section regarding their applicability to long-term coastal modelling. This is followed by section 2.8 which identifies and discusses the fundamental mechanics and numerics behind a coastline model. This includes potential improvements to previous methods.

The next section (Sect. 2.9) reviews various statistical methods for synthesising wave records as well as their usefulness in improving observed datasets. Furthermore, the methodology for generating stochastically simulated regional wave climates conditioned on synoptic scale meteorology is discussed.

### 2.2 Coastal Erosion

Coastal erosion is of concern to developed shorelines worldwide (Pilkey et al., 1991). It presents a complex physical process influenced by various human-induced or natural factors (Prasad and Kumar, 2014). Pilkey et al. (1991) identify sea level rise and a reduction of sand supply to shorelines as major causes behind coastal erosion. Corbella and Stretch (2012*b*) identified a further potential cause as meteorological changes that directly affect wave climates. Furthermore, as sea level rise continues together with climate change, global erosion rates are expected to increase in the coming decades (Pilkey et al., 1991). Although coastal erosion has always existed, it has been largely intensified by anthropogenic influences (Van Rijn, 2011).

Historically, human intervention in coastal zones has regularly led to non-sustainable levels of resource exploitation (Turner et al., 1996). Activities such as damming and sand mining have depleted sand discharges to coastlines, resulting in severe damage to shorelines (Pilkey et al., 1991). Increased investment and development has created a sustained demand for land reclamation and protection of infrastructure. This has necessitated the installation of engineering defence structures such as sea walls which has affected local coastline behaviour (Perkins et al., 2015). Soft engineering solutions such as beach nourishments also serve to counteract erosion however these solutions are costly (Pilkey et al., 1991). Maintenance of shorelines is significant to coastal settlements. Coastlines act as buffers to waves and storm surges while also reducing exposure to potential sea level rises (Arkema et al., 2013). They also provide coastal cities with a socio-economic benefit, contributing greatly towards recreational activities and the tourism industry. Given the potential repercussions of this behaviour, coastal cities have prioritised coastal management to maintain and preserve their shorelines. Operation and management of coastal defence schemes are challenging due to the inability to quantitatively account for long-term ecosystem dynamics (Bouma et al., 2014). Numerical models may prove advantageous in this aspect.

Numerous models have been previously developed to aid with coastal management. These vary in complexity and application and are becoming increasingly important in the management and planning of soft and hard engineering solutions. The following literature highlights the impacts of human activities along coastlines and major sediment sources such as rivers. Remediation measures to these impacts are discussed together with available methods for predicting coastline change. Available models are reviewed and discussed, with a focus on one-line models in particular. Furthermore, the numerics required for the development of a coastline model that may be used to predict long term coastal changes are explored.

## 2.3 Coastal Sediment Sources

Shorelines have a unique combination of sediment sources (Pilkey et al., 1991). Sedimentary budgets represent the different sediment inputs and outputs of coastlines which may be used to predict changes along a coastline for a particular time period. It is essentially the sum of gains and losses, also termed sources and sinks, within a specified control volume over a specified interval of time. Sediment budgets are useful in coastal planning, however Parsons (2012) raises concerns over what timescale estimated budgets may be valid over. Parsons (2012) goes on to state that any budget with an unequal input to output is untenable over the long term.

Sediment sources of coastlines may be categorised as primary or secondary sources. Primary sources consist of wave eroded material from cliffs and submarine platforms and are usually representative of linear or areal sources (Carter, 1988). Secondary sources consist of sediment produced by rivers, glaciers or ice sheets, human activity such as waste disposal and eolian action. These are commonly considered as point sources while exhibiting high variability along the coastline (Carter, 1988). The continental shelf serves as an important sediment source which is provided by onshore transport (Pilkey et al., 1991). Within the active beach system, common sources of sediment are derived from upland erosion of rivers, longshore transport from adjacent coastline segments and erosion of shore face and inner shelf deposits (Schwab et al., 2013). Figure 2.1 below details the various sources of sediment within a coastal system. The greatest influence on coastal sediment supplies is that of humans (Pilkey et al., 1991).

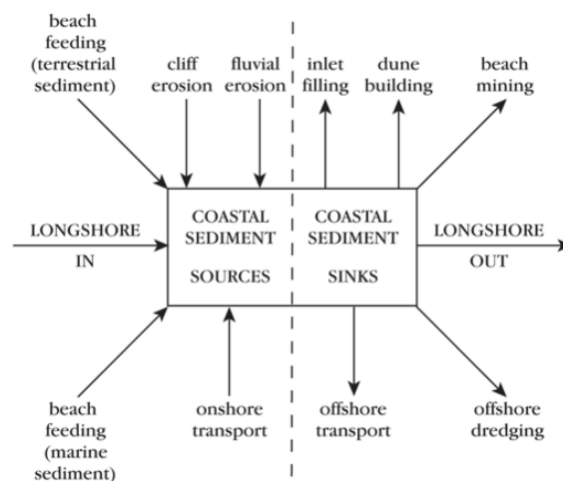


Fig. 2.1 Sediment sources of active coastal systems (Rosati, 2005)

## 2.4 Impacts on Sediment Supplies

### 2.4.1 Coastal Structures

Coastal structures are constructed features along a coastline that serve various purposes. Groins and breakwaters form part of coastal defence schemes whereas ports and harbours form part of a cities infrastructural network. With coastal cities growing in both population and physical assets, the need for coastal defences has greatly increased (Genovese and Green, 2015). These structures are typically installed following a major storm event in a process referred to as “*coastal armouring*” (Dugan et al., 2011). Structures are generally installed along beaches experiencing erosion in an attempt to halt the process. Dugan et al. (2011) state that the placement of a coastal structure fundamentally alters hydrodynamics and the flow of water together with sediment dynamics and depositional processes which proves advantageous to eroding coasts. Although they have proven to be effective in protecting infrastructure from storms and erosion, concerns still remain relating to their construction.

Dugan et al. (2011) infer that little is understood regarding the ecological consequences of these structures on native environments. Furthermore, even less is known about the impacts of these structures on open-coast systems such as beaches. This notion is shared by Airoidi et al. (2005) who add that construction of defences may lead to disruption of soft-bottom environments together with the introduction of artificial hard-bottom environments. This also has a knock-on effect on species diversity in the area, allowing for the spread of non-native species which increases habitat homogeneity (Airoidi et al., 2005). In addition to habitat destruction and alteration, coastal defence structures impact coastline evolution by altering natural sediment transport processes. Dugan et al. (2011) identified potential changes to coastlines following the installation of varying defence structures;

- Initial reduction of beach widths seaward of shore-parallel structures responding to placement losses as well as continuous processes of active and passive erosion.
- Beach area reduction and passive erosion.
- Scour up-drift of the structure together with flanking erosion due to stronger physical processes induced by wave reflection and surf zone narrowing during storms.
- Accelerated erosion of coastlines down-drift of groins and jetties as a result of abrupt discontinuities in littoral sediment transport.

Dugan et al. (2011) add that these effects scale based on the amount of interaction between the structure and the wave climate. In addition to coastal defence structures, port and harbour developments are known to cause local environmental problems (Davis and Macknight, 1990). These structures alter wave conditions and act as a sink for sediment, limiting supply to longshore drift systems and causing down-drift coastal regions to become vulnerable (Haslett, 2016). Storm conditions with high surge levels result in hard structures such as groins and breakwaters providing little relief (Van Rijn, 2011). Furthermore, hard structures may cause an increase in coastal variability. Figure 2.2 illustrates the interaction of littoral transport with a harbour breakwater and the formation of a discontinuity.

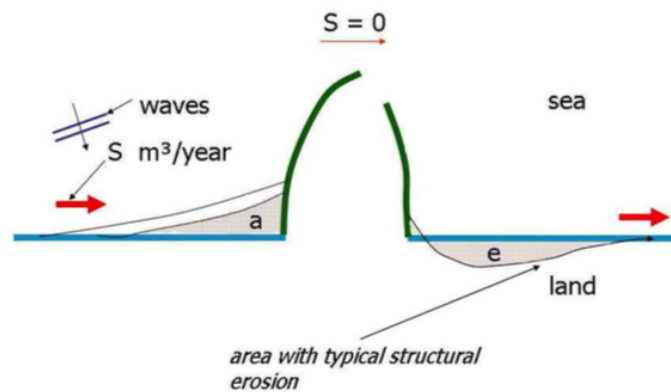


Fig. 2.2 Sediment transport around a harbour mouth (Bosboom and Stive, 2015)

It is however important to make a distinction between infrastructural installations such as harbours and coastal defence structures such as groins. The former commonly has negative implications whereas the latter is introduced to remediate ongoing issues. A study by Bernatchez and Fraser (2012) found that the effects of coastal defence structures are compounded on beaches with a high level of sediment transport due to the reflective nature of the structure. Vaidya et al. (2015) suggest that decisions on whether to build structures should include a thorough analysis of past shoreline behaviour and projected future developments.

### 2.4.2 Fluvial Sediment Yields

Rivers are a key pathway for land-ocean sediment transfer, forming an integral part of the coastline evolution scheme. On a global scale, Theron et al. (2008) found that coastlines rely on rivers for approximately 80% of their sediment load. Contemporary data on numerous river sediment loads have given clear indications of significant recent

## Literature Review

---

changes in sediment fluxes as a result of human activity (Walling, 2006). A range of human activities occur within drainage basins, with Chu et al. (2009) identifying dams, reservoirs, water conservation schemes, water consumption and sand mining as the primary causes behind sediment load reductions. Given increased demand for sand required in construction and infrastructure sectors, sand mining has become common practice along the flood-plains of rivers (Amponsah-Dacosta and Mathada, 2017).

Sand mining refers to the extraction of sand predominantly from an open pit or by means of dredging along ocean floors and river beds (Amponsah-Dacosta and Mathada, 2017). Syvitski and Saito (2007) demonstrated that sand mining had caused mega-deltas along the Asian coastline to shrink due to reduced sediment yields whereas pre-mining studies showed consistent accretion. With sand mining experiencing a rise in popularity, regulation of the activity has proved troublesome in many countries which compounds the problem. South Africa serves as an example, where sand mining regulations are split into three categories; mineral, environmental and land use planning regulations. It was found that mineral regulations are favoured ahead of the others, with Green (2012) implying that all three classes should hold equal importance. This notion is shared by Amponsah-Dacosta and Mathada (2017) who found that most mining activities have little regard for environmental protection. Furthermore, South Africa is experiencing a high amount of illegal sand mining where miners have not received official permits for their operations (Theron et al., 2008). This worsens resource exploits and also makes prediction of sediment budgets inaccurate.

Dams have also played a significant role in sediment load reductions. Snoussi et al. (2002) studied the impacts of dam construction on water and sediment fluxes. Findings showed that the cumulative volume of sand trapped by three dams along the Sebou River in Morocco resulted in a 95% reduction in sediment load. Yang et al. (2018) present similar findings showing significant sediment load reductions due to damming. In contrast, Yang et al. (2018) initially found a 30% increase in load due to surface erosion resulting from an increase in human population, inferring that certain activities lead to increases in sediment load.

The combined effect of dams and sand mining have demonstrated how severely sediment yields of rivers may be affected. Rivers also intermittently transact sand to the ocean, typically during flooding events (Michaelides and Singer, 2014). This behaviour is exacerbated when considering the sedimentation pattern of the river. Estuaries that are in a state of non-progressive sedimentation maintain a state of long-term dynamic equilibrium. This means that a constant sediment volume is always retained within the estuary (Theron et al., 2008). These are also referred to as river-dominated estuaries,

## 2.5 Coastal Management & Planning

where sediment volumes recover to the equilibrium volume following flooding events (Cooper, 1993). Estuaries experiencing progressive sedimentation or wave-dominated estuaries experience a consistent increase in stored sediment over time. Figure 2.3 below illustrates the differences between non-progressive and progressive sedimentation scenarios, showing how sediment volumes vary over time. Finally, Theron et al. (2008) explains that the sedimentation rate of the river also plays an important role in defining how quickly sediment loads accrete within estuaries.

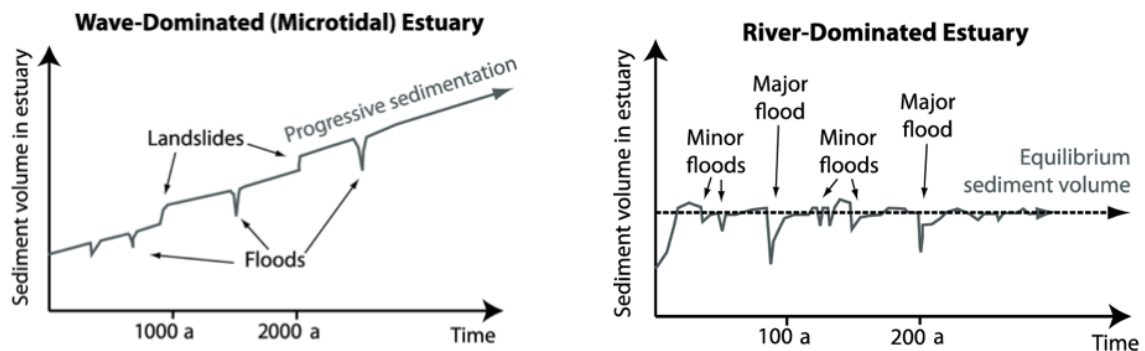


Fig. 2.3 Graphic representations of river-dominated and wave-dominated estuaries (Cooper, 1993)

## 2.5 Coastal Management & Planning

The link between global and local activities and coastal management is significant given the intense pressure coastal resources will always experience (Kay and Alder, 2005). Coastal management involves the implementation of defence schemes to maintain beaches. This process is split into two categories; namely soft and hard engineering schemes (Corbella and Stretch, 2012a). Hard engineering schemes are predominantly permanent fixtures designed to resist natural processes using structures like breakwaters and seawalls. Soft engineering solutions aim to replicate, emulate or manipulate natural processes, such as nourishment schemes (Hansom, 1999). Defence schemes vary in form and function with groins, breakwaters and revetments primarily designed to prevent beach erosion. Sea dikes, seawalls and storm surge barriers are more purposed towards flood prevention (Burcharth and Hughes, 2003). Thomas (1994) further states that these structures form elements of a coastal defence system, and rarely operate individually. Coastal management is increasingly leaning towards 'soft' engineering having been historically rooted in 'hard' solutions (Winter and Checkland, 2003).

### 2.5.1 Shore Nourishments

Unexpected shoreline losses are often the result of improper planning prior to design and construction of coastal structures (Noble, 2011). In countries such as the United Kingdom, beach nourishments are commonly implemented to complement more traditional forms of coastal defence (Hanson et al., 2002). Beach nourishments are defined as the placement of large volumes of sand within the nearshore region in an attempt to advance the shoreline seaward (Dean, 1991). Shore nourishment are an alternative term due to high variability in the cross shore direction (Hamm et al., 2002).

Benefits of nourishments include storm damage reduction along with recreational and environmental enhancement while serving as an effective energy absorber during persistent periods of high water levels and storm waves (Dean, 1991). These schemes provide a reservoir of sand for transportation to adjacent segments of coastline, improving beach width (Dean, 1991). The fundamental thinking behind beach nourishment is to deposit sediment into starved regions and allow for nature to take its course as opposed to counteracting natural forcing factors to retain remaining sediment (Hamm et al., 2002). An example of a mega-nourishment scheme is the Sand Engine along the coast near Ter Heijde in the Nertherlands. The project entails the deposition of  $21.5 Mm^3$  of sediment resulting in the formation of a peninsula (fig. 2.4) (Stive et al., 2013) . The project is aimed at evaluating the efficacy of local mega-nourishments as a means for combating enhanced coastal erosion (Stive et al., 2013). The single mega-nourishment is expected to be more efficient, environmentally friendly and economical as compared to traditional beach and shoreface nourishments (Stive et al., 2013).

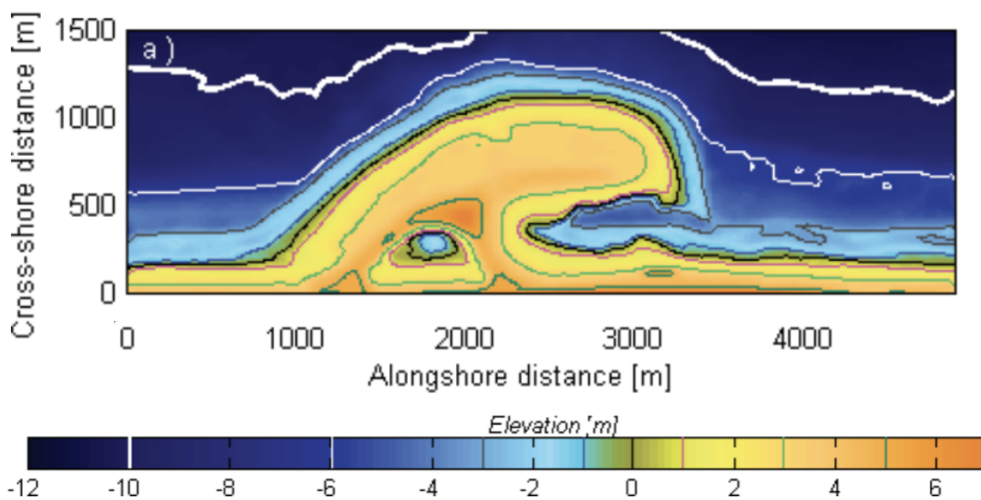


Fig. 2.4 The Sand Engine at the initial stage of deposition (Stive et al., 2013)

## 2.5 Coastal Management & Planning

---

Although these soft engineering techniques provide an environmentally friendlier option, questions remain over the long term sustainability of this technique given climate change and sea level rise. Given the alteration of wave climates, storm intensity and frequency as well as mean sea levels, the extents of beach nourishments will undoubtedly be significantly increased which may make them economically unfeasible (Van Rijn, 2011). Hamm et al. (2002) state that although tricky, evaluation of effectiveness and performance of these schemes plays a major role in the appraisal of this method.

Evaluation criteria relating to design and accreditation of nourishment schemes are primarily dependant on technical issues and public policy (Capobianco et al., 2002). Examples of technical issues include design frequency, pre and post-fill erosion rates, project length and long term sand resources, among a number of others. Public policy issues are composed of monitoring, periodic nourishment, rehabilitation and environmental permitting, however complexities arise when considering nourishment frequency from a technical and policy standpoint (Capobianco et al., 2002).

Performance of beach nourishments are highly variable and depend on a number of factors. Brown et al. (2016) found that a number of smaller, well-placed nourishment schemes were as effective as larger schemes over the short-term (0-20 years). Long-term (50-100 years) benefits become more apparent regarding larger schemes, however results indicated initial phases of erosion due to sediment deposition, interrupting natural sediment drift processes. This raises the issue of sediment losses, with Verhagen (1996) stating that only around 52% of nourished material becomes a permanent part of the coastal volume. Verhagen (1996) suggests an increase of 40% to the calculated design value to account for these losses. Charlier and Meyer (1995) infer that sediment losses may be minimised by constructing structures along the ends of nourished regions.

A number of environmental impacts are linked to the use of artificial nourishment schemes. These include burying of shallow reefs, degradation of other beach habitats and reductions in densities of invertebrate prey for shorebirds, fish and crabs (Peterson et al., 2014). This is a result of changing water levels and currents, turbidity and disturbances of sediment within the appropriate region (Vidal and van Oord, 2010). Additionally, a number of marine fish and turtle species may be affected during mining, as well as the water column and benthic fauna (Greene, 2002). Peterson et al. (2014) add that much uncertainty still exists relating the the biological impacts of nourishment schemes. A review of 46 beach monitoring studies yielded 49% of these failing to meet publication standards. This highlights the importance of a comprehensive environmental impact assessment before any nourishment schemes are implemented.

### 2.5.2 Sand-bypassing

Sand-bypassing as a “*soft-engineering*” solution is still open to discussion, however their usefulness in beaches that are sediment starved is unquestionable (Charlier and Meyer, 1995). Sand-bypassing schemes operate on a combination of basic principles; dredging, transporting and depositing of sand (Loza, 2008). River mouths and entrances to lagoons or embayments act as natural initiators of littoral drift processes. Should currents not be strong enough to carry sediments to the downcast side of the feature, erosion is likely to occur (Charlier and Meyer, 1995). Man-made inhibitors include harbour mouths that extend seaward. They may cause almost complete inhibition of littoral drift process depending on the extent of the protrusion.

Loza (2008) states that there are two different operating modes when referring to bypassing schemes, namely interception systems and storage systems. Furthermore, structures such as groins and harbours aid in concentrating sediment volumes for interception, with these schemes requiring a high degree of certainty regarding longshore drift rates. An alternative to dredging is the use of fixed plants, however Clausner (2000) states that fixed plants are relatively rare worldwide. This is due to significantly higher efforts required to estimate costs and performance as opposed to more conventional dredging techniques.

Shore nourishments together with sand-bypassing often lead to the formation of coastal features such as sand waves and spits which integrate their own unique behaviour under the influence of wave action. In the long term, these features may be used to explain erosive or accretive behaviour at particular points along the coastline. Understanding how these features form and how they influence coastline evolution is significant in modelling coastline evolution. Additionally, understanding how these features move through coastal systems may aid in identifying behavioural patterns and will improve coastal management.

### 2.5.3 Set-back Lines

Set-back lines may be defined as the amount of open space that should be left between infrastructure such as buildings and the shoreline (Breetzke et al., 2012). USACE (1984) further define a set-back line as an allocated zone along the coast wherein prescribed development activities are prohibited or restricted. DEA (2008) states that these zones are being increasingly implemented to prevent non-sustainable and inappropriate development in sensitive coastal zones to reduce the risks posed by climate change.

The Integrated Coastal Management Act 24 of 2008 details that special permissions are required for any person wishing to erect structures seaward of this zone.

### 2.5.4 Dune Management

Sand dunes are an accumulation of sediment which occurs under general conditions, and is thereafter released and transferred to the beach and offshore regions following the occurrence of a storm (CEP, 1998). Over time, these dunes will rebuild themselves following a storm event through the accretion process however this results in high variability along beaches. Furthermore, conflicts arise when considering immovable coastal properties (CEP, 1998). CEP (1998) states that sand dunes are so interdependent that it is crucial for them to be managed in unison as they have complex physical, economic and social implications. The Integrated Coastal Management Act 24 of 2008 protects these structures by preventing development in regions that are subject to serious erosion during storms or areas characterised by drift-sand movement (DEA, 2008). Loss of vegetation along dunes causes these structures to become vulnerable to erosion due to surface winds. Funnelling of winds onto low-lying dunes results in rapid sand removal as well as the development of an exposed dune region, also termed a blow-out (CEP, 1998). CEP (1998) states that methods for dune conservation include implementation of physical barriers to trap sand, mechanical stabilisation of ridges and reforestation of the dune ridge.

### 2.5.5 Restricted Beach Access

Coastal public property is a zone of land and water along the coastline which may be regarded as common property to the citizens of the relevant country (DEA, 2008). In order for effective coastal and regulation to be possible along these public property areas, restrictions and controls are also required in areas that form part of coastal ecosystems. Identification and restriction of these regions is crucial in managing development along sensitive areas and is essential in reducing the risks faced by properties bordering the coastal region (DEA, 2008). These include coastline erosion, flooding and sea-level rise as a result of global warming. This has been incorporated into the Integrated Coastal Management Act 24 of 2008 allows for demarcation of these zones which are thereafter referred to as coastal protection zones. The distance to which the zone extends inland from the high-water mark is variable, with previous demarcations ranging from 100 to 1000 metres depending on the land use purposing (DEA, 2008).

## 2.6 Coastline Behaviour

### 2.6.1 Sand Wave Formation

Relatively minute gradients in alongshore sediment transport may result in substantial alongshore changes (Ashton and Murray, 2006). Expected behaviour of longshore sediment transport is to smooth out undulations on a generally straight coastline as described by the diffusion equation by Pelnard-Considère (1956). Ashton et al. (2001) demonstrated that sandy shorelines become unstable when deepwater wave crests approach the coastline at high angles. These “*high angle*” result in self-organisation of coastlines into quasi-periodic, large scale features such as sand waves and cusped spits (Ashton et al., 2001).

Instabilities manifest when waves approach the coastline at angles greater than that corresponding to maximum sediment transport, typically around 45 degrees. Longshore transport decreases accordingly as the angle between waves and the shoreline progressively increases. These instabilities have been found to grow for sufficiently large wave angles of approach, eventually interacting with each other to form large scale features (Ashton et al., 2001). Ashton et al. (2001) add that when dealing with interactions between multiple features, analytically predicting instabilities becomes very difficult. Falqués et al. (2011) state that high angle wave instabilities have profound implications for one-line models whose linearised governing equation is a diffusion equation. Thevenot and Kraus (1995) add that longshore sand waves are associated with intermittent sediment supplies as well as episodic river discharges.

Falqués and Calvete (2005) identified that traditional one-line models over-predict the diffusivity coefficient by a factor of between 2.5 and infinity as they assume wave height at breaking constant and hence does not rely on coastline orientation. Given the dependence of refraction on coastline orientation, this invalidates the assumption. Ashton et al. (2001) and Falqués and Calvete (2005) implement two significant simplifications: 1) changes to the coastline occur in deep water along the same bathymetric line and 2) the modified bathymetric lines are both rectilinear and parallel. Falqués and Calvete (2005) further analysed diffusivity and instability by relaxing these simplifications. Changes in coastline position affect nearshore bathymetry however these changes extend up to a finite distance from the shoreline (Falqués and Calvete, 2005). This results in the departure from rectilinear, parallel contours to contours that are perturbed. In using one-line models, anticipating unstable behaviour is important in obtaining reliable results. The aforementioned points highlight serious phenomena that should be considered for one-line modelling.

### 2.6.2 Sand Wave Advection

Shoreline undulations are often along sandy coasts (van den Berg et al., 2012). Sand waves are wave-like forms that retain their shape while migrating alongshore, commonly formed by the periodic opening of an inlet (Thevenot and Kraus, 1995). These features emerge from interactions between morphology and hydrodynamics through sediment transport (Castelle et al., 2016). Sand waves cause temporal and spatial variations in shoreline position which often exceeds usual trends for the region, making them important regarding coastal management (van den Berg et al., 2012). van den Berg et al. (2012) argue that although this behaviour has not been observed in nature, coastlines experiencing sand waves are commonly associated with wave climates dominated by very oblique wave incidence.

Besio et al. (2004) stated that for practical purposes, modelling the migration of sand waves is important. The Pelnard-Consideré equation (equation 2.4) follows classical coastline theory and is purely diffusive. This makes it difficult to reproduce propagation behaviour (Roelvink and Reniers, 2011). Roelvink and Reniers (2011) explained that for propagation behaviour to occur, longshore transport rates must vary in the alongshore and cross shore directions. Thevenot and Kraus (1995) modified Pelnard-Consideré's equation 2.1 to obtain:

$$\frac{\partial y}{\partial t} + V \frac{\partial y}{\partial x} = \epsilon \frac{\partial^2 y}{\partial x^2} \quad (2.1)$$

where  $V$  is the propagation velocity of the feature and  $\epsilon$  is an empirical coefficient relating to the longshore transport formula and the vertical cross-shore extents. Thevenot and Kraus (1995) calculate longshore transport rates ( $Q$ ) using the CERC formula:

$$Q = Q_0 \sin(2\theta_b) \quad (2.2)$$

where  $Q_0$  is the longshore transport rate amplitude and  $\theta_b$  is the relative wave angle at breaking. This formula leads to  $\epsilon = 2Q_0/(D_c + D_b)$  where  $D_c$  is closure depth and  $D_b$  is berm height, resulting in  $\partial^2 y/\partial x^2 = (2Q_0)^{-1} \partial Q/\partial x$ . Substitution into equation 2.1 produces:

$$\frac{\partial y}{\partial t} + V \frac{\partial y}{\partial x} = \frac{1}{D_c + D_b} \frac{\partial Q}{\partial x} \quad (2.3)$$

where  $V$  is a function of hydrodynamic conditions and offshore bathymetry which vary in time. It is evident that the sand wave will migrate with the propagation velocity  $V$  while simultaneously diffusing by means of the right hand term in equation 2.1.

## Literature Review

---

Migration of sand waves could potentially have important consequences on distribution of nourishments, seeing that there are numerous possible mechanisms through which longshore transport may depend on absolute coastline position (Roelvink and Reniers, 2011). These include:

- In the presence of groins which function more effectively on sediment starved beaches as opposed to when they are engulfed in sand.
- In the presence of a beach wall or revetment on sediment starved beaches, wave energy is expended on rocks rather than sand, reducing longshore transport rates.

Figure 2.5 below graphically represents the difference between varying longshore transport rates based on cross-shore position. The upper plot shows a purely diffusive outcome when maintaining constant longshore rates along the cross-shore. The lower plot represents equation 2.1 where longshore transport is varied linearly in the cross-shore direction, producing a diffusive and migratory outcome for the same starting scenario.

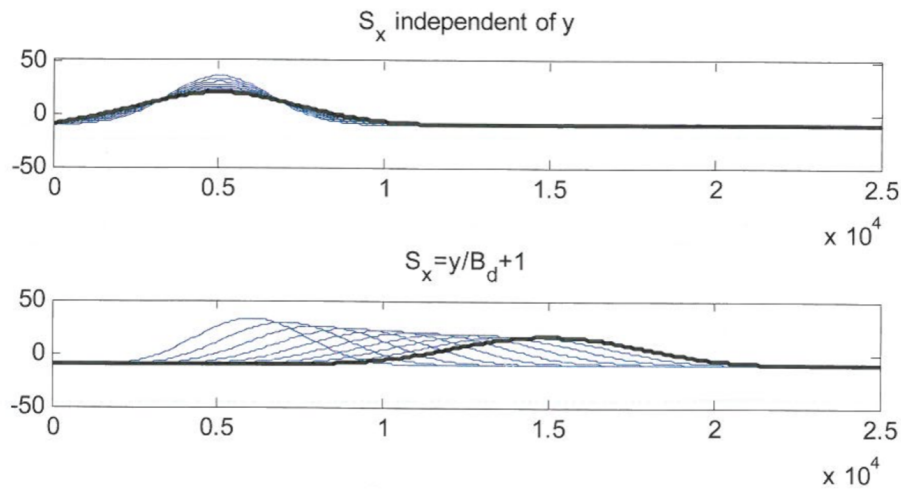


Fig. 2.5 Propagation of perturbations with cross-shore variations in longshore transport (Roelvink and Reniers, 2011).

Numerical models provide a useful framework for analysing coastline behaviour having been developed and refined over a number of decades. Hanson (1989) made widely available a model which allowed for any arbitrary combination of common coastal protection structures. Although it is a useful planning tool, modelling changes over the long term require lengthy periods of observed data that may be used to obtain a representative wave climate for the modelled region.

## 2.7 Numerical Modelling

### 2.7.1 Overview of Coastal Models

Models form an integral part in coastal studies and will increase in importance as coastal environments become more complex and rigorous (Woodroffe, 2002). Their usefulness is demonstrated by virtue of real world simplifications, allowing for control and focus on specific variables (Woodroffe, 2002). Numerical models are mathematical models that integrate a time-stepping procedure to approximate model behaviour over a specified time period. Analytical models use a sequence of equations to obtain exact answers whereas numerical models often require an iterative process to obtain an approximate solution. Pelnard-Considère (1956) first introduced the one-line theory of shoreline change. Through advances in computing and modelling techniques, 2D and 3D models were developed that investigate coastal change in greater detail (Baykal, 2014). 2D and 3D models distinguish themselves from one-line models by integrating separate models for wave transformations, sediment transport and bottom evolution. Quasi-3D models or fully 3D models incorporate vertical distributions of current velocities, increasing accuracy at a cost. Baykal (2014) states that these models are preferable to short periods, commonly less than a year.

The greatest challenge faced by model developers is balancing accuracy and computational effort (Vitousek and Barnard, 2015). In increasing model resolution (number of grid points), accuracy is proportionately increased however computational effort is also increased. Additionally, an increase in model resolution requires an appropriate time step adjustment to maintain model stability (Vitousek and Barnard, 2015). Long term modelling faces numerous challenges regarding computational effort with a number of techniques developed to overcome this obstacle. These include the “brute-force” approach where the full time history is simulated, morphologic acceleration, input reduction and model reduction (de Vriend et al., 1993).

One-line models are computationally advantageous in comparison to other models for various reasons. One-line models present reduced-physics and reduced-dimension models regarding conservation of sediment (Vitousek and Barnard, 2015). They provide a satisfactory alternative to 2D and 3D models that may be used as a tool for experimentation and extrapolation given a broad set of scenarios (Woodroffe, 2002). One-line models are less computationally intensive and require no reduction of forcing conditions (Tonnon et al., 2018). Well known examples of one-line models include GENESIS, LONGMOR and UNIBEST models.

### 2.7.2 Examples of One-line Models

#### GENESIS Model

The Generalised Model for Simulating Shoreline Change (GENESIS) was developed and funded by the US Army Corps of Engineers (USACE) in collaboration with the University of Lund around 1989. The model is currently available in two major versions; an implicit numerical solution scheme and an explicit solution scheme specifically developed by Hans Hanson and Nicholas Kraus to investigate tombolo formations (GENESIS-T). The current user interface for GENESIS is the Coastal Engineering Design and Analysis System (CEDAS). USACE recently developed the GenCade model which combined the capabilities of the GENESIS (regional-scale, engineering design-level model) and Cascade (regional-scale, planning-level model) (Frey, 2012). As with most one-line models, GENESIS uses a linear 1D grid with shoreline positions represented by scalar values at specified grid points. Longshore transport is calculated based on breaking wave parameters using the CERC formula (Thomas and Frey, 2013). Use of simplified grids are problematic given that shoreline evolution tends to emulate the original grid shape with both linear and curvilinear spaces (Thomas and Frey, 2013). One-line models therefore perform optimally over regions of straight coastlines, with GENESIS addressing this problem by integrating a regional contour. This model is useful for simulations of between 1 and 100 months over longshore distances between 1 and 100 kilometres (Thomas and Frey, 2013). It allows for an arbitrary combination of coastal structures, includes diffraction of waves around structures and allows for sand transmission at detached breakwaters. Limitations include no wave reflection from structures and no provisions for change in tidal levels (Thomas and Frey, 2013).

#### UNIBEST Model

The Uniform Beach Sediment Transport (UNIBEST) model was funded and developed by Deltares Inc. currently operating through the UNIBEST-CL+ user interface. Unlike GENESIS, UNIBEST uses a curved grid, with shoreline positions normal to the curve at each grid point. UNIBEST also includes a wave transformation model for shoaling and refraction. Unlike GenCade, this model is able to capture wave-current interactions directly. Longshore transport rates are computed through a rigorous process of calculating transport over a cross-section spanning from dune to sea (Thomas and Frey, 2013). Table 2.1 illustrates numerous significant differences between similar one-line models, highlighting the limitations and applications depending on the intended use.

Table 2.1 Notable process inclusions/exclusions of various one-line models (Thomas and Frey, 2013)

<b>Table 8. Other included processes, modules, or features in evaluated models.</b>				
	<b>GenCade</b>	<b>GENESIS</b>	<b>LITPACK</b>	<b>UNIBEST</b>
Direct provision for changing tide level	Y	Y	Y	Y
Tidal/other non-LST currents	Y	Y	Y	Y
Offshore contour	Y	Y	Y	NA
Wind-driven transport	N	N	N	Y
Regional contour	Y	Y	NA	NA

### 2.7.3 Long-term Modelling

Long-term prediction of coastal behaviour due to human interference is becoming increasingly important (de Vriend et al., 1993). Threats such as accelerated sea level rise and climate change are directly impacting sustainable development. Long-term predictions focus on coastline behaviour but does not exclude more complex regions such as estuaries and lagoons (de Vriend et al., 1993). Millions of civilians together with billions of dollars in infrastructural assets will face the threat of shoreline retreat by the year 2100 (Yuan and Cox, 2013). A severe limitation in terms of adaptive planning for climate change and sea-level rise is an inability to predict potential changes in coastal sediment processes (Yuan and Cox, 2013) however Stive et al. (2011) proposed a coastal evolution concept able to account for morphodynamic processes from the shelf to the first dune-row.

de Vriend et al. (1993) state that although certain models allow for coverage of significant time spans, long term modelling of coastal behaviour remains in it's early stages. This was partially attributed to models simulating processes at time scales which are orders of magnitude smaller than those which should be of major interest (de Vriend et al., 1993). An investigation into existing coastal models by Yuan and Cox (2013) found that existing models show adequate capabilities in predicting erosion linked to storm events. Conversely, these models fall short when simulating beach recovery and accretion over short and long time scales. Another concern is the computational power required to carry out long term simulations. de Vriend et al. (1993) further explain that should the required computing power be obtained for running a small scale model for a lengthy period, this does not necessarily represent the best approach to long-term modelling.

With greater availability of field monitoring data, data-driven modelling has been extensively developed in recent years (Alvarez and Pan, 2016). An example of this is

the Empirical Orthogonal Functions (EOF) technique that is widely used to understand shoreline trends and associated morphological change. Problems with this method arise due to the dependence on the quantity and quality of available data. Additionally, linking these models to hydrodynamics proves difficult due to the incomplete inclusion of physics (Alvarez and Pan, 2016). Recent approaches by Alvarez and Pan (2016) aimed to combine physical processes of process-based models with statistical aspects of data-driven techniques. The purpose was to reduce dependence on field data while improving accuracy of morphological predictions. Results indicated that volumetric changes may be used to calculate shoreline changes using a defined depth of closure however the model showed discrepancies towards the lateral boundaries. Overall, this method provided encouraging evidence of computationally efficient long-term models that may be developed.

## 2.8 Coastal Hydrodynamics

### 2.8.1 One-line Theory

Coastline models integrate simplicity by using one-line theory as the underlying fundamentals. One-line theory suggests that all contours lines have and retain similar shapes, moving landward and seaward in unison up to a limiting offshore depth. The contours behave as if they were a single contour line (Ergin et al., 2006). Given that this model does not account for numerous cross-shore changes and processes, a number of assumptions are necessary for stable and efficient model performance. Thomas and Frey (2013) list the basic assumptions common to all one-line models below:

- Beach profile shape remains constant throughout period.
- Specified shoreward and seaward vertical limits of the profile remain constant.
- Sediment is transported in the alongshore direction by breaking wave action and longshore currents.
- Complex nearshore circulation structures are ignored.
- There is evidence of long-term shoreline trends.
- An adequate supply of sand is available.

Pelnard-Considère (1956) derived an analytical solution for shoreline changes under numerous cases, with the major assumption being that the beach profile translates

parallel to itself up to the depth of closure (Ergin et al., 2006). Further assumptions of the Pelnard-Consideré equation are listed below, as explained by Mascarenhas et al. (1996):

- Longshore transport is proportional to wave breaking angle and is considered to be small
- Longshore transport occurs within and is bounded by the zone between the top of the berm and the depth of closure
- Beach profile is considered to be in equilibrium

Sediment motion beyond the depth of closure is considered negligible (Ergin et al., 2006). Equation 2.4 below shows Pelnard-Consideré's diffusion equation. This equation explains behaviour such as accretion and erosion adjacent to groins, development of river deltas and dispersion of nourishments in the longshore direction (Roelvink and Reniers, 2011). The equation states:

$$\frac{\partial y}{\partial t} = \frac{1}{D_c + D_b} \frac{\partial Q}{\partial x} \quad (2.4)$$

where  $t$  is time in seconds,  $D_c$  is the closure depth in metres,  $D_b$  is the berm height in metres,  $Q$  is the volumetric longshore transport rate in  $m^3/s$  while  $x$  and  $y$  represent spatial dimensions in metres.

### 2.8.2 Wave Transformation: Refraction

As waves propagate from deep to shallow or intermediate depths, their lengths, heights and directions are transformed until they break and disperse their energy. This transformation takes place through interactions between waves and the seabed through processes such as refraction, shoaling, bottom friction and wave-breaking (Bosboom and Stive, 2015). In the presence of a current, energy is not conserved due to potential transfers between waves and currents. In the absence of a current, energy is conserved and hence the wave action balance reduces to the energy balance (Bosboom and Stive, 2015).

Wave refraction is the process by which the wave ray bends towards depth contours due to a change in depth (Bosboom and Stive, 2015). This occurs due to the deeper section of the wave moving faster than the shallower section, causing the wave to bend in the process. Figure 2.6 illustrates the phenomenon for parallel depth contours.

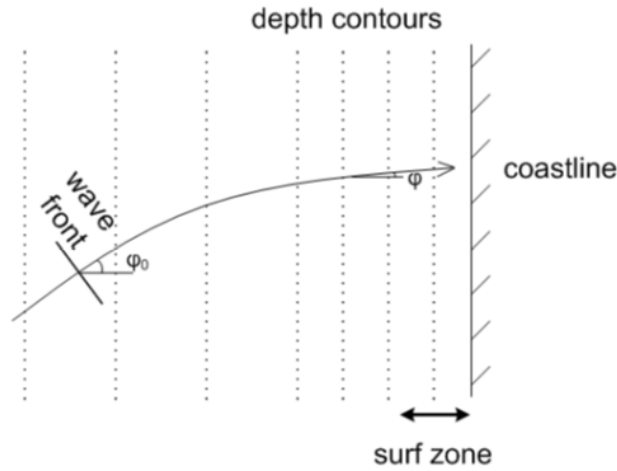


Fig. 2.6 Obliquely incident waves propagating on uniform depth contours (Bosboom and Stive, 2015)

As with light waves, directional changes in ocean waves may be calculated through proportionality of propagation speeds at two different points using Snell’s Law, represented in equation 2.5 below:

$$\frac{\sin \theta_1}{c_1} = \frac{\sin \theta_2}{c_2} \quad (2.5)$$

where the subscripts 1 and 2 denote different positions along the wave path,  $\theta$  denotes relative wave angles and  $c$  represents wave phase speed. Importantly,  $\sin \theta/c$  remains constant for deepwater and shallow or transitional depths, however equation 2.5 only holds for parallel, straight depth contours (Bosboom and Stive, 2015). Relative wave angle is a major component in calculating longshore transport rates, with wave climates comprised of primarily “*high-angle*” waves resulting in complex shoreline evolution (Ashton and Murray, 2006). Furthermore, these high wave angles may give rise to perturbations along the coastline.

### 2.8.3 Wave Transformation: Shoaling

Shoaling is the process by which waves increase in height due to a decrease in water depth. Consider a linear long-crested wave propagating in water that becomes consistently shallower. The propagation speed of the wave will be impacted by the seabed when the depth of water falls below approximately half the wavelength. A decrease in water depth proportionally decreases the wavelength and wave celerity by virtue of the dispersion relationship shown in equation 2.6 (Bosboom and Stive, 2015).

$$L = \frac{g}{2\pi} T^2 \tanh(kh) \quad (2.6)$$

where  $g$  is acceleration due to gravity,  $T$  is wave period in seconds,  $k$  is the wave number and  $h$  is the water depth in metres. A consequence of wave shoaling is non-linearity of waves in shallow water as well as wave asymmetry, influencing the onshore movement of sediment (Bosboom and Stive, 2015).

### 2.8.4 Wave Transformation: Wave Breaking

Wave breaking is the physical limit governing the extent of wave height increases due to shoaling. A wave crest experiences instability when the particle velocity exceeds the wave velocity, causing the wave to break. This angle of breaking was found to be approximately 120 degrees, as illustrated in figure 2.7 below.

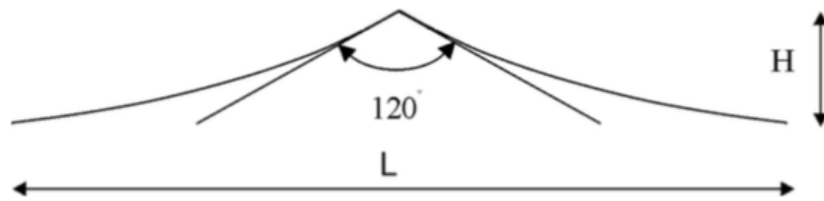


Fig. 2.7 Maximum crest angle governing wave breaking (Bosboom and Stive, 2015)

Miche (1944) derived an expression for limiting wave steepness based on Stokes wave theory, finding that when deepwater wave steepness, or the ratio between wave height and wavelength exceeded approximately 0.142, white capping occurred. This represented the breaking conditions for deep water, with the shallow water expression shown in equation 2.7 below, also referred to as the breaker index. Solitary wave theory suggests a slightly different value of 0.78. The breaker index may vary depending on coastlines under consideration however 0.78 presents a realistic value for coastlines subjected to monochromatic waves (Bosboom and Stive, 2015). Equation 2.7 states:

$$\frac{H}{L} = 0.142 \tanh(kh) \quad (2.7)$$

where  $H$  is wave height in metres,  $L$  is wavelength in metres,  $k$  is wave number and  $h$  is water depth in metres.

## 2.8.5 Longshore Sediment Transport

Longshore transport is the cumulative migration of beach and nearshore sediment parallel to the shoreline induced by tides, wind, waves and currents (Seymour, 2005). These driving forces commonly result in a continuous movement of sediment in both suspension or bed load flows. Total longshore sediment transport (LST) rates represent an important quantity in coastal engineering, aiding in undertakings such as infilling of dredged channels, dispersion of nourishment schemes and morphodynamic responses of coastlines to engineering projects (Bayram et al., 2007).

The CERC formula is arguably the most widely used longshore transport formula, developed by USACE (Smith et al., 2003). The fundamental basis of the equation is that longshore transport rates are proportional to wave power  $P$  per unit length of beach, with the equation calibrated using field data from beaches (van Rijn, 2014). Equation 2.8 shows the CERC equation. van Rijn (2014) argued that this equation only used wave characteristics as the input for calculating transport rates, inferring that more realistic values may be obtained by accounting for sediment size and beach profile. Smith et al. (2003) shared a similar notion, adding that calibration of the  $K$  coefficient was difficult and that this formula commonly under-predicted transport rates during storms.

$$Q = \frac{K}{16\sqrt{\gamma_b}} \rho_w g^{\frac{3}{2}} H_b^{\frac{5}{2}} \sin(2\theta_b) \quad (2.8)$$

Kamphuis (1991) developed his own formula, built on the CERC formula by including a number of parameters. Kamphuis (1991) formulated a relationship for estimating longshore transport rates primarily based on physical laboratory experiments, represented in equation 2.9 (Bayram et al., 2007). The expression related sediment transport to wave steepness, beach slope, relative grain size and breaking wave angle (Kamphuis, 1991). This equation omits any integration of wind-induced currents, which were found to increase longshore transport rates by up to a factor of 100 (Bayram et al., 2007). Bayram et al. (2007) also added that although there was no inclusion of wind or tide driven currents, inclusion of physical factors such as sediment diameter and wave characteristics were highly significant.

$$Q = K \rho_w \left(\frac{g}{2\pi}\right)^{1.25} H_b^2 T^{1.5} m^{0.75} D_{50}^{-0.25} \sin^{0.6}(2\theta_b) \quad (2.9)$$

where  $K$  is a calibration coefficient,  $\rho_w$  is seawater density,  $H$  is wave height in metres,  $T$  is wave period in seconds,  $m$  is beach slope,  $D_{50}$  is median sediment diameter in metres and  $\theta_b$  is relative wave angle. The subscript  $b$  denotes breaking conditions.

### 2.8.6 Boundary Conditions

Boundary conditions act to restrict or free longshore transport of sand at the lateral boundaries of a project region (Young et al., 1995). They are generally separated into two categories; open and closed boundary conditions. Closed boundaries represent physical boundaries that exist in reality such as land or coastal boundaries. Open boundaries are artificial, typically used to define model domains (Shabangu, 2015). Two primary types of boundary conditions are recognised by Hanson (1989), namely pinned and gated boundary conditions. Hanson (1989) emphasise the importance of boundary conditions on the calculation of coastline positions, with the entire grid region depending on these constraints. Long headlands, long jetties and inlets make for ideal lateral restraints, given that they are terminal points of littoral cells. Additionally, presence of coastal structures such as groins and seawalls behave similarly to boundary conditions, inhibiting longshore transport and constraining shoreline movement. They may also introduce a non-steady constraint potentially resulting in an eventual bypass. These features may have significant influences on coastline evolution and must be accounted for (Hanson, 1989).

A pinned-beach boundary represents a point that exhibited no observable change in historical position. This is achieved by enforcing a zero sediment transport gradient. In mathematics, this is referred to as a Neumann boundary condition. This condition assumes no restriction of transport across the boundary and may represent a seawall or an open, natural beach (Young et al., 1995). Equation 2.10 below represents the pinned-beach boundary, and given that  $\Delta Q = 0$ , it must follow that  $\Delta y = 0$  from the equation below. Recommendations are made to place a pinned-beach boundary far away from the project area to prevent interactions between the boundary and the project area (Young et al., 1995).

$$Q_{n+1} = Q_n \quad (2.10)$$

A gated boundary represents a point where longshore transport of sand is either partially or completely restricted (Young et al., 1995). In reality, this may take the form of a man-made structure such as a groin or jetty, and in natural cases, a headland that forms the end of a natural littoral cell (Young et al., 1995). The effects of a groin, headland or similar feature is estimated based on the permeability and amount of sediment allowed to pass around the structure. Additionally, considerations must be given to the amount of sand passing through the grid (Hanson, 1989). An example of one-way sediment movement is the presence of a jetty next to a deep inlet, where

sand would occasionally be allowed to flow into the channel during periods of high waves. The reverse would not be possible. The Dirichlet boundary condition is one which specifies the value at the boundary of the domain. It is also possible to use a combination of Dirichlet and Neumann boundaries.

Another form of boundary condition is sand-bypassing or sand-transmission. Bypassing occurs when sand moves around the seaward end of the structure whereas transmission is migration of sediment over the structure (Young et al., 1995). Equation 2.11 governs the extent of bypassing, calculated using the depth at the tip of the structure ( $D_G$ ) and the depth of active longshore transport ( $D_{LT}$ ). It is clear that should the  $D_G$  equal or exceed  $D_{LT}$ , bypassed volumes of sand reduces to 0. This value will vary with wave conditions given the dependance of  $D_{LT}$  on wave conditions, shown in equation 2.12 (Young et al., 1995). Depth at the tip of the groin is simply calculated using the equilibrium profile function. The equations state:

$$BYP = 1 - \frac{D_G}{D_{LT}} \quad (2.11)$$

$$D_{LT} = \frac{1.27}{\gamma_b} H_b \quad (2.12)$$

where  $\gamma_b$  is the breaker index and  $H_b$  is breaking wave height in metres. Boundary conditions play significant roles in model stability. Specification of boundary conditions are not based on equations being modelled but rather on the nature of the model domain or sundries of the domain (Shabangu, 2015). It is difficult to specify a set of boundary conditions that will guarantee the existence of a stable, unique solution. With some over-specification, the discrete approximation may be somewhat stable however the solution may not be continuous while the interior solution may speedily obtain contaminations in the form of errors (Marchesiello et al., 2001).

Open boundary conditions (OBCs) are a necessity in the case of uncertain physical principles as the foundation. Røed and Cooper (1986) suggested that open boundaries should not retain perturbations within the computational domain and should not interfere with the internal model solution. Marchesiello et al. (2001) argued that physically important external information should be occasionally conveyed inward, with omission of this leading to under-specification of the system.

### 2.8.7 Equilibrium Beach Profile

Interpretation of nearshore processes and rational engineering designs rely on a quantitative understanding of equilibrium beach profiles (Dean, 1991). Well-known features associated with equilibrium profiles are listed below (Dean, 1991);

- Commonly have concave upward profiles.
- Milder and steeper slopes are linked to smaller and larger sediment diameters respectively.
- The beach face is approximately planar.

Several attempts were made to characterise equilibrium beach profiles, with Bruun (1954) following the simple relationships shown in equation 2.13. The study undertaken by Bruun (1954) involved analysis of beach profiles from the Danish North Sea coast and from Mission Bay, California (Dean, 1991). In accordance with Dean (1991), Bruun (1954) discovered that beaches commonly presented concave upward shapes and followed the two-thirds power law.

$$h = Ax^{\frac{2}{3}} \quad (2.13)$$

where  $h$  is the calculated depth in metres,  $A$  is a dimensionless profile shape parameter and  $x$  is distance seaward measured from the shoreline in metres. Moore (1982) showed that the scale parameter  $A$  in equation 2.13 has a dependence on grain size. A design curve by Moore (1982) was approximated using a series of line equations as a function of the median nearshore beach grain size, represented by equations 2.14 to 2.17 below (Hanson, 1989).

$$A = 0.41(D_{50})^{0.94} \quad , \quad D_{50} < 0.4 \quad (2.14)$$

$$A = 0.23(D_{50})^{0.32} \quad , \quad 0.4 \leq D_{50} < 10.0 \quad (2.15)$$

$$A = 0.23(D_{50})^{0.28} \quad , \quad 10.0 \leq D_{50} < 40.0 \quad (2.16)$$

$$A = 0.46(D_{50})^{0.11} \quad , \quad 40.0 \leq D_{50} \quad (2.17)$$

where  $D_{50}$  is the median nearshore beach grain size in millimetres.

Given the assumption that beach profiles remain constant and translate in one-line models, it may appear that equilibrium profiles are of minimal significance. When

considering the Kamphuis (1991) equation which includes beach slope when calculating longshore sediment transport, the significance is highlighted. Corbella and Stretch (2012*b*) found that some South African beaches required approximately 2 years to recover from severe erosive storm events and return to pre-storm state. This indicates that these beaches experience cyclic offshore and onshore sediment migration.

## 2.9 Statistically Modelled Wave Climates

Long term records containing important information on potential wave states, storm inter-arrival times and their temporal grouping are fundamental in accurately quantifying coastal vulnerability (Pringle et al., 2015). Accurate quantitative prediction of beach erosion hazards within a probabilistic framework are being increasingly sought out (Callaghan et al., 2008). Prior to the availability of remote sensing wave data, limited real time wave data was widely available with most buoy locations being inappropriate due to their locations (Lefèvre and Aouf, 2012). Pringle et al. (2015) adds that wave data is limited to observations from wave buoys, ships and satellites that primarily focus on the Northern Hemisphere. Furthermore, wave buoys are region specific and only provide data over limited periods of 30-40 years. Increased availability of satellite wind and wave data in recent years has seen an increase in operational assimilation of data for wave prediction (Lefèvre and Aouf, 2012). Quantity and quality of wave data restrict their application, hence Pringle et al. (2015) suggest an approach to simulate long wave records that may supplement and extend current records.

Previous approaches used a benchmark event to assess beach erosion. This approach provided limited information on return periods of events and failed to include confidence level estimations (Callaghan et al., 2008). This method also fails to merge independent meteorological events into a single beach erosion event. Callaghan et al. (2008) explain that two equal magnitude events in quick succession will result in more severe beach erosion as opposed to the same storms further apart, allowing for the beach to recover from the first event. Callaghan et al. (2008) proposed four alternative parameters methods that could replace the benchmark method, listed below;

- Fitting distributions directly to erosion measurements
- Structural variable method (SVM)
- Joint probability method by integration
- Full temporal simulation

Statistical models are subject to limitations, with Corbella and Stretch (2012*c*) identifying that their copula model has no links to physical meteorological forcing. This made identification of independent events and delineation of wave sources difficult. Evaluation of dependance between variables may be erroneous, with Callaghan et al. (2008) finding no interrelationship between wave direction and height. Pringle et al. (2015) add that weather systems driving wave development link different characteristics to wave climate variables, implying interdependence of wave height, direction and period. Finally, many statistical models do not include physical mechanisms of generation for extreme waves of engineering concern (Muir & El-Shaarawi, 1986).

### 2.9.1 Stochastically Simulated Regional Wave Climates

Pringle et al. (2015) developed a method that simulates regional wave climates based on the occurrence of atmospheric circulation patterns. This is done by exploiting strong links between synoptic scale meteorology and regional wave climates. The method provides a physically meaningful way to describe changes in wave state and to identify independent storm events. This mixed approach presents a new method for modelling regional wave climates based on interrelationships between variables such as wave height, direction and period. Two approaches were considered; simulation of entire climates and simulation of individual storm events with different inter-arrival times and durations. The major difference between approaches is that storm simulation requires the definition of a wave height threshold that signifies the start and end of a storm. Simulation of the full climate reproduces natural changes in wave state between extreme events.

The general approach involves a fuzzy rule based algorithm that was applied to graded anomalies at a 6-hour temporal resolution. This delineated circulation patterns that are commonly associated with wave development, with a transition matrix used to calculate migration between classes. Archimedian copulas serve to evaluate dependance structures within circulation patterns, with distributions of wave climate variables also calculated. A linear combination of objective functions were used to locate the optimal set of circulation pattern classes by using a simulated annealing optimisation algorithm.

Wave climate simulation is difficult given that modelling involves a multivariate dependance structure. High dimensional environments make it difficult to derive relationships between variables therefore circulation patterns provide useful insight into these complex relationships, simplifying the modelling process. Pringle et al. (2015) explain that a temporal sequence of wave climate variables may have strong

## Literature Review

dependance on the occurrence of a circulation pattern, therefore that pattern is likely to dictate changes in wave climate. Additionally, circulation patters may be associated with calm periods or extreme events, hence natural transitions can provide a physically meaningful temporal sequence of wave climate variables.

Transitions between circulation patterns was done using a Markov Chain, with the sequence being 100 years long at a 6-hour temporal resolution. This process was carried out 101 times to obtain a suitable sample size and to account for any potential variations in scenarios. Fundamental properties of wave mechanics were integrated such as the temporal dependance of wave heights e.g. large waves are likely to follow large waves and vice versa. Figure 2.8 below shows selected observed and simulated wave climates linked to the relevant circulation pattern. Pringle et al. (2015) highlight the significance of demonstrating that the method is able to correctly reproduce wave direction statistics. From figure 2.8, it is evident that the simulated waves correctly reproduce wave direction data for the given circulation pattern. Furthermore, it may be seen that distributions of high and low pressure zones may be linked to wave rose shapes.

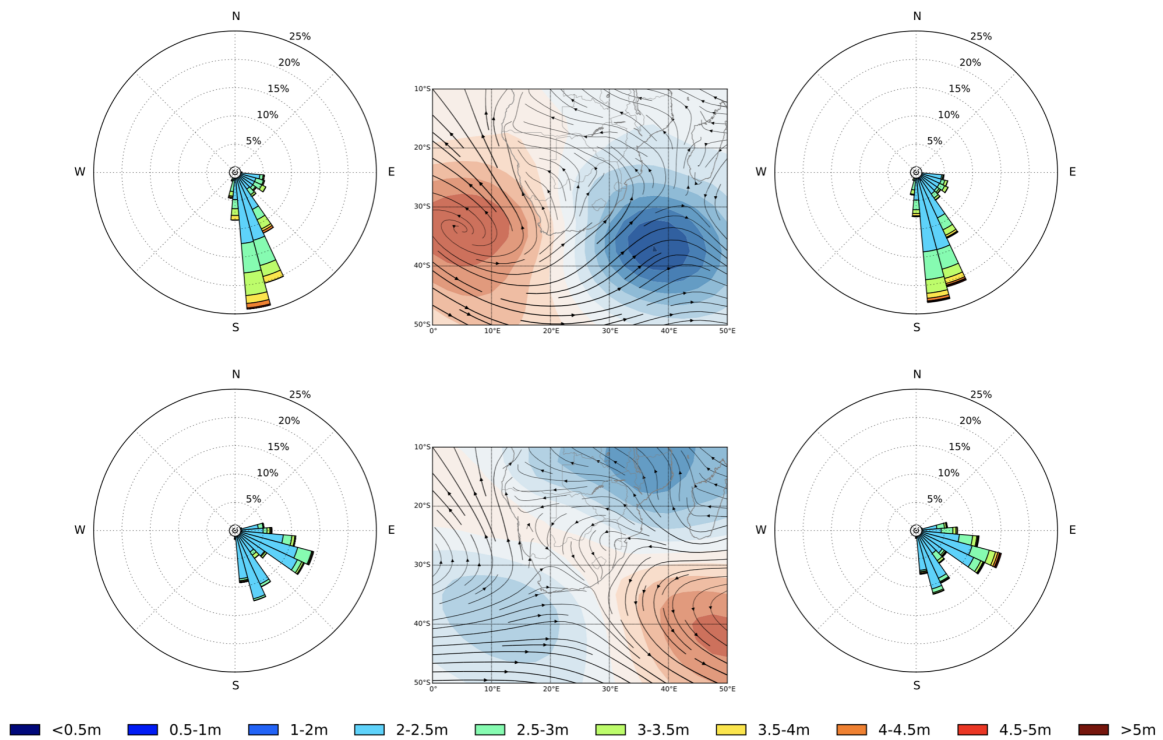


Fig. 2.8 Observed (*left*) and simulated (*right*) wave roses for the given circulation pattern (*middle*). Line widths indicate relative magnitudes of wind velocity. Significant wave heights are given in the colour legend below (Pringle, 2015).

### 2.10 Potential Inclusion of Climate Change Phenomena

In order to secure the future of our society, the influence of global climate change resulting from greenhouse gasses will require impact assessment, mitigation and adaptation (Mori et al., 2010). Storm surges and ocean waves are expected to experience changes in characteristics, presenting a dynamic phenomena for coastal disaster prevention (Mori et al., 2010). Significant wave height increases have been recorded off the Irish and Canadian coastlines however the Scandinavian coastline reflected less significant changes Mori et al. (2010). A study by Grabemann and Weisse (2008) predicted wind speed and significant wave height increases in the North Sea based on anthropogenic emission activities. Findings expect wind speeds and significant wave heights to increase by 7% and 18% respectively within the next 30 years. Storm intensities are also predicted to increase substantially, with Knutson et al. (2010) anticipating up to an 11% increase in tropical cyclone storm intensity by the year 2100.

Pringle et al. (2015) formulated a method to improve statistical wave modelling by identifying features within atmospheric circulation patterns that drive extreme wave events. The method classifies circulation patterns into classes based on strength and size and associates certain wave conditions to the class. In using this technique, changes in atmospheric conditions may be reflected in simulated wave climates which may be used as a data source for numerous coastal models. Prevalence of more extreme circulation patterns will increase peak significant wave heights for a certain simulation period. This may help with future planning of coastal defence schemes, such as coastal structure construction and nourishment schemes.

Sea-level record and climate models have suggested accelerated sea level rise since the mid 1950's (Church and White, 2006). Although no substantial acceleration has been detected in the 20th century, current rates of acceleration predict a  $310 \pm 30$  mm increase in sea levels between 1990 and 2100 (Church and White, 2006). Consequences such as flooding, shoreline retreat and infrastructure damage will occur as a result of changes in frequency and intensity of extreme sea-level events (Church and McInnes, 2006). In accounting for sea level rise in simulations over the long term, improvements may be made in terms of required sediment budgets within coastal defence schemes.

The combined potential of storm surges and sea level rise pose major risks to coastal cities worldwide. These change are expected to present a major challenge to coastal cities this century, with millions of civilians and thousands of billions of USD in assets exposed to this risk (Hallegatte et al., 2010). Planning and mitigation strategies will

be at the forefront of coastal cities in preserving assets and minimising damage costs, highlighting the usefulness of a long term model able to account for these effects.

### 2.11 Summary

Coastal erosion is of significant concern to coastal settlements worldwide. Major causes behind erosion have been identified as sea level rise, meteorological changes to wave climates and reductions in sediment supplies. Rapid urbanisation along coastlines has increased anthropogenic influences on coastal environments. This population expansion has resulted in higher demand for resources necessary for the development of coastal cities. The need for building materials and necessities such as sand and water respectively have warranted activities such as sand mining and damming along major rivers. Additionally, following construction and development of infrastructure, coastal cities are implementing coastal defence schemes to protect valuable assets from impacts of climate change and sea level rise. The cumulative result of these activities is the loss of beach width due to negative influences on coastal sediment sources. Rivers subject to mining and damming have reflected significantly reduced sediment yields to coastlines, with coastal structures such as harbours and breakwaters inhibiting natural littoral drift processes. Reduction in beach widths together with climate change and sea level rise leaves coastal regions vulnerable to saltwater intrusion and storm surges. Additionally, climate change is expected to increase frequency and severity of storms over the next 100 years. Long term planning is essential in preventing damage to infrastructure, however no models are able to predict changes in sediment transport due to changes in climate and sea levels.

Coastal models exist over a range of complexity and application. The complex “process based” models are accurate in predicting coastline changes over the short to medium term however these models are computationally intensive. One-line models present a simple, efficient method to speedily predict shoreline changes however this method does not integrate mechanics integrated into process based models. One-line models operate on a number of assumptions to simplify reality into a representative framework. One-line theory forms the basis of these models, assuming that depth contours remain parallel, with coastal profiles retaining their shape throughout the simulation period. For model stability, user defined boundary conditions play a substantial role in producing reliable estimates. Furthermore, wave climates dominated by high angle waves govern the formation of large scale coastline features, which is

significant in long term modelling. One-line models are advantageous as they are all to run the full wave climate within a simulation.

Long term simulations rely on lengthy records of wave data which is often unavailable or unreliable. Statistical models aim to improve upon these records by filling in periods lacking information and even extend them. Stochastically simulated regional wave climates conditioned on synoptic scale meteorology serve as a statistical method for simulating long term wave records based on the prevalence of particular atmospheric patterns. The method identifies the circulation patterns that drive extreme wave events, therefore providing a method to integrate climate change effects into simulated wave records. This is significant as coastline models integrating simulated wave climates will aid in coastal planning over the long term, potentially preventing severe damage to infrastructure and assets.



# Chapter 3

## Case Study: Durban

### 3.1 Site Location

The city of Durban, South Africa, situated on the east coast in the KwaZulu-Natal province. The stretch of coastline between the uMngeni River mouth and the uMhlanga Lighthouse along the Durban coastline served as the site for this case study. Figure 3.1 depicts the study region where the model domain is denoted by markers with associated coordinates. This coastline has a general clockwise orientation of 22.44 degrees relative to North with a median sediment diameter ( $D_{50}$ ) of approximately 1.17 millimetres.

### 3.2 Selection Criteria

The east coast of South Africa has experienced numerous coastal developments in recent years (Corbella and Stretch, 2012*a*). The wave climate in this region is described as being highly energetic (Mather et al., 2009). The stretch of coastline between the uMngeni River mouth and the uMhlanga Lighthouse presents a complex and dynamic environment with numerous sediment sources as well as consistent erosion in recent years. According to annual beach surveys by the eThekweni Municipality (Durban's local authority), the region experienced a net sand loss of 270,000  $m^3$  between 2011 and 2017. Furthermore, Corbella and Stretch (2012*b*) analysed comprehensive records of beach profile data from 1973, concluding that Durban's beaches have been eroding. The study region obtains sediment from two major sources: the uMngeni River and littoral drift. Given the periodic nature of river sediment transactions and the high variability of sand-bypassing schemes, this site is optimal for exploring the impacts of varied sediment supply on coastline evolution.

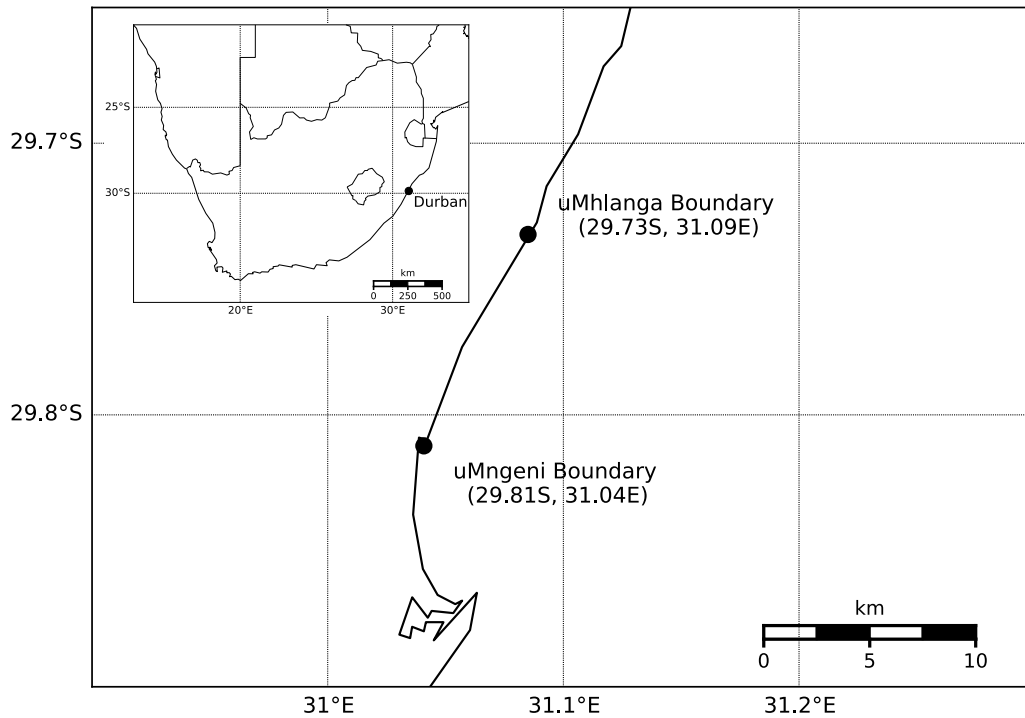


Fig. 3.1 Locality plot of study region in national and local context.

### 3.3 Data For Study

#### 3.3.1 Coastline Coordinates

Coastline coordinates were obtained using data from eThekweni Municipality’s beach monitoring program. Surveyed coordinates integrating latitude, longitude and elevation were used to obtain the land levelling datum (LLD) contour by means of linear interpolation. Beach profile data was used to estimate beach heights and widths and. Figure 3.2 features an example of a cross-shore profile taken from the survey. Technical information for the survey is provided in appendix A.

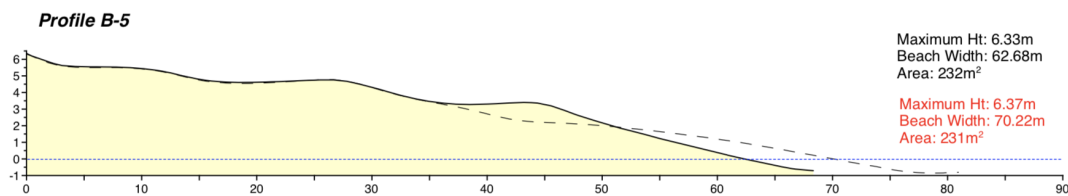


Fig. 3.2 Surveyed cross-shore profile from study region. Dashed line and red text indicate measurements from previous survey. Solid line and black text refer to current surveyed data. Beach heights are measured from LLD (eThekweni Municipality, 2017)

### 3.3.2 Wave Climate: Simulated Data

Wave data was obtained from the statistical method for generating stochastically simulated regional wave climates conditioned on synoptic scale meteorology by Pringle et al. (2015). Long-term wave records spanning 100-year periods at 6-hour temporal resolutions were used for numerical simulations. The wave climates provide significant wave height ( $H_s$ ), peak period ( $T_p$ ), and wave direction ( $\theta$ ) at the aforementioned time interval. Wave sequences were simulated 101 times to account for any variations in wave scenarios. These wave climates served as a further check for model calibration. Seasonal variations in wave behaviour plays an important role in shaping the coastline. Table 3.1 below defines seasonal occurrences with a year in South Africa. See appendix B for more information.

Table 3.1 Annual seasonal occurrences in South Africa (After Pringle, 2015)

Season	Months
Summer	January - March
Autumn	April - June
Winter	July - September
Spring	October - December

Furthermore, selected seasonal wave roses are presented in figure 3.3, showing variations in wave climates accordingly.

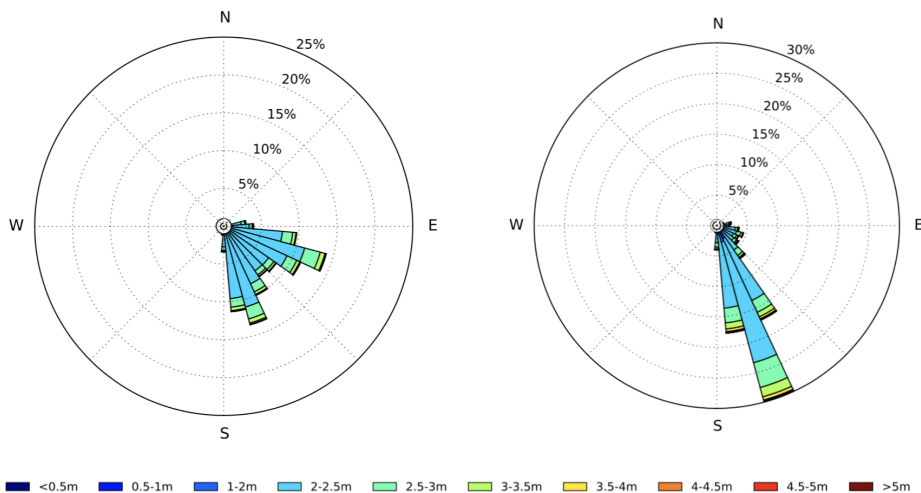


Fig. 3.3 Simulated data wave roses for summer (*left*) and winter (*right*). The legend indicates significant wave heights (Pringle, 2015)

### 3.3.3 Wave Climate: Observed Data

Waverider buoys along the KwaZulu-Natal coastline at Richards Bay and Durban provide relatively long data sets of 18 years (Corbella and Stretch, 2012c). The observed wave records span from 1992 to 2009 however periods do exist where either significant wave height, direction or period is unavailable. Wave characteristics are generally recorded at 30 minute intervals. Corbella and Stretch (2012c) found a strong correlation between wave data from both sites, making it possible to supplement Durban wave data with Richards Bay data during periods of missed observations. This data was also used by Pringle et al. (2015) in verifying the accuracy of simulated wave climates. Figure 3.4 shows seasonal wave roses for the KwaZulu-Natal wave climate, generally indicating a strong SSE wave incidence. See appendix B for more details.

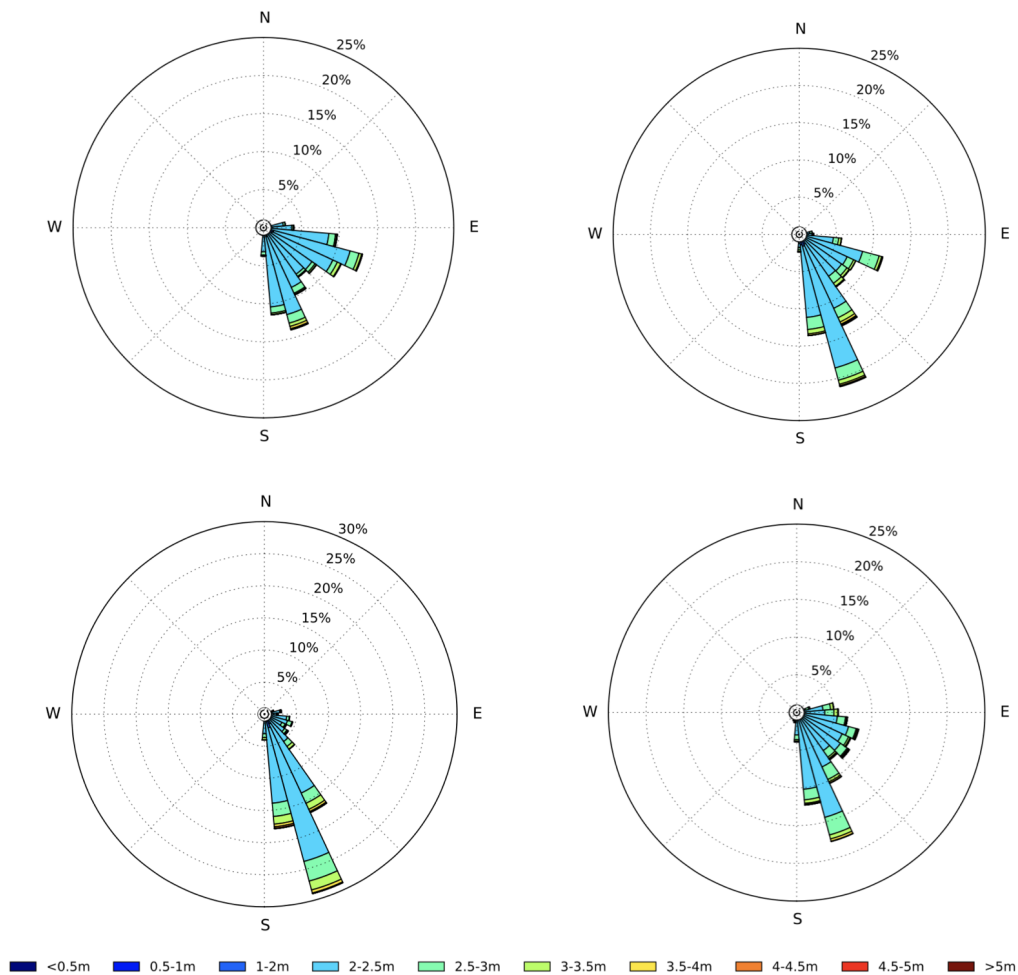


Fig. 3.4 Observed summer (*upper left*), autumn (*upper right*), winter (*lower left*) and spring (*lower right*) wave roses for the East Coast. The legend indicates significant wave heights (Pringle, 2015)

### 3.3.4 River Sediment Discharges

The uMgeni River represents a major source of sediment for the study region. This river integrates five dams along its course together with a recent emergence of sand mining. Figure 3.5 shows the uMgeni River catchment together with the dam locations along its course. Theron et al. (2008) estimated annual sediment yields for this river using the ACRU model which served as an estimate for annual fluvial discharge ranges. Table 3.2 shows sand yields from the uMgeni River under various scenarios. Theron et al. (2008) assume 10% and 15% sand contents of the total sediment yield. This assumption is based on previous literature relating to rivers in KwaZulu-Natal (eg. Cooper, 1993) which state that sand loads are approximately between 5% and 15%. Table 3.2 shows a substantial reduction between pre-dam and net yield volumes due to anthropogenic influences.



Fig. 3.5 Map of the uMgeni River catchment (der Zel, 1975)

Table 3.2 Annual sand yields in the uMgeni River (Theron et al., 2008)

Scenario	Mean annual volume ( $m^3$ )	
	10% Sand	15% Sand
Pre-dam	112594	168892
Post-dam	25271	37907
Sand Mining	13920	13920
Net Yield	11351	23987

### 3.3.5 Longshore Transport Volumes

Littoral drift constitutes the second major source of sediment for the site under investigation. Littoral drift processes cause natural migration of sediment due to wave action. Given the presence of the Durban harbour entrance, sand-bypassing and nourishment schemes are necessary to preserve beaches northward of the structure. Nourishment is achieved by pumping sand from the sand trap along the beaches of the Durban Bight (Schoonees, 2000).

Corbella and Stretch (2012*b*) analysed 37 years of beach profile data along the east coast of South Africa to estimate recovery times following the occurrence of a storm. The sand-bypass scheme affecting the Durban bight allowed for this region to be studied in terms of the sediment balance by analysing profile changes together with bypassed volumes. Figure 3.6 shows annual sediment losses at a particular observation point in the Durban Bight calculated by Corbella and Stretch (2012*b*). Furthermore, the sediment balance accounts for pumped sand from the bypass scheme, hence loss of sediment is still possible even with increases in profile volume. Schoonees (2000) states that there is arguably no major net cross-shore loss of sand in the long term along this region. The Bight loss rate was therefore used for this investigation as the time period correlated with observed wave data mentioned in section 3.3.3. These values were also used in calibrating the longshore sediment transport formula, discussed in chapter 4.

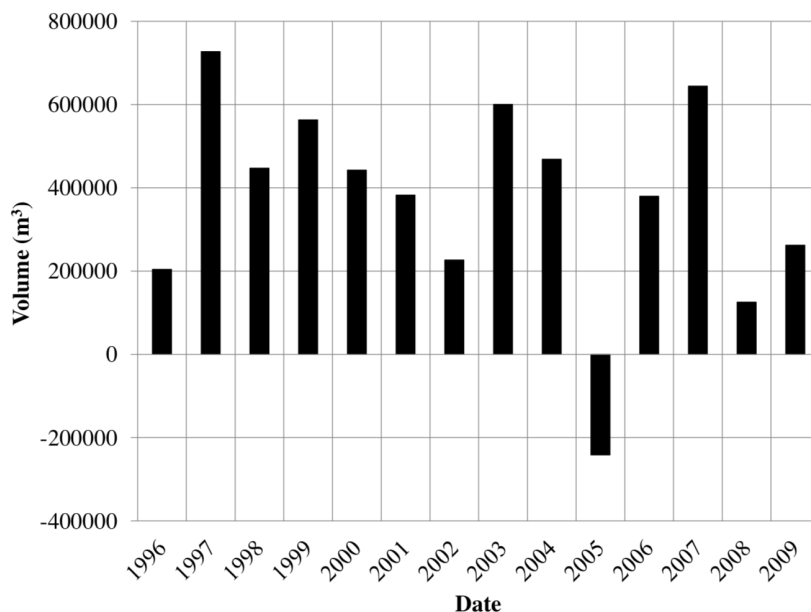


Fig. 3.6 Annual sediment losses for the Durban Bight accounting for sediment volumes contributed by the bypass scheme (Corbella and Stretch, 2012*b*)

# Chapter 4

## Model Development

### 4.1 Model Overview

An overview of the one-line model is given in this section. The model was programmed using Python. A brief description is provided regarding model structure, indicating the sequence in which calculations are done. A flow chart of the model structure is presented in section 4.2. Details of the numerics are discussed from section 4.5 onward.

The one-line model requires a number of data inputs to function. These include coastline coordinates, wave data and the simulation period. Numerous processes are carried out to initialise the model before any simulations are done. Importing and storage of wave data, grid space resolution and simulation of storm sequences for river inputs are a few examples. These preliminary processes are detailed in section 4.4.

Following resolution of the grid space and importing of wave data, a time-step loop is initiated. Interpolated coordinates are used to calculate relative wave angles using shore normals and directional wave data. An iterative loop is thereafter initiated to transform waves from deepwater to breaking conditions due to shoaling and refraction. The transformed wave conditions are used to compute longshore sediment transport rates for each grid cell. Boundary conditions are applied to the grid space. Internal checks verify whether river sediment should be introduced to the grid space. Computed longshore rates are used to calculate coastal changes using the diffusion equation. Where necessary, nourishments are introduced and advected. The sum of coastline changes from river input and longshore transport are applied to the latest iterated coastline. This looped process is repeated until the specified analysis period is completed.

The GENESIS model served as a template for model development with omission of certain aspects such as wave diffraction. Occasionally, equations used in GENESIS have been substituted by others following review of literature. An example of this

## Model Development

---

is substitution of the CERC formula with the Kamphuis (1991) formula to calculate longshore transport rates. Comparison of numerous longshore transport equations by Schoonees and Theron (1996) found that the Kamphuis equation yielded the smallest relative standard error. Additionally, when compared to alternate longshore transport prediction methods, the Kamphuis formula proved to be relatively consistent and did not yield excessive outliers (Schoonees and Theron, 1996).

### 4.2 General Model Structure

Figure 4.1 shows the coastline model breakdown with individual input files. The model consisted of an input file PARAMS which housed all constants and general operating conditions. The values were imported by the main model structure MODEL which used INITIALISE to set up all grids, import wave data and generate storm sequences. The model then used the BATHY and SHORELINE files to carry out all coastline calculations such as wave transformations and longshore sediment transport rates. Included in these files are any necessary checks to ensure model stability. Finally, the OUTPUT file produced relevant plots and beach volume data for analysis.

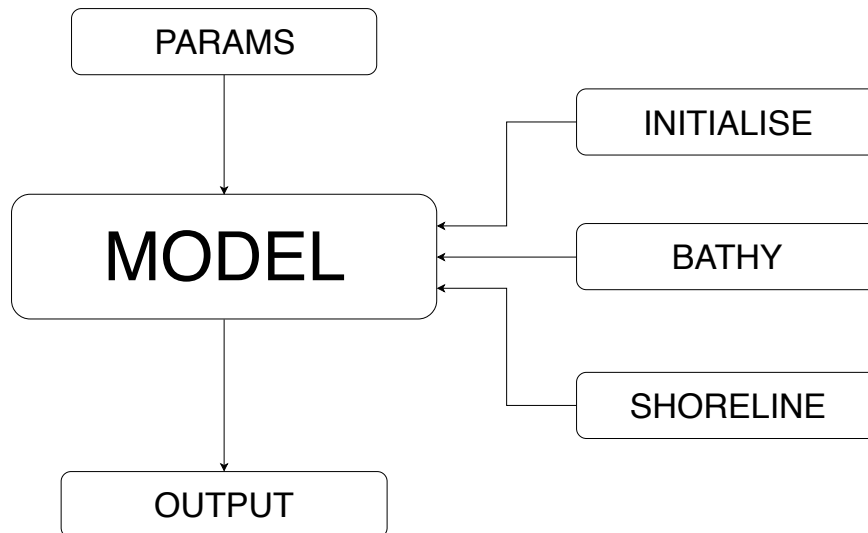


Fig. 4.1 Schematic of general coastline model structure.

### 4.3 Internal Model Structure

Figure 4.2 below illustrates the internal model structure described in section 4.1. Outlines signify different file inputs, where the main model is outlined using the dotted line. The nourishment grid uses the same numerics as the coastline for diffusion, hence the parallel flow of arrows. A legend is provided in the lower left corner.

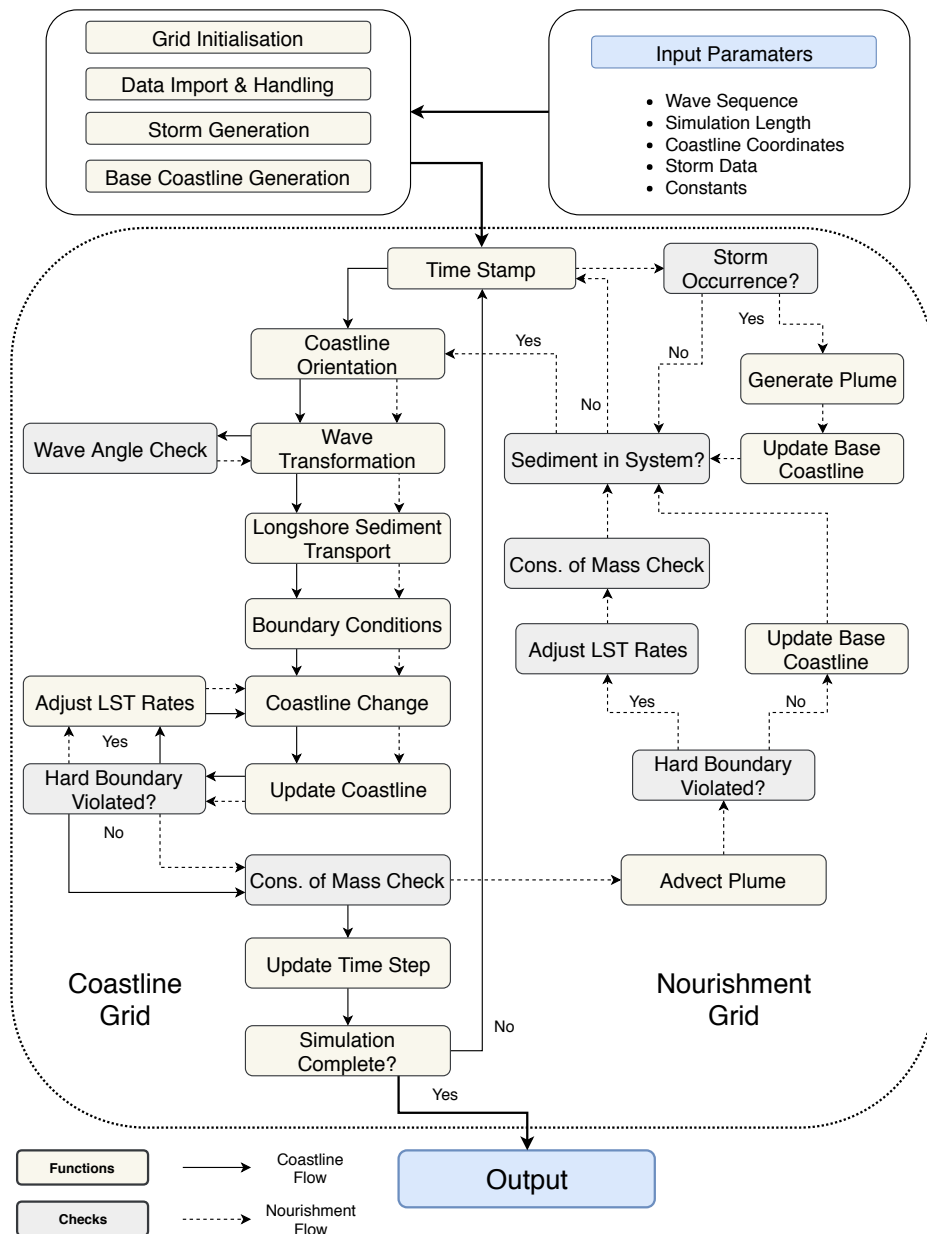


Fig. 4.2 Flow chart detailing the internal model structure.

## 4.4 Initialisation Process

### 4.4.1 Grid Resolution

The model domain uses a right-hand Cartesian coordinate system, similar to that employed by GENESIS. The system is drawn with the x-axis parallel to the shoreline with the y-axis defining the offshore direction. Offshore distances are adjusted such that only positive values are dealt with. This has no effect on the end result of the simulation as all shifts are relative to the initial shoreline.

User supplied coordinates are resolved into an equally spaced grid along the x-axis using an interpolation algorithm. The spacing was made sufficiently small in order to preserve coastline shape while including small scale features. Interpolated grid points represent scalar quantities that were subject to change with sediment transport points positioned centrally between grid points. Figure 4.3 illustrates the grid setup used by the GENESIS model, showing the division of the coastline into individual, equally spaced cells. A similar grid setup was used within this model. Calculated changes in coastline positions due to longshore transport are assumed to occur along a fixed vertical axis, intersecting each grid point along the domain. This is discussed in detail further on in this chapter.

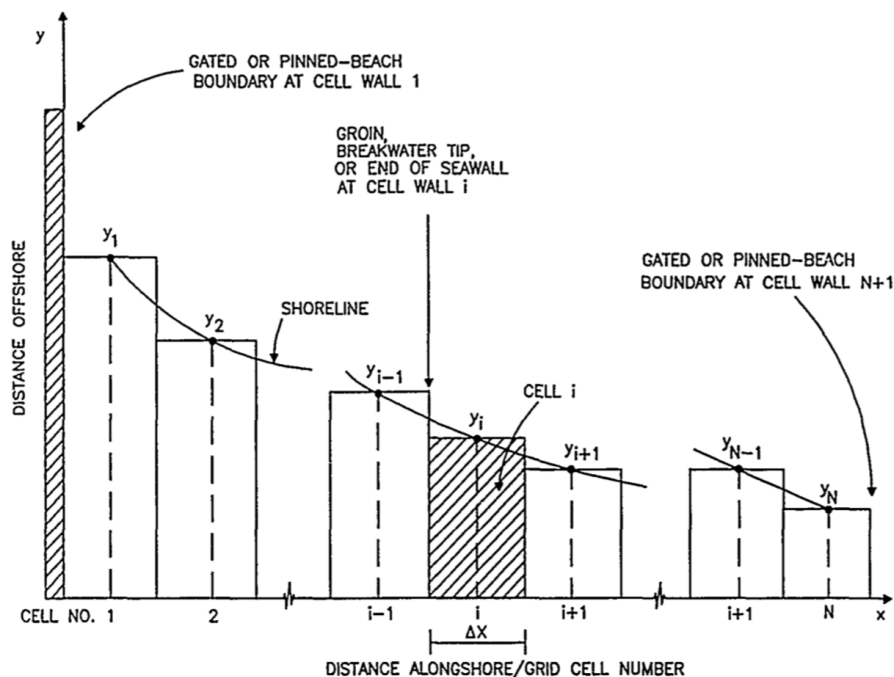


Fig. 4.3 Coastline grid setup used in GENESIS (Hanson, 1989)

### 4.4.2 Data Import & Handling

Simulated wave sequences serve as the input source of wave data. These simulated wave climates have temporal resolutions of 6 hours which is substantially longer than the time-step used in the model. The user specified sequence is imported into the model where it is managed by an interpolation algorithm. This algorithm linearly interpolates significant wave height and wave period to the specified model time-step. Wave direction is assumed to remain constant over the 6-hour period.

This data is thereafter stored into a dictionary with the corresponding time stamp. Figure 4.4 shows an example of interpolated data between two 6-hour data points stored in the form of a Python dictionary. The first value is the date and time of the wave occurrence, tuple refers to the type of method used to store the data and the number 3 refers to the length of the tuple or list. The list in the last segment stores the three important wave characteristics in the following order; significant wave height ( $H_s$ ) in metres, peak wave period ( $T_p$ ) in seconds and wave direction ( $\theta$ ) in degrees. Wave direction is measured clockwise from North.

1990-01-01 00:00:00	tuple	3	(1.93507136713, 12.08550231186013, 100.10588843171699)
1990-01-01 01:00:00	tuple	3	(1.9006523848616665, 12.584959320963641, 100.10588843171699)
1990-01-01 02:00:00	tuple	3	(1.8662334025933334, 13.08441633006715, 100.10588843171699)
1990-01-01 03:00:00	tuple	3	(1.831814420325, 13.583873339170658, 100.10588843171699)
1990-01-01 04:00:00	tuple	3	(1.7973954380566666, 14.083330348274169, 100.10588843171699)
1990-01-01 05:00:00	tuple	3	(1.7629764557883334, 14.58278735737768, 100.10588843171699)
1990-01-01 06:00:00	tuple	3	(1.72855747352, 15.082244366481188, 100.10588843171699)

Fig. 4.4 Stored wave data for a randomly selected wave climate

### 4.4.3 River Flooding Sequence

The uMngeni River is a major source of sediment for Durban coastline, specifically the stretch immediately North of the uMngeni river mouth. The river previously yielded annual sediment volumes of around 100,000 cubic metres before the construction of dams and the prevalence of sand mining (Theron et al., 2008). Although greatly reduced, the river continues to make significant contributions during storm events (Cooper, 1993). This model assumes that the uMngeni River only contributes sediment to the coastline during flooding caused by storms. This is in agreement with Theron et al. (2008) who state that sediment is stored within the floodplains of rivers, usually

## Model Development

---

only reaching the ocean via floods. Another major source of sediment, being the sand-bypass scheme at the harbour mouth, is discussed in section 4.5.4.

To account for the annual fluvial contributions, an algorithm was designed to simulate a specified number of storm events within a year. This algorithm requires the user to input storm frequency, storm duration and a range for annual fluvial discharge volume. Annual yields are selected by a random number generator operating within the specified range of discharge. A seasonal probability distribution of rainfall events acts to proportion the seasonal frequency of storms throughout the year as well as the seasonal discharge volume. Table 4.1 below shows the mean seasonal rainfall distributions obtained from a 10-year observation record. The data was obtained from rainfall records provided by the Department of Water Affairs and Forestry. The algorithm then picks out numerous random dates corresponding to the seasonal storm frequency and assigns them a time to signify the start of a storm. The aforementioned seasonal volumes are divided by the seasonal storm frequency to obtain individual storm volumes which implies storms are of equal discharge volume within each season. This data is stored into a Python dictionary.

Table 4.1 Mean seasonal rainfall and probability distributions (DWAF, 2011)

Season	Rainfall (mm)	Probability (%)
Spring	188.8	28.32
Summer	265.9	39.88
Autumn	130.6	19.59
Winter	81.4	12.21

### 4.4.4 Base Coastline Generation

Although this part of the model utilises all of the numerics explained from section 4.5 onward, it is carried out prior to the iterative model loop to provide a baseline coast for use further on in section 4.7. The initialised grid is used for this calculation. An incoming wave angle equal to the general coastline normal is used to smooth out and diffuse and undulations along the coastline. The result is a smooth coastline generally resembling the measured coastline which is thereafter used as a baseline for further calculations. This coastline is updated at regular intervals to continuously reflect the general coastline shape at the given time step.

## 4.5 Model Numerics

### 4.5.1 Grid Orientation

The first undertaking of the time-stepped loop is to calculate orientations of individual grid cells. This includes grid inclination, shore parallels and shore normals. Equation 4.1 is used to calculate the slope of a grid cell. The equation states:

$$\theta = 2\pi - \arctan\left(\frac{y_{i+1} - y_i}{x_{i+1} - x_i}\right) \quad (4.1)$$

where  $x$  and  $y$  refer to the cartesian grid points. Given that grid spacing is kept constant throughout the simulation period, the denominator will not vary in equation 4.1. Figure 4.3 demonstrated that coastal coordinates were transformed such that the shoreline trend falls parallel to the x-axis. This transformation is shown in figure 4.5, where the coastline is rotated from quadrant 1 to quadrant 2. The purpose of this transformation is to have all angles relative to a single datum and to simplify graphical representations.

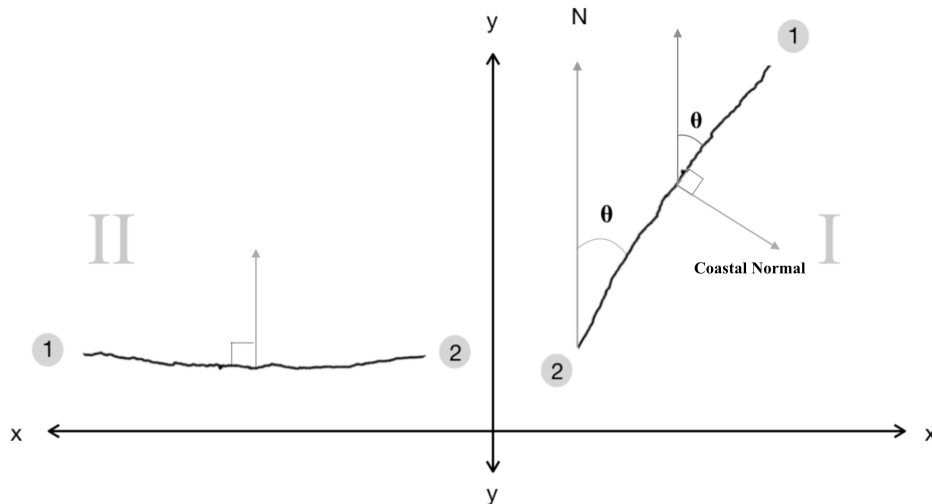


Fig. 4.5 Transformation of a coastline section from quadrant 1 to 2. N indicates north and theta indicates the relative coastline orientation. Grey arrows perpendicular to the coast indicate coastal normals.

Coastal normals (labelled) are calculated by adding 90 degrees to the calculated slope from equation 4.1. This may be seen in quadrant 1 on figure 4.5 and is done for all individual grid cells. All values are measured clockwise from North.

### 4.5.2 Wave Transformation

Prior to carrying out the wave transformation, relative wave angles are computed as they are an input requirement for the calculations that follow. Equation 4.2 uses deepwater wave angles and shore normals to calculate relative wave angles for each grid cell. This value represents deepwater conditions. Equation 4.2 is expressed as:

$$\varphi = \theta - \phi_o \quad (4.2)$$

where  $\varphi$  is the relative wave angle,  $\phi_o$  is the deepwater wave angle and  $\theta$  is the shore normal angle in degrees. Figure 4.6 depicts the orientation of deepwater and breaking waves. It must be noted that figure 4.6 shows all angles measured from the x-axis, however the model uses the y-axis (North) as the zero degree datum. Individual grid cells may vary greatly in terms of shore normals, hence relative wave angles will vary proportionately.

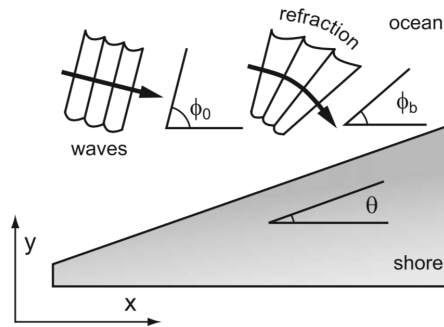


Fig. 4.6 Relative orientations of breaking and deepwater waves (Ashton and Murray, 2006)

Transformation of waves involves an iterative loop that is halted when specified requirements are met. Initial calculations involve values that remain constant throughout the iteration period, usually relating to deepwater conditions. Wavelength was calculated using equation 4.3 below:

$$L_0 = \frac{gT_p^2}{2\pi} \quad (4.3)$$

where  $T_p$  is wave period in seconds. Note that the subscript 0 denotes deepwater conditions. Thereafter, wave steepness is checked by the ratio between deepwater significant wave height ( $H_{s0}$ ) and deepwater wavelength ( $L_0$ ). Exceedance of the 0.142 steepness limit results in an adjustment of wave height to meet this threshold. The wave number and wave celerity are calculated using equations 4.4 and 4.5 respectively:

$$k_0 = \frac{4\pi^2}{gT_p^2} \quad (4.4)$$

$$c_0 = \frac{gT_p}{2\pi} \quad (4.5)$$

where  $T_p$  is wave period in seconds. The iterative loop is thereafter initiated, taking an initial assumption for the depth at breaking along the entire grid space. The wavelength at this assumed depth is then computed using equation 4.6:

$$L_b = L_0 \tanh\left(\frac{2\pi h}{L_b}\right) \quad (4.6)$$

where  $L_0$  is the deepwater wavelength and  $h$  is the water depth at breaking.  $L_b$  is obtained iteratively. The computed wavelength at the breaker depth ( $L_b$ ) is then used to calculate further parameters. Equations 4.7 and 4.8 are used to calculate wave number ( $k$ ) and  $n$  respectively.  $n$  is the ratio between group velocity and higher phase velocity. Whence:

$$k = \frac{2\pi}{L_b} \quad (4.7)$$

$$n = \frac{c_g}{c_{phase}} = 0.5\left(1 + \frac{2kh}{\sinh 2kh}\right) \quad (4.8)$$

$$c_{phase} = \frac{gT_p}{2\pi} \tanh(kh) \quad (4.9)$$

where  $c_g$  denotes group velocity and  $L_b$  denotes breaking wavelength. Phase velocity is obtained from equation 4.9, with group velocity  $c_g$  calculated by multiplying  $n$  by  $c_{phase}$ .

Refraction of waves occur when gradients in velocity are present as a result of varying depths (Bosboom and Stive, 2015). Snell's Law provides a way to estimate changes in wave direction proportional to changes in wave propagation speed shown in equation 4.10:

$$\frac{\sin \varphi_1}{c_1} = \frac{\sin \varphi_2}{c_2} \quad (4.10)$$

where  $\varphi$  represents relative wave angles at two points along the wave ray and  $c$  represents phase velocities at the corresponding points. Hanson (1989) interchanged phase velocity with wavelength, however both equations provide the same solution given the dependance of phase speed on wave number which in turn relies on wavelength.

## Model Development

---

Bosboom and Stive (2015) relate wave power at two arbitrary points to derive a formula for calculating the refraction coefficient, given by equation 4.11:

$$K_r = \sqrt{\frac{\cos \phi_0}{\cos \phi}} \quad (4.11)$$

where  $\phi_0$  and  $\phi$  denote relative wave angles at deepwater and breaking conditions.

Similarly, Bosboom and Stive (2015) showed that this approach allows for derivation of a shoaling coefficient. Shoaling is the process by which waves decrease in velocity and wavelength but increase in height due to a reduction of water depth (Bosboom and Stive, 2015). Equation 4.12 shows this formulation:

$$K_{sh} = \sqrt{\frac{1}{\tanh kh} \frac{1}{2n}} \quad (4.12)$$

where  $k$  is the wave number,  $h$  is the assumed breaker depth and  $n$  is the ratio between group velocity and higher phase velocity. Multiplication of both coefficients with the deepwater significant wave height gives the breaking wave height.

Breaking criteria for the loop is based on two values. Given the absence of a current, the wave action balance reduces to the energy balance (Bosboom and Stive, 2015). This principle was exploited by ensuring deepwater and breaking depth wave energy is conserved using equation 4.13 which states:

$$U_1 = U_2 = \frac{1}{8} \rho_w g H^2 n c \cos \varphi \quad (4.13)$$

where  $H$  is significant wave height,  $\rho_w$  is the density of sea water,  $n$  is the velocity ratio,  $c$  is the phase velocity and  $\varphi$  is the relative wave angle at the given point.  $H$ ,  $n$ ,  $c$  and  $\varphi$  vary depending on the position at which values were calculated. Should deepwater and breaking wave energies be equal, a further check is done using the breaker index. Linear wave theory suggests a value of 0.78 (Bosboom and Stive, 2015). Breaker index is calculated by dividing wave height by water depth at the breaker line. Should the calculated indices not equal this value, a new assumed depth is calculated using equation 4.14:

$$h_{new} = \frac{H_b}{0.78} \quad (4.14)$$

This process is repeated until convergence of breaker index and wave height and is done for individual grid cells throughout the model domain.

### 4.5.3 Longshore Sediment Transport

Longshore transport is the cumulative migration of beach and nearshore sand parallel to the shoreline. This is caused by the combined action of tides, wind and waves that result in shore parallel currents (Seymour, 2005). Model computes longshore transport using equation 4.15 developed by Kamphuis (1991):

$$I_m = K \rho_w \left( \frac{g}{2\pi} \right)^{1.25} H_{sb}^2 T_p^{1.5} m^{0.75} D_{50}^{-0.25} \sin^{0.6}(2\varphi_b) \quad (4.15)$$

where  $K$  is a calibration coefficient,  $\rho_w$  is the density of seawater,  $H_b$  is the breaking significant wave height,  $T_p$  is peak wave period,  $m$  is beach slope,  $D_{50}$  is median sediment diameter and  $\varphi_b$  is relative wave angle at breaking. Equation 4.15 produces units of kg/s which represents the immersed mass transport rate. Conversion to volumetric transport rate is done using equation 4.16 below:

$$Q = \frac{I_m}{(\rho_s - \rho_w)(1 - p)} \quad (4.16)$$

where  $I_m$  is immersed mass transport rate,  $\rho_s$  is the density of sand,  $\rho_w$  is the density of seawater and  $p$  is the porosity of sand. Commonly used values for these parameters are  $\rho_s = 2650 \text{ kg/m}^3$ ,  $\rho = 1030 \text{ kg/m}^3$  and  $p = 0.4$ . The sign convention of this model defined northward transport as negative and southward transport as positive.

Beach slope is the ratio between depth of breaking and the distance from the shoreline to the breaking depth, assuming a linear slope. The equation for calculating beach slope is given below in equation 4.18, incorporating the cross shore profile function from equation 4.17. The equation states:

$$y = Ax^{\frac{2}{3}} \quad (4.17)$$

where  $y$  is the depth of water,  $x$  is offshore distance and  $A$  is a shape factor dependent on the median sediment size for the beach. Changing the subject of the formula and substituting  $h$  for  $y$ , we get equation 4.18 which states:

$$m = \frac{A^{\frac{3}{2}}}{\sqrt{h}} \quad (4.18)$$

where  $h$  is depth of water. Longshore sediment transport is calculated for each grid cell and may vary significantly given the equations dependance on relative wave angle. The shape factor  $A$  is solely based on median sediment diameter.

#### 4.5.4 Lateral Boundary Conditions

Boundary conditions are important in allowing for stable model performance while producing reliable results. The lack of coastal structures required for the specification of two boundary conditions at either end of the model domain.

Considering the general direction of longshore sediment migration (northward), the uMhlanga boundary essentially served as the outflow point of the domain. In order to prevent interaction between the boundary point and the model domain, the left side of the domain was extended by 5000 metres using a constant slope encountered at the end of the domain. This extension is presented in figure 4.7. A Neumann (zero gradient) boundary was imposed at the end of the full domain under the assumption that this point is unlikely to move significantly over time. This allowed for appropriate behaviour of the surveyed study region while being adequately far away from the study domain to not receive any influence.

The uMngeni boundary presented a dynamic situation whereby sediment inputs would be varied to investigate their influence on coastal evolution. Given that a sand-bypassing scheme is operated at the harbour mouth together with a general northward migration of sediment, time-varying fluxes of sand are to be expected at the uMngeni boundary. For this reason, a Dirichlet (specified value) boundary condition was enforced such that an inflow rate may be specified at each time step which emulates the periodic bypassing scheme as a source of sediment. For simplicity in this study, the uMngeni River was not included in the model domain and the effects of the groyne at the river mouth were ignored. Coordinates used for the model domain were limited at a point to avoid inclusion of the coastal features formed by the river mouth. Due to the specification of lateral boundary conditions, coastline behaviour is likely to be erratic for certain simulation scenarios. The inclusion of vertical boundary conditions are therefore also necessary to ensure relatively reliable results, which is discussed further in section 4.7.1.

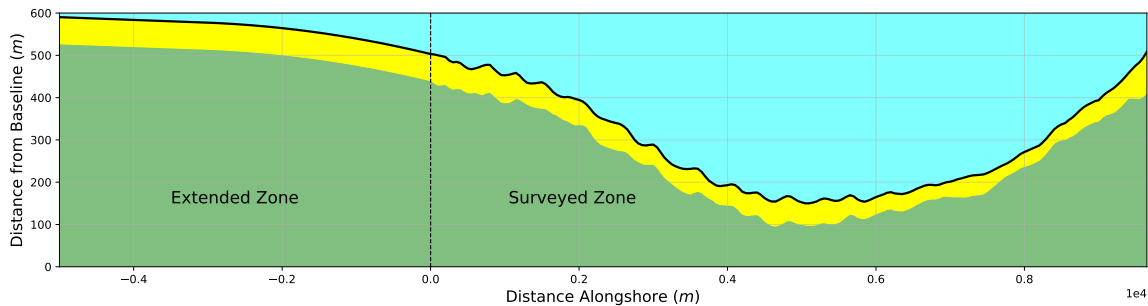


Fig. 4.7 Shoreline extension used for the uMhlanga boundary.

### 4.5.5 Coastline Changes

Morphological changes may occur as a result of numerous physical processes along the coastline. These include gradients in longshore transport and introduction of sediment from sources and loss of sediment to sinks. Approximation of these changes require a number of assumptions explained in chapter 2. The coastline model accounts for changes due to longshore transport. Equation 4.19 provides a graphic representation of coastline change. Calculation processes are detailed below.

$$y_{i+1} = y_i + \Delta y_{longshore} \quad (4.19)$$

Consider an arbitrary stretch of coastline resolved into equally spaced rectilinear grid cells shown in figure 4.8 below. The curved line represents the coastline shape in plan. Individual grid points are denoted by  $y$  with the relevant subscript, with  $Q$  representing points of longshore transport computation as explained in section 4.5.3.

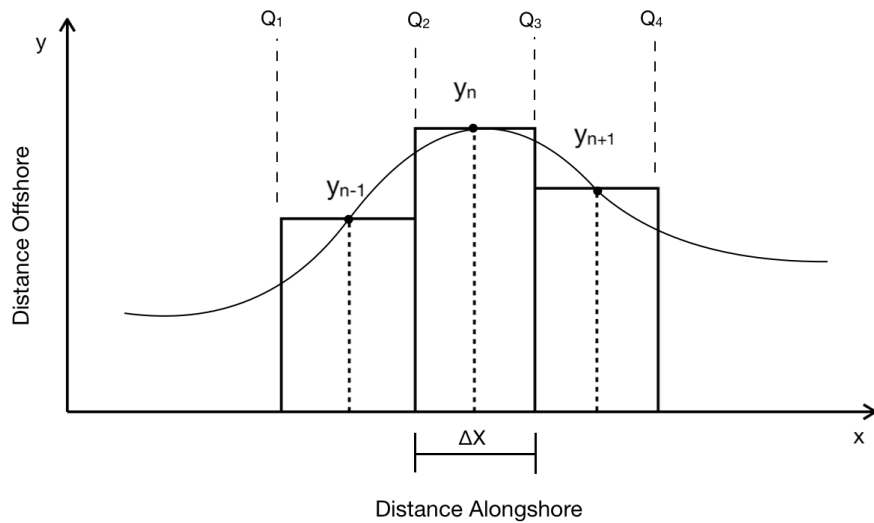


Fig. 4.8 Model domain setup showing grid and longshore transport points

The change in position  $\Delta y$  at any point  $y$  caused by longshore transport may be computed using equation 4.20 which states:

$$\frac{\partial y}{\partial t} = \frac{1}{D_c + D_b} \frac{\partial Q}{\partial x} \quad (4.20)$$

where  $D_c$  and  $D_b$  are depth of closure and berm height respectively and  $Q$  refers to longshore sediment transport. This equation is an extension on Pelnard-Consideré's

## Model Development

---

diffusivity approach. Longshore induced changes are assumed to occur along a fixed vertical axis parallel to the  $y$ -axis for the given grid cell. This assumption may result in unreliable results for coastlines integrating large curvatures however given the relatively minute curvature of the study region, it was assumed to be of a sufficient accuracy.

The depth of closure and berm height variables serve to limit vertical extents of the cross-shore profile where both values remaining constant throughout the simulation period. Berm height is obtained from beach survey data mentioned in chapter 3 while beach profile heights are averaged across all 41 measured profiles. Profile heights were measured from land levelling datum (*LLD*).

The depth of closure represents the seaward extent of longshore sediment transport, beyond which no significant changes in morphology occurs. Birkemeier (1985) derived an equation to calculate this parameter, modifying an equation previously developed by Hallermeier (1980) shown in equation 4.21 which states:

$$D_c = 1.75H_s - 57.9\left(\frac{H_s^2}{gT^2}\right) \quad (4.21)$$

where  $H_s$  is the effective wave height falling just outside of the breaker zone, that is exceeded for 12 hours per year,  $g$  is acceleration due to gravity and  $T$  is the period associated with the value of  $H_s$ . Effective wave height is essentially the significant wave height with a probability of yearly exceedance of 0.137%. To calculate this quantity, all wave heights across all 101 simulated wave sequences were used, with the corresponding  $T$  value identified. Verification of this value involved substitution of the depth of closure into the cross-shore profile function (eqn. 4.17) and solving for offshore distance. The depth and related distance were compared to the findings of Mather & Stretch (2011) who studied wave run up on natural beaches. Both approximations showed good agreement. Berm height ( $D_b$ ) was calculated using eThekweni Municipality's beach survey data for the region. A mean value was calculated using the measured beach profile heights at regular intervals along the coastline.

## 4.6 Beach Nourishments

In addition to coastline changes caused by longshore sediment transport, the model also accounts for introduction of sediment in bulk volumes, otherwise referred to as nourishments. This is necessary for large river sediment deposits following storms as well as for analysing longshore sediment supplies in the form of large, episodic influxes. The numerics for both river and longshore sediment is the same.

### 4.6.1 Nourishment Shape

Dispersion of the sediment discharge is assumed to take on a Gaussian distribution in plan, hence equation 4.22 below is used to calculate changes in coastline position. The equation states:

$$g(x) = \frac{1}{\sigma\sqrt{2\pi}} e^{-\frac{1}{2}\left(\frac{x-\mu}{\sigma}\right)^2} \quad (4.22)$$

where  $x$  is the shoreline position,  $\mu$  is the point about which the discharge is centred and  $\sigma$  is the width of the discharge, where the first term in the equation normalises the area of the plot. The probability distribution was therefore multiplied by the discharge volume is divided by the sum of vertical extents (berm height and depth of closure) to obtain coastline changes.

Given the presence of a groin at the uMngeni River mouth together with a strong south-south-east angle of wave incidence, a number of assumptions have been made regarding the addition of this discharge into the model domain. Modelling river mouth dynamics are complex and beyond the scope of this study, hence the river has been simplified into a sediment source with no hydrodynamics accounted for.

### 4.6.2 River Discharges

While the model is running, a check is carried out at each time step to ascertain whether the current date and time is linked to a storm occurrence. Should an event occur, the relevant discharge volume is obtained from the previously generated storm dictionary. The discharge volume is thereafter proportioned based on the model time-step and storm length to calculate the dispersion pattern.

### 4.6.3 Longshore Sediment Supply

Longshore transport rates for intermittent sediment supply simulations were also calculated using Gaussian distributions. It was assumed that the pumping effect of a sand-bypass scheme would result in a bulk volume of sediment that would advect through the coastline. Once this sand reaches the study region, application of the sand is done using a Dirichlet boundary condition corresponding to the position along the bulk nourishment using equation 4.22. Longshore transport rates are calculated by initially assuming an annual sediment volume influx. This volume is divided equally by the pumping frequency for the year and is thereafter proportioned using the distribution.

## 4.7 Nourishment Diffusion & Advection

Sand waves are large scale features that move under the influence of the incoming wave climate. Inclusion of these features into the model may be significant in explaining the erosion behaviour observed along the Durban coastline. Given that the basic coastline model is based on a diffusive mechanism, a variation of the Pelnard-Considerere equation was implemented to replicate the advective nature of sand waves, namely:

$$\frac{\partial y}{\partial t} + \frac{S_{x,0}}{(D_c + D_b)B} \frac{\partial y}{\partial x} = \frac{1}{D_c + D_b} \frac{\partial Q}{\partial x} \quad (4.23)$$

where  $S_{x,0}$  is the longshore transport rate at the zero degree coastline orientation and  $B$  is the amplitude of the nourishment. The nourishment is advected by a velocity equal to that of the second term on the left hand side of equation 5.6. The value of  $\partial y/\partial x$  is calculated using the central difference theorem.

For application in the model, a baseline coast was used as the reference plane for added nourishments (see sect. 4.4.4). For model stability and accuracy, a numerical process was devised to ensure that sand waves behave appropriately. The first step involved calculating the relative orientations of coastline segments without the nourishment added onto the baseline coast. The nourishment was thereafter added to the baseline coast. Given that coastline positions will only change for the region where the nourishment was added, it was possible to isolate baseline coast orientations within the region of the nourishment. These base coastline orientations were averaged to obtain essentially a tangent to the coastline where the nourishment is situated (see fig. 4.9). The tangent is a straight line that is inclined at the previously calculated average coastline orientation. Use of a straight baseline is advantageous as  $\partial y/\partial x$  values are simpler to calculate. Furthermore, corrections due to over-erosion is made simpler. Considering the relative size of nourishments with regards to the total domain, it was assumed that curvature effects would not be significant.

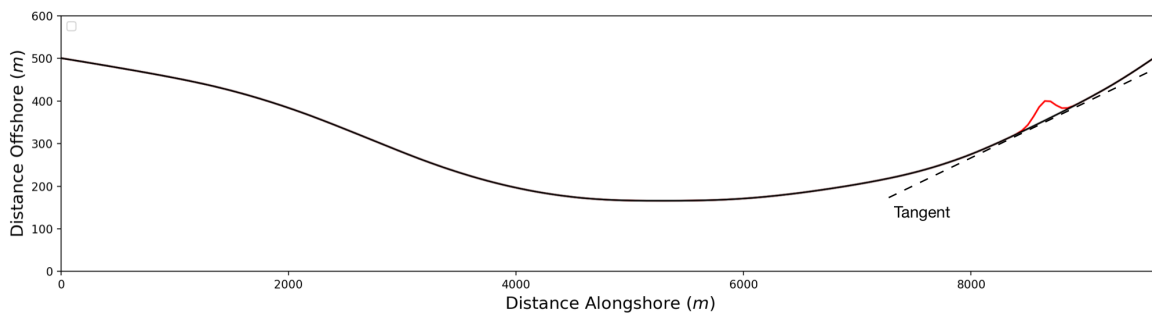


Fig. 4.9 Visualisation of tangent method used for diffusing and advecting sand waves.

## 4.7 Nourishment Diffusion & Advection

The process then assumed that the nourishment was placed along the tangent coastline, and was thereafter adjusted to account for diffusion effects as detailed in section 4.5.5. Alteration of the tangent baseline is prevented by using the tangent as a hard boundary limit (see sect. 4.7.1). The diffused nourishment is thereafter advected using equation 5.6. Using the incoming wave angle,  $S_{x,0}$  is computed using for the tangent coastline orientation by subtracting the wave angle from the tangent normal (see fig. 4.10).  $B$  is the maximum value of the plume, which does not vary along the coastline. Finally,  $\partial y/\partial x$  is thereafter computed. The tangent base is thereafter subtracted from the now diffused and advected coastline inclusive of the nourishment. This isolates the nourishment such that it may be added back onto the curved baseline. Figure 4.11 shows the advection and diffusion of an arbitrary nourishment along a straight coastline over a period given a fixed deepwater wave angle.

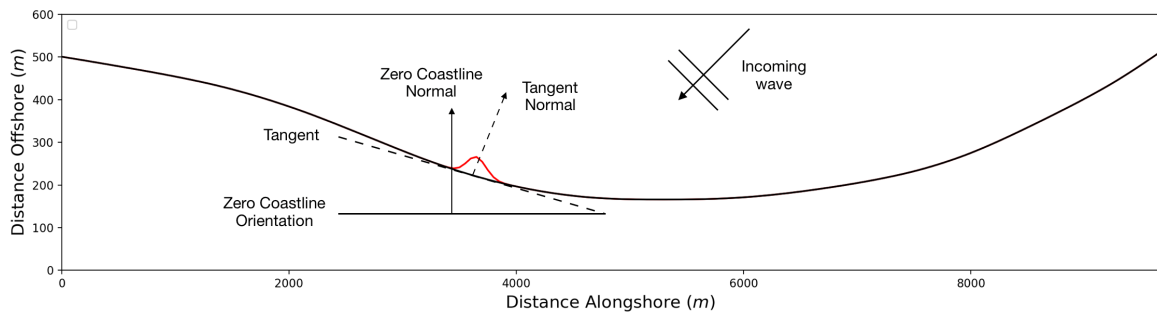


Fig. 4.10 Coastline orientations used for calculating  $S_{x,0}$ .

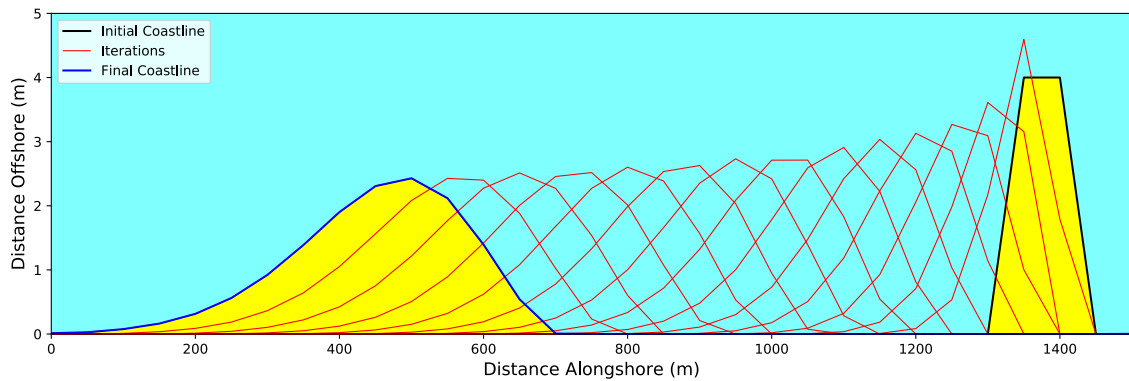


Fig. 4.11 Example of an advected and diffused sand wave.

### 4.7.1 Vertical Boundary Conditions

Given that this study investigates coastline evolution due to varying sediment supply schemes, the possibility of beach profiles being completely eroded must be accounted for in terms of the model. The inclusion of an erosion limit is important when considering availability of sediment for longshore transport and the resulting coastal evolution. Numerically, the computed longshore transport rate is independent of available sediment, hence a computed rate within a cell that has been exhausted of sediment could provide unrealistic results. This limit is introduced in the form of a vertical boundary condition where the erosion limit essentially represents a seawall.

Hanson and Kraus (1986) detail a procedure for implementing a seawall boundary condition into the capabilities of a one-line model. They base their method on the following principles:

- The shoreline in front of a seawall may not recede landward of the structure.
- Sand volume must be conserved.
- Direction of alongshore sand transport must be conserved in accordance with the natural direction of the potential local transport.

This erosion limit was introduced by using beach widths obtained from eThekweni Municipality's beach survey program by averaging measured widths for 41 profiles. During the initialisation process, the model interpolated beach widths from the entered data and subtracted them from the zero contour. This essentially produced an offset beach width contour that provided limits for erosion activity. Should sufficient erosion occur such that this limit is exceeded in any cell, the following process is implemented.

Individual grid cells breaching the limit are analysed to identify whether they are regular, minus or plus area cells. Figure B.1 depicts the differences between these classifications. This classification is based on the direction of longshore transport rates. Following this classification, the necessary adjustment to the longshore transport rate is carried out using the appropriate formula. Minus cells (fig. 4.13a) use equation 4.24 to adjust transport rates whereas regular cells (fig. 4.13b) use equation 4.25 to adjust transport rates. Notably, plus area cells require no adjustment of transport rates as they represent a convergence of sediment.

$$Q_{i+1}^* = Q_{i+1} \frac{y_i - y_{s_i}}{y_i - y_{i'}} \quad (4.24)$$

$$Q_{i+1}^* = Q_i - \frac{y_{s_i} - y_i}{2B} \quad (4.25)$$

## 4.7 Nourishment Diffusion & Advection

Longshore transport rates with asterisks correspond to adjusted rates equations 4.24 and 4.25, with  $y_i$  referring to the original coordinate,  $y'_i$  being the shifted coordinate using equation 4.20 and  $y_{si}$  referring to the hard boundary position. Corrections to longshore transport rates often propagate through the system, hence this correction is continued throughout the model domain until either the end or a plus area cell is reached (Hanson and Kraus, 1986). For this section of the model, the pseudocode provided by Hanson and Kraus (1986) was converted from FORTRAN to Python and implemented. See appendix D for more details.

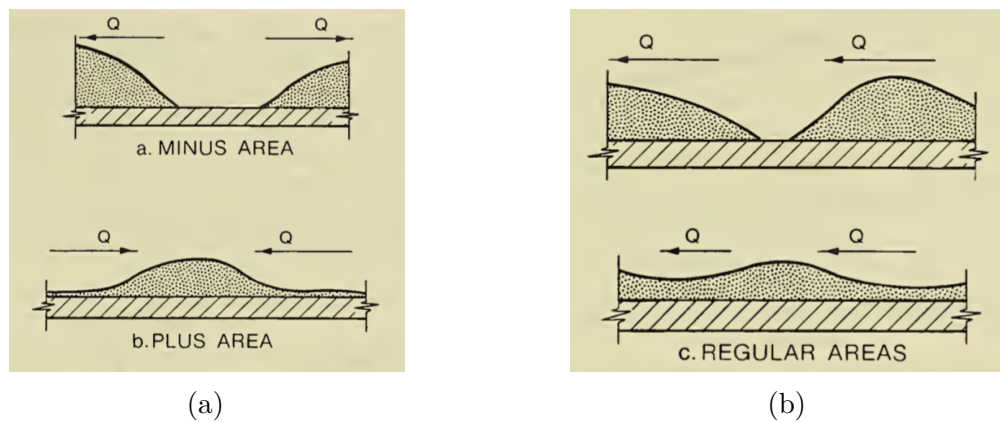


Fig. 4.12 Conceptual diagram showing cell classifications for minus and plus area (a) and regular (b) cells (Hanson and Kraus, 1986).

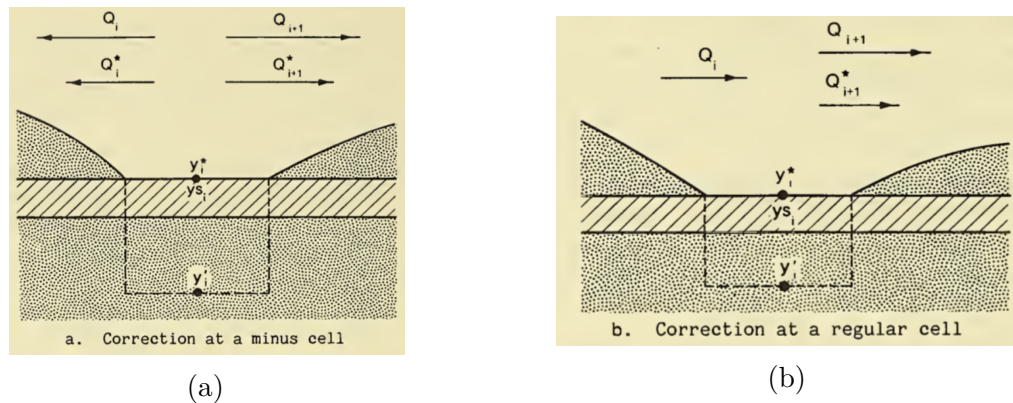


Fig. 4.13 Conceptual diagram showing shoreline and transport corrections for minus (a) and regular (b) (Hanson and Kraus, 1986).

## 4.8 Model Checks

### 4.8.1 Wave Transformation Limits

In order to prevent unrealistic changes in relative wave angles after the wave transformation, a limit is applied following completion of this calculation. As mentioned in the literature review, Ashton et al. (2001) found that sandy coastlines become unstable when approached by waves at high incidence angles. These instabilities are known to grow and eventually form large scale features such as sand waves. In order to prevent this from occurring during model operation, a limit relating to wave direction is enforced. A check is carried out where relative wave angles at deepwater and breaking conditions are subtracted to obtain the net change. The algorithm identifies any grid cells where the net change in relative wave angle has exceeded 90 degrees, following which the longshore transport rate for that cell is equated to 0.

### 4.8.2 Conservation of Mass

As explained in section 4.7.1, adjustment of longshore transport rates is significant in obtaining realistic results from the model. A further check included is the conservation of mass. The model domain is analysed to ensure that all sediment entering or leaving the domain is accounted for. A simple, triangular profile is used to calculate the volume of sediment contained within each grid cell. This value is calculated by multiplying the cell width ( $\Delta x$ ) by the vertical profile extents ( $D_c + D_b$ ) and the mean height of the beach segment ( $y$ ). The sum of cell volumes plus the net sediment transport at the boundaries for the current iteration is checked against the sum of cell volumes for the previous iteration. The domain volume is calculated using the trapezoidal rule multiplied by the cross shore extents. Volumes are allowed to fluctuate within 0.1% of the previous iteration while allowing the model to continue. Violation of this range halts the simulation.

## 4.9 Model Calibration

Calibration of the longshore sediment transport equation involved using annual net loss rates for the Durban Bight from Corbella and Stretch (2012*b*) and observed regional wave data obtained from waverider buoys located at Durban and Richards Bay. The Durban Bight loss data from Corbella and Stretch (2012*b*) was applied to the Durban Sand Trap due to the operation of a sand-bypassing scheme at the Durban Port entrance. This served as the best estimate of measured longshore transport volumes over a period that coincided with the observed wave data. The Kamphius longshore transport formula (eqn. 4.15) is calibrated through the coefficient  $K$  which linearly scales computed transport rates values. The calibration process is explained below.

Observed wave data was imported into Python and filtered. This filtering ensured that only data points containing a wave height, direction and period were retained, with the remainder removed. The wave data was thereafter stored into arrays by year, with each entry being a list containing wave characteristics ( $H$ ,  $T$ ,  $\theta$ ) and the timestamp. The model sorted each data point into a 2D array based on wave height and direction. The sorting also summed wave characteristics in their respective bins while keeping an entry count to compute mean values. This provided a more accurate representation of the wave data as opposed to using a mean of the bin location. Figure 4.14 shows distributions of wave height and period along with a probability distribution of wave events.

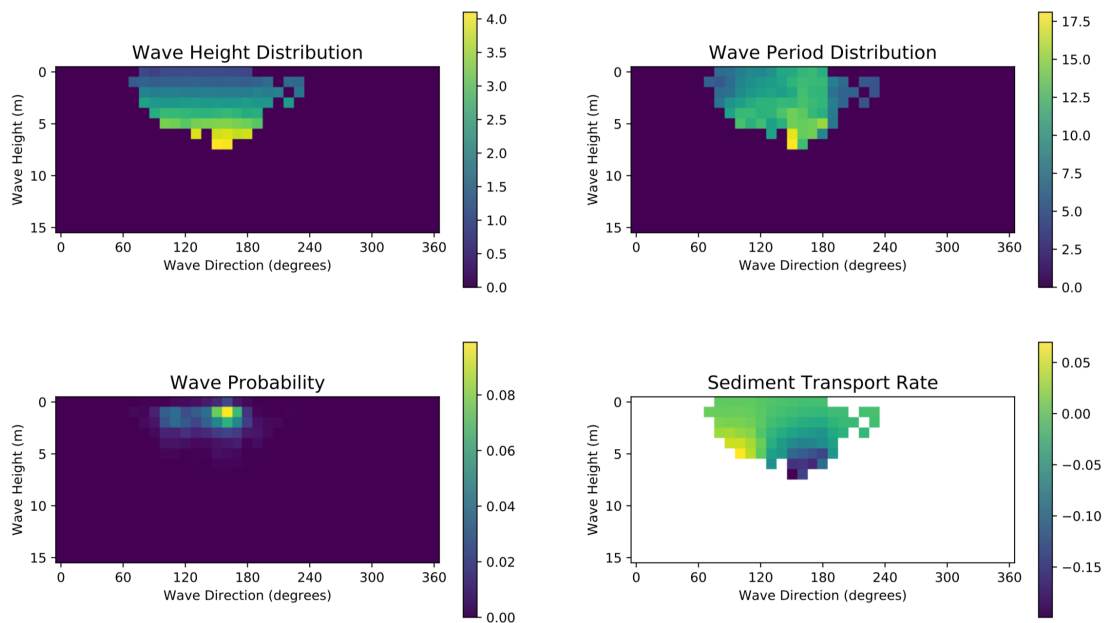


Fig. 4.14 Distributions of various datasets used for model calibration.

## Model Development

---

The algorithm was initiated using a constant coastline orientation and an uncalibrated Kamphuis equation with  $K$  equal to 1. Following sorting of data, the model performed a wave transformation. Using the transformed wave heights and directions together with mean wave periods, longshore sediment transport rates were calculated for each bin (fig. 4.14). These transport rates were thereafter scaled using the probability array to obtain a final transport rate array for the given wave climate in  $m^3/s$ . To obtain annual longshore transport volumes, the computed rates were multiplied by a time period, which in this case was the average length of a year. The sediment transport arrays were thereafter summed to obtain a final representative value for the annual longshore transport rate. This was done for each individual year in the observed wave record. Use of this process was favoured over running a time series through the model as the wave data incorporated numerous periods of missing data. In not accounting for certain wave occurrences, longshore transport rates may be skewed by measured wave events which may not necessarily be as significant as unmeasured data.

In order to calculate the calibration coefficient, the following process was used. The observed and computed longshore volumes were split into two halves, with the first half used to calibrate the equation and the second half serving to validate the calibration. The datasets were split as shown in table 4.2. The 2005 annual loss rate, which indicated a net gain of sediment, was excluded from the dataset as it represented an outlier. By plotting uncalibrated, computed longshore volumes against observed longshore volumes for the same period, a linear regression analysis may be used to obtain the slope of the best-fit line which represents the calibration coefficient. This coefficient was thereafter applied to second half of the computed dataset. Calibrated longshore volumes were once again plotted against observed volumes for the second half of the datasets to check the effectiveness of the calibration. Results of the model calibration are shown in chapter 5.

Table 4.2 Allocation of observed longshore transport rates for model calibration.

Years	Period (Years)	Allocation
1997 - 2002	6	Calibration
2003 - 2009	6	Validation
2005	1	Excluded

## 4.10 Sensitivity Analysis

### 4.10.1 Input Error Effects

A sensitivity analysis was carried out to assess model sensitivity to small changes in input wave data. Accurate measurement of wave characteristics is difficult therefore determining the effects of uncertainties on model predictions are important (Hanson, 1989). The model is centred around the calculation of longshore sediment transport rates which is subsequently used to calculate coastline changes. The Kamphius equation (eqn. 4.15) is used in this model, which uses three wave characteristics together with physical coastline parameters to calculate a longshore sediment transport rate. Throughout the simulation period, wave characteristics are varied within the equation while other quantities remain constant. The effect of small changes to significant wave height at breaking ( $H_s$ ), peak wave period ( $T_p$ ) and relative wave angle at breaking ( $\theta_b$ ) are used as criteria for this sensitivity analysis. Additionally, beach slope ( $m$ ) has also been included due to its dependence on the breaking wave height. Ignoring all constant values in the beach slope equation, it may be represented as:

$$m = H_b^{-\frac{3}{8}} \quad (4.26)$$

Substituting this into the Kamphius equation yields:

$$Q = H_b^{\frac{13}{8}} T_p^{1.5} \sin^{0.6}(2\theta_b) \quad (4.27)$$

A numerical analysis was carried out to quantify the effects of small errors in wave input values. Errors were computed using a first order Taylor series approximation for each input variable. Combined error effects were also estimated by arithmetically multiplying the relevant input errors. An error of 10% was assumed such that the results may be compared to a similar analysis conducted by Hanson (1989) on the CERC formula. Table 4.3 details the values used for the sensitivity analysis.

Table 4.3 Wave characteristic values for sensitivity analysis.

Parameter	Unit	Value	Change
$H_s$	$m$	2.0	$\pm 10\%$
$T_p$	$s$	13.0	$\pm 10\%$
$\theta_b$	$^\circ$	15	$\pm 10\%$

### 4.10.2 Model Stability and Accuracy

The coastline model uses an explicit solution technique as the new shoreline position is entirely dependent on calculated values at the previous time step. Explicit solution schemes are advantageous in the sense that programming is made easier along with boundary conditions being more easily expressible (Hanson, 1989). A major flaw however is the numerical stability, represented by the Courant Number ( $R_s$ ) which is defined as the ratio between the time step and finite grid length (see eqn. 4.28). The explicit scheme used in this model is second order correct however unlike implicit schemes, is not unconditionally stable (Dutykh, 2016). Hanson (1989) infers a maximum Courant Number of 0.5 when using explicit solution schemes for diffusion models while adding that numerical model results should be grid and time step independent. Equation 4.28 arithmetically represents the Courant number, which states:

$$R_s = \kappa \frac{\Delta t}{\Delta x^2} \quad (4.28)$$

where  $\kappa$  is a diffusivity constant,  $\Delta t$  represents the model time step and  $\Delta x$  represents the spatial grid intervals used in the model. Equation 4.20 may be alternatively expressed as:

$$\frac{\partial y}{\partial t} = \frac{s_x}{D_c + D_b} \frac{\partial^2 y}{\partial x^2} \quad (4.29)$$

where  $s_x$  is the coastal constant, represented as follows:

$$s_x = \frac{\partial Q_x}{\partial \phi} \quad (4.30)$$

where  $Q_x$  refers to calculated longshore transport rates and  $\phi$  refers to relative wave angles. Hence, we may represent diffusivity as:

$$\kappa = \frac{s_x}{D_c + D_b} = \frac{\partial Q_x}{\partial \phi (D_c + D_b)} \quad (4.31)$$

This analysis focused on the effect of varying time steps and grid intervals on model stability and result accuracy. A hypothetical beach was initialised with constant wave parameters. The time step was varied with a constant grid interval to estimate the effects of a varying time step. The opposite was carried out to test the effect of varying grid intervals.

# Chapter 5

## Results & Discussion

This chapter presents the findings of this study. Comparison of observed and simulated wave climates are presented within this chapter together with the model calibration. Outcomes of the sensitivity analysis are also shown. Finally, results of long-term simulations using varying sediment input schemes are presented.

### 5.1 Wave Climate Comparison

A comparison of the observed and simulated wave climate was carried out to assess similarity between datasets. Table 5.1 summarises both wave climates with selected statistical properties. The simulated climate covers all 101 iterations of 101 year wave sequences while the observed data corresponds to the 18 years of recorded data.

Table 5.1 Statistical properties of observed and simulated wave climates.

Property	Observed Climate			Simulated Climate		
	Mean	Min.	Max.	Mean	Min.	Max.
$H_s$ (m)	$1.56 \pm 0.51$	0.01	8.5	$1.70 \pm 0.60$	0.1	30.24
$T_p$ (s)	$10.84 \pm 2.72$	2.5	40.0	$10.38 \pm 3.93$	1.05	20.0
$D$ ( $^\circ$ )	$137.71 \pm 27.52$	32.0	233.0	$133.89 \pm 30.42$	30.0	210.0

Mean and standard deviation values for both wave climates show close resemblance regarding all wave parameters. A notable difference between the two wave climates is the maximum significant wave height ( $H_s$ ) that occurs within the simulated wave climate. This value (30.24 metres) is sizeably larger than that of the observed wave climate (8.5 metres). Both values correspond to storm occurrences where the difference

## Results & Discussion

---

may be attributed to the relative return periods of the storm events. The simulated data consists of 101 iterations of 101 year sequences, hence the likelihood of a 1:100 or 1:200 storm event occurring within one of the sequences is relatively high. Pringle et al. (2015) substantiates this by stating a key feature of simulated waves is the inclusion of the correct number of extreme events. Another significant difference between wave climates is the observed maximum wave period (40.0 seconds) which is double that of the simulated climate (20.0 seconds). This value may be considered an outlier as it only occurs once in the entire dataset. The next highest value from the observed dataset is 22.0 seconds which varies from the simulated maximum by only 2.0 seconds. Additionally, the same was found for the minimum wave height ( $H_s$ ) for the observed wave data. The value (0.01 metres) was considered an outlier given its single occurrence, with the next highest value of 0.41 metres being a more common reading. An analysis of the wave climate distributions was then carried out.

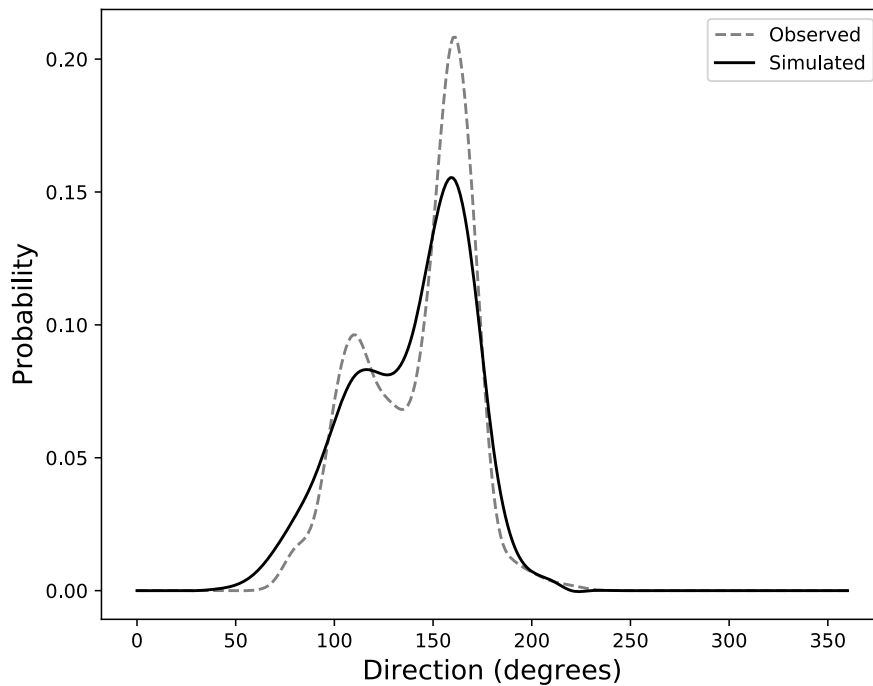


Fig. 5.1 Probability distribution of wave heights based on direction.

Figure 5.1 shows the probability distribution of wave occurrences based on direction. The simulated curve is representative of all 101 wave sequences. The two datasets show good correlation between probabilities across the entire wave spectrum. The observed data curve shows two distinct peaks at around 110 ( $P = 0.096$ ) and 160 ( $P = 0.208$ ) degrees separated by a distinct low around 130 ( $P = 0.070$ ) degrees. This is replicated by the simulated data however not to the same extents. In comparison,

the simulated data yields probabilities of 0.081, 0.082 and 0.155 at 110, 130 and 160 degrees respectively. This may be attributed to the relative dataset sizes. Taking this into consideration, it may be said that both wave climates bear close resemblance in terms of directional occurrences of waves.

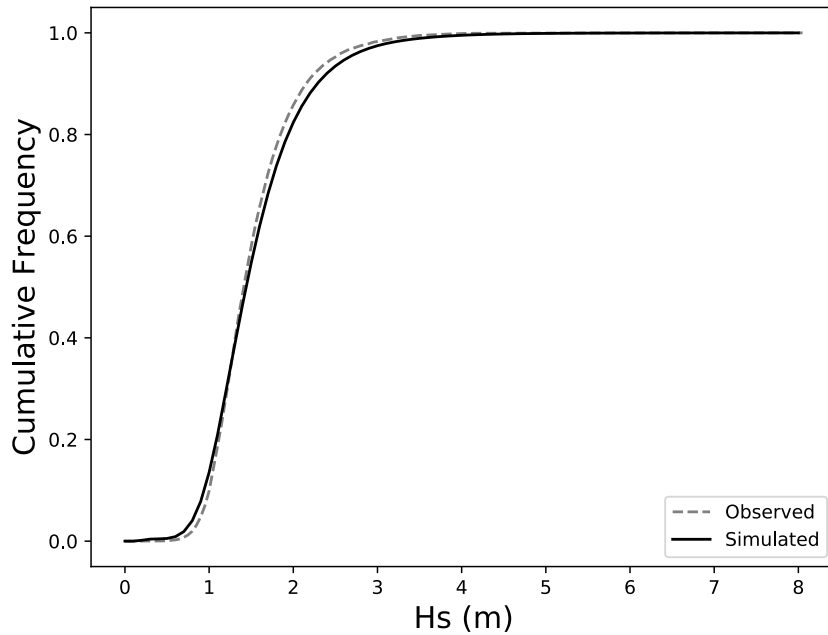


Fig. 5.2 Cumulative frequency distribution for observed and simulated wave heights.

Figure 5.2 shows the cumulative frequency distributions for the observed and simulated wave heights. The simulated curve (*black line*) corresponds to wave heights across all 101 iterations of wave sequences. It is evident that both are very similar regarding distributions of wave heights. The intersection point between curves at approximately 1.3 metres may be used to show the slight variations between datasets. Visibly, the simulated data contains a greater number of wave occurrences below 1.3 metres compared to the observed wave data. In contrast, the observed data exceeds the simulated data for essentially all wave heights above the intersection point until both graphs effectively asymptote at their peak cumulative frequencies.

Taking into consideration the statistical properties of both datasets together with a comparison of wave parameter distributions, it may be said that the simulated wave climate accurately assimilates the observed wave data. Use of the simulated wave climates for long-term model simulations should therefore provide an accurate indication of coastline behaviour.

## 5.2 Model Calibration

### 5.2.1 Longshore Sediment Transport Coefficient

The longshore sediment transport equation was calibrated using the process described in section 4.9. The coastline orientation remained constant at 26.13 degrees clockwise from north. This represented the general orientation of the study region. Figure 5.3 shows the correlation between observed and calibrated data points for both datasets. The calibration coefficient  $K$  was calculated using linear least squares fitting technique which fitted calculated annual transport rates to observed annual transport rates. The regression line was forced through the origin. This method produced a  $K$  value of 0.00030782.

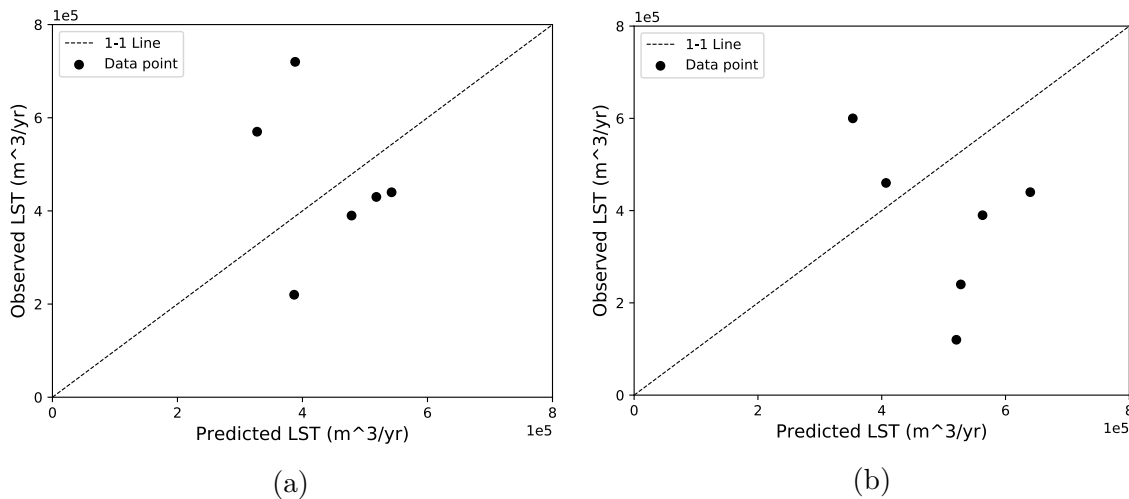


Fig. 5.3 Linear regression plots of calibration (a) and validation (b) data sets showing annual longshore transport (LST).

Although both datasets show no visible correlation to the plotted 1-1 lines in figure 5.3, the calibration data (fig. 5.3a) produces a regression slope of 1. Figure 5.3b depicts a similar correlation, however the regression slope is equal to 0.7. This reduction in correlation may be due to high variability between datasets. Additionally, the size of the dataset given is limited to 12 years which may potentially contribute towards the variation. Schoonees (2000) studied the required measurement periods to obtain a mean long-term longshore transport rate. Schoonees (2000) suggests a measurement period of between 5 and 8 years to obtain an accurate mean longshore transport rate with a deviation within 10% of the long-term mean. Additionally, Roussow (1989) suggests that measurements of at least 5 years are sufficient in representing the long-term wave climate.

## 5.2 Model Calibration

This suggests that the limited data used for model calibration is sufficient in obtaining a relatively accurate calibration coefficient. This suggestion is further justified when considering the 95% confidence interval for the data. Sample size is an important parameter in calculating the confidence interval. The calculated interval is therefore relatively high given the sample size however all data points fall within this range. Schoonees and Theron (1996) identified the same trend, stating that the confidence intervals for the Kamphius equation are very wide. The suggested minimum sample size to produce a statistically significant confidence level exceed the available data by orders of hundreds which may be problematic. Schoonees and Theron (1996) do however state that outliers are points that lie beyond the 95% confidence interval. Significantly, no points fall beyond this threshold.

Schoonees and Theron (1996) carried out a similar calibration of the Kamphius equation however with a sizeably larger dataset. They state that a few data points representing high transport rates are highly influential to the least squares method. Both datasets in this study exhibit points that depict high transport rates. Schoonees and Theron (1996) overcame this by removing the identified points from the dataset which yielded a greater correlation and an improved calibration. This is not possible with this calibration given the limited size of the dataset. The overall predicted longshore transport rates showed relatively strong correlation to the observed data with a regression slope of 0.83. Given the aforementioned points, this is assumed to be sufficient for model calibration. Figure 5.4 illustrates a time series of the observed and predicted data.

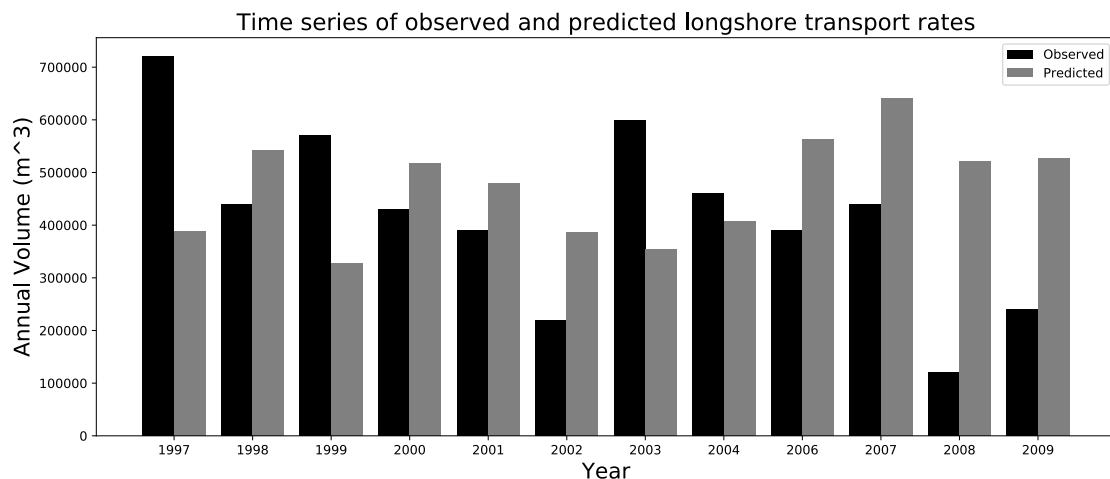


Fig. 5.4 Time series of observed (*black*) and predicted (*grey*) longshore transport rates.

### 5.2.2 Data Correlation

A summary of the calibration data is provided in table 5.2. The table shows a close correlation between mean values for calibration and validation datasets.

Table 5.2 Summarised model calibration results. Slope is the correlation between validation and calibration datasets. Mean is an average annual longshore transport rate for the respective datasets with the associated standard deviation.

Data	Years	Slope	Mean ( $m^3/year$ )
Calibration	6	1.0	$440,302 \pm 77,786$
Validation	6	0.70	$501,910 \pm 95,675$

Upon comparing means for the calibration and validation datasets, the calibration is considered to be sufficiently accurate. Applying the calibration coefficient to the entire simulated dataset yielded a mean of  $471,106 \pm 92,472 m^3/year$ . Comparatively, the observed dataset yielded a mean of  $418,133 \pm 161,133 m^3/year$  with both mean values falling within one standard deviation of the other. These values are also comparable with both the calibration and validation means of  $440,302 \pm 77,786$  and  $501,910 \pm 95,675 m^3/year$  respectively. Figure 5.5 shows this information graphically using a normalised plot.

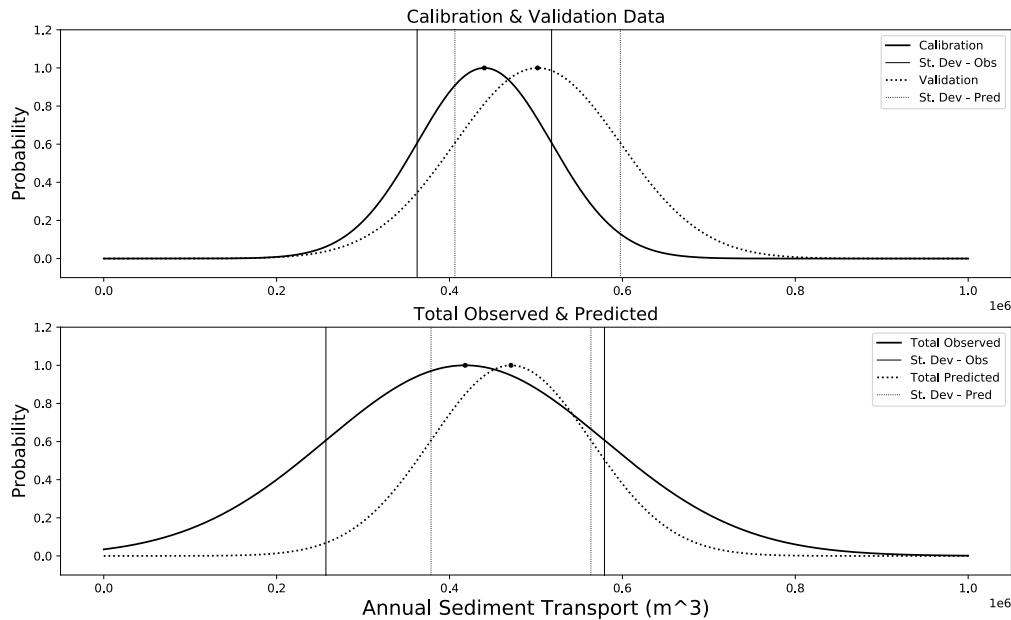


Fig. 5.5 Normalised probability distributions for datasets used in model calibration. Vertical lines correspond to one standard deviation from the mean.

### 5.2.3 Residual Values

In order to validate the assumptions behind a linear regression analysis, Chatterjee and Hadi (1986) suggest the use of a residual plot. A residual plot is essentially the difference between the observed and predicted value plotted relative to a horizontal datum. Figure 5.6 shows the residual plot for the model calibration results.

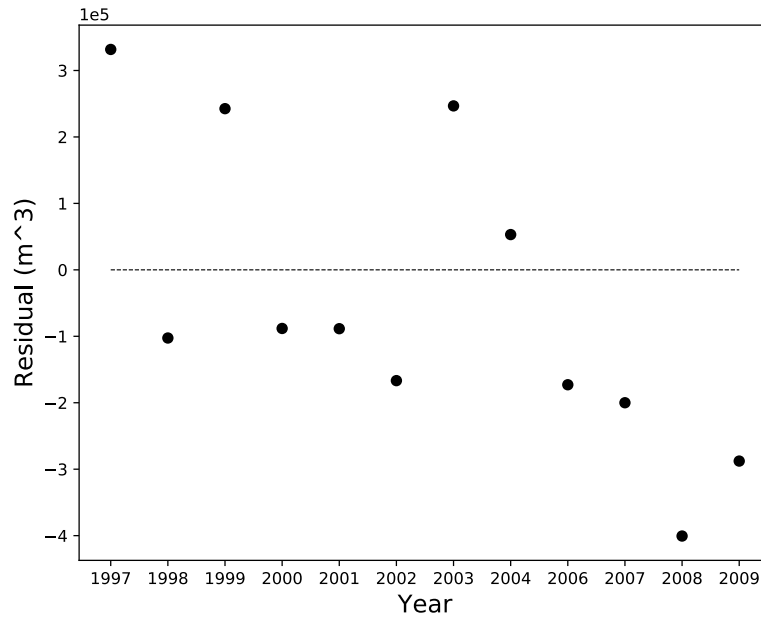


Fig. 5.6 Residual values for calculated and observed longshore transport rates.

It is evident that the residual values are highly variable in the y-direction. Chatterjee and Hadi (1986) suggest that ideal residual plots have the following characteristics:

- Plots are symmetrically distributed with a tendency to cluster centrally.
- Plots cluster around the lower single digits along the y-axis.
- Clear patterns are not visible.

Taking these suggestions into consideration, the following may be said. The plot is relatively symmetrically distributed about the x-axis however there is no clustering. This is likely due to the size of the dataset. With regards to clustering around the x-axis, it is evident that the values do not vary extremely from this datum. There are clear outliers within this dataset however the majority of data is within relatively close proximity to the x-axis. Finally, the plot does appear to be randomly distributed with no clear patterns visible. Considering the following points together with the size of the dataset, it may be said that the calibration is of sufficient accuracy.

## 5.3 Sensitivity Analysis

### 5.3.1 Input Errors

Accurate measurement of wave characteristics (height, direction and period) is difficult. Use of this data within numerical models requires careful consideration of uncertainties involved with obtaining wave input data. Uncertainties may produce erroneous model predictions hence understanding these effects are significant. This section shows the results of a simple sensitivity analysis which attempts to quantitatively predict the effects of small errors in wave input data (height, direction and period). Given the importance of longshore sediment transport ( $Q$ ) in approximating shoreline change, this equation has been selected as the criteria for evaluating model sensitivity. By using a first order Taylor approximation, results may be accurate to within 2 percent. Consider equation 4.15 which requires wave characteristics at breaking conditions. Ignoring all constant quantities and omitting subscripts, 4.15 may be reduced to:

$$Q = H^2 T^{1.5} m^{0.75} \sin^{0.6}(2\theta) \quad (5.1)$$

Given the dependance  $m$  on wave height ( $H$ ), 5.1 may be further reduced to:

$$Q = Q(H, T, \theta) = H^{\frac{13}{8}} T^{1.5} \sin^{0.6}(2\theta) \quad (5.2)$$

Assuming an error  $dH$  in breaking wave height, the relative error in longshore sediment transport ( $Q$ ) may be determined using a first order Taylor series approximation, shown below:

$$\frac{Q(H \pm dH, T, \theta)}{Q(H, T, \theta)} = \frac{H^{\frac{5}{8}}(H \pm \frac{13}{8}dH)}{H^{\frac{13}{8}}} = 1 \pm \frac{13}{8} \frac{dH}{H} \quad (5.3)$$

Similarly, the same analysis may be carried out for an error  $dT$  in wave period, which yields the following:

$$\frac{Q(H, T \pm dT, \theta)}{Q(H, T, \theta)} = \frac{T^{\frac{1}{2}}(T \pm \frac{3}{2}dT)}{T^{\frac{3}{2}}} = 1 \pm \frac{3}{2} \frac{dT}{T} \quad (5.4)$$

Finally, this analysis is done for an error  $d\theta$  in relative wave angle which produces the following result using the small angle approximation:

$$\frac{Q(H, T, \theta \pm d\theta)}{Q(H, T, \theta)} = 1 \pm \frac{1.2 \cos 2\theta}{\sin 2\theta} d\theta = 1 \pm \frac{3}{5} \frac{d\theta}{\theta} \quad (5.5)$$

### 5.3 Sensitivity Analysis

---

This analysis may be expanded to quantify the effects of multiple variable errors. Consider the same errors  $dH$ ,  $dT$  and  $d\theta$  which represent wave height, period and direction respectively. The combined effect may be defined as:

$$\begin{aligned} \frac{Q(H \pm dH, T \pm dT, \theta \pm d\theta)}{Q(H, T, \theta)} &= \left(1 \pm \frac{13}{8} \frac{dH}{H}\right) \left(1 \pm \frac{3}{2} \frac{dT}{T}\right) \left(1 \pm \frac{3}{5} \frac{d\theta}{\theta}\right) \\ &= 1 \pm \frac{13}{8} \frac{dH}{H} \pm \frac{3}{2} \frac{dT}{T} \pm \frac{3}{5} \frac{d\theta}{\theta} \\ &\quad \pm \frac{39}{16} \frac{dH}{H} \frac{dT}{T} \pm \frac{39}{40} \frac{dH}{H} \frac{d\theta}{\theta} \pm \frac{9}{10} \frac{dT}{T} \frac{d\theta}{\theta} \\ &\quad \pm \frac{117}{80} \frac{dH}{H} \frac{dT}{T} \frac{d\theta}{\theta} \end{aligned}$$

Table 5.3 below shows the effect of combined input variable errors on  $Q$ . The variable input error for all calculations is assumed to be 10%. The upper half of the table corresponds to a positive error with the bottom corresponding to a negative error.

Table 5.3 Relative error in longshore sediment transport ( $Q$ ) due to combined input errors.

	$H$	$T$	$\theta$
H	-	1.337	1.232
T	0.663	-	1.219
$\theta$	0.768	0.781	-

As indicated by table 5.3, the combination of wave period and wave height produce the highest relative error of approximately 33.7% in  $Q$ . The combination of either height or period with direction result in a sizeably lower error of 23.2% and 21.9% respectively. This is attributed to the relative exponents operating on the variables in equation 4.15. Comparatively, a 10% error in all input variables results in a 41.7% change in  $Q$ . Taking equation 4.20 into consideration, deviations in shoreline change may be expected of the same order. A study by Hanson (1989) found a 50% error in  $Q$  using the CERC equation for the same input variable error.

### 5.3.2 Accuracy and Stability of Solution Scheme

Model accuracy and stability was investigated in terms of coastline change at a selected position relative to a baseline value. To accomplish this, a hypothetical beach spanning 500 metres was set up using a constant grid spacing of 50 metres. The coastline incorporated no undulations and coastline width was 8 metres throughout. A hard boundary was situated at the interface between the coastline and the hinterland. The simulation period was 240 hours using constant wave height, period and direction of 2.5 metres, 10 seconds and 125 degrees respectively. The beach is bounded by a zero gradient Neumann boundary at the right end and a zero flux Dirichlet boundary at the left end. This hypothetical situation replicates sediment buildup on the up-drift side of an impermeable groin. Coastline positions are measured at the left boundary as this represents the point of most movement. Results are presented in table 5.4, with the upper half of the table presenting the effect of varying time steps and the lower half presenting the effects of varying grid intervals.

Table 5.4 Stability and accuracy of explicit numerical scheme for labelled schemes.

<b>Constant <math>\Delta x</math>, Varying <math>\Delta t</math></b>				
$\Delta t(hrs)$	Courant No. ( $R_s$ )	Coastline Position ( $m$ )		
		$t = 60 hrs$	$t = 120 hrs$	$t = 240 hrs$
0.5	0.03	14.77	18.15	23.03
1	0.07	14.75	18.14	23.04
2	0.14	14.70	18.10	23.05
6	0.41	14.48	17.95	23.09
12	0.83	14.70	17.72	23.13
24	1.65	-	17.27	23.21

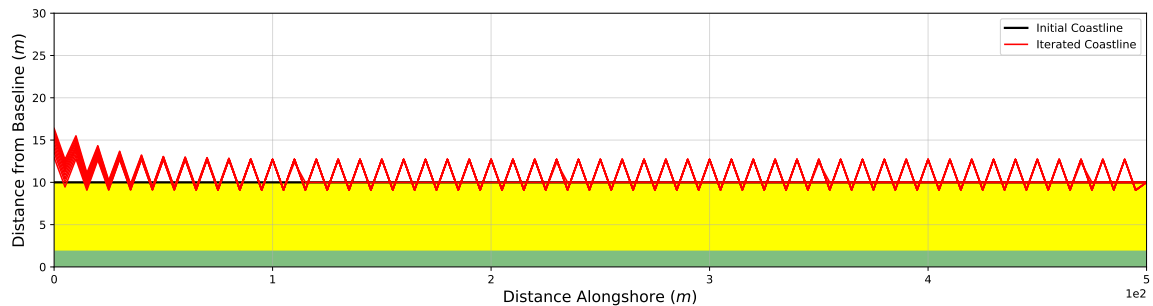
  

<b>Constant <math>\Delta t</math>, Varying <math>\Delta x</math></b>				
$\Delta x(m)$	Courant No. ( $R_s$ )	Coastline Position ( $m$ )		
		$t = 60 hrs$	$t = 120 hrs$	$t = 240 hrs$
5	5.09	Unstable		
10	2.01	17.59	21.08	25.83
25	0.46	16.46	19.91	24.83
50	0.07	14.75	18.14	23.04
100	0.02	12.74	15.26	19.57

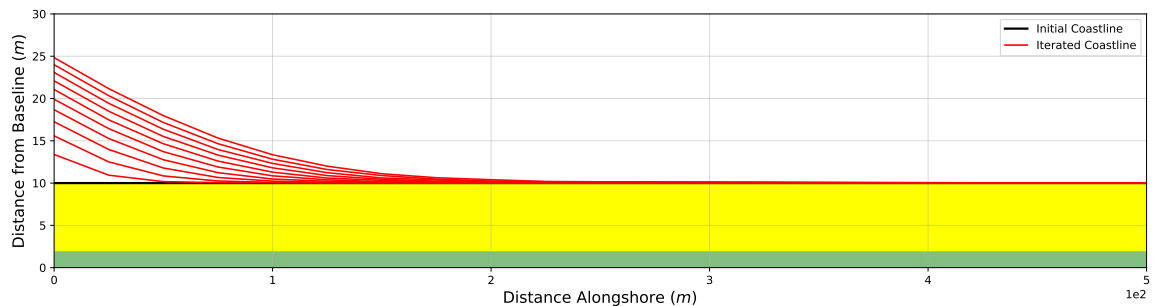
### 5.3 Sensitivity Analysis

Taking into consideration the coastline positions in the upper half of table 5.4, it is evident that for time steps less than 6 hours, the values vary minimally across the entire simulation period. Furthermore, the corresponding stability parameters ( $R_s$ ) fall into the stable region defined by Hanson (1989) who defines 0.5 as an upper limit for explicit scheme stability. Beyond this threshold, coastline positions show minimal variation. Significantly, coastline positions corresponding to the 60 and 120 hour elapsed simulation time exhibit similar behaviour, decreasing with an increase in time step whereas the 240 hour column increases with an increase in time step. This may be indicative that an increase in time step leads to slower convergence of the model.

From the bottom half of table 5.4, low grid intervals expectedly yielded high stability parameters given the formulation of equation 4.28. Coastline positions for the elapsed times show the same behaviour as the stability parameter, decreasing with an increase in grid interval. Furthermore, coastline positions vary significantly more than for varying time steps, indicating that time step adjustments should be favoured over grid interval adjustments. Large grid spacings prevent accurate representation of small scale coastline features. Figure 5.7 shows examples of unstable and stable simulations with a grid spacing of 25 metres due to the domain length. Intervals of 50 metres were adequate for the study domain (10,000 m) as well as for computational efficiency.



(a)



(b)

Fig. 5.7 An unstable simulation (a) and a stable simulation (b).

## 5.4 Continuous Sediment Supply

Littoral drift of sediment is the primary supplier of sand to the study region. This section explores the effects of a continuous supply on coastline evolution. Table 5.5 summarises all necessary input data required for long term simulations.

Table 5.5 Input data for model simulations with descriptions and the associated value.

Variable	Value	Unit	Description
$K$	0.00030782	-	Calibration coefficient
$D_c$	15.14	$m$	Depth of closure
$D_b$	5.78	$m$	Berm height
$\Delta t$	1	$hour$	Model time step
$\Delta x$	50	$m$	Grid Interval
$D_{50}$	1.19	$mm$	Median sediment diameter
$\rho_w$	1030	$kg/m^3$	Saltwater density
$\rho_s$	2650	$kg/m^3$	Sand density
$p$	0.4	-	Porosity

### 5.4.1 Sediment Demand

In order to simply approximate the annual sediment demand for the domain, simulations were carried out with a constant, specified sediment influx at the uMngeni boundary (see fig. 3.1 for domain). A Dirichlet boundary at uMngeni and a Neumann boundary at uMhlanga were implemented to achieve this. Using measured data as a guideline, the fixed annual sediment supply ranged from 300,000 to 600,000  $m^3/year$  at 50,000  $m^3/year$  intervals, imposed in the form of a constant longshore transport rate obtained by dividing the annual supply volume by the number of seconds in a year. The simulation period was 50 years. Simulations were run 10 times for the 300,000, 450,000 and 600,000  $m^3/year$  supply rates using differing set of randomly selected wave sequences while all remaining supply rates were simulated once.

Figure 5.8 indicates a strong linear relationship between annual sediment supply and net sediment change. The trend line has a slope of 0.994 with a  $R^2$  value of 0.991. All simulation results fall within or in close proximity to the 95% confidence interval shown on figure 5.8. Using this linear relationship, it was estimated that an annual longshore sediment supply of around 460,961  $m^3/year$  would produce a zero

## 5.4 Continuous Sediment Supply

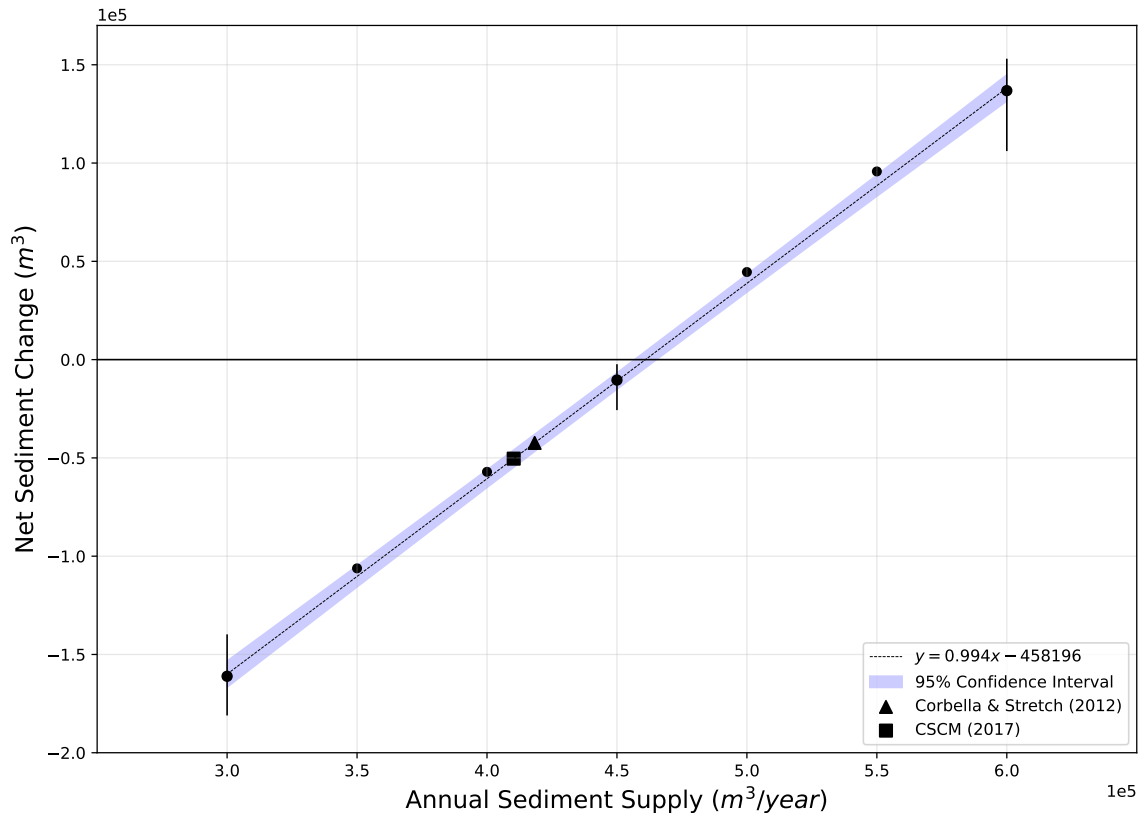


Fig. 5.8 Sediment influx versus net sediment change in model domain with the associated trend line. Labelled markers indicate measured rates by the respective studies and bars indicate value ranges.

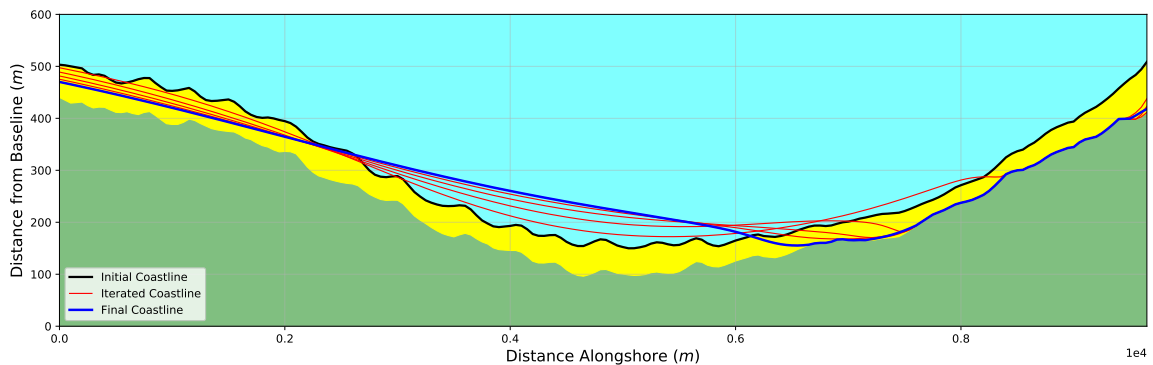
net sediment change within the model domain. This value represented the minimum influx required to maintain a sediment balance assuming a continuous supply of sand. This value was compared to observed and estimated sediment changes obtained from a number of studies carried out in the region. Figure 5.8 also shows observed supply rates or net sediment changes from different studies along the Durban coastline. Corbella and Stretch (2012b) analysed the sediment balance for the Durban Bight between 1996 and 2009, estimating the mean sediment supply from the Durban sand trap to be approximately  $418,333.3 \text{ m}^3/\text{year}$ , represented by the triangle on figure 5.8. This supply corresponded to an annual sediment change of  $-42,372.7 \text{ m}^3$  for a continuous sand supply. The observed beach erosion observed by the eThekweni Municipality of approximately  $-50,382.2 \text{ m}^3/\text{year}$  (square) between October 2011 and January 2017 corresponds to a mean sediment supply of  $410,275.5 \text{ m}^3/\text{year}$ . Both loss rates show good correlation and fall below the x-axis which may indicate that inadequate longshore sediment supplies are the primary cause of erosion. Notably, the observed sediment loss

## Results & Discussion

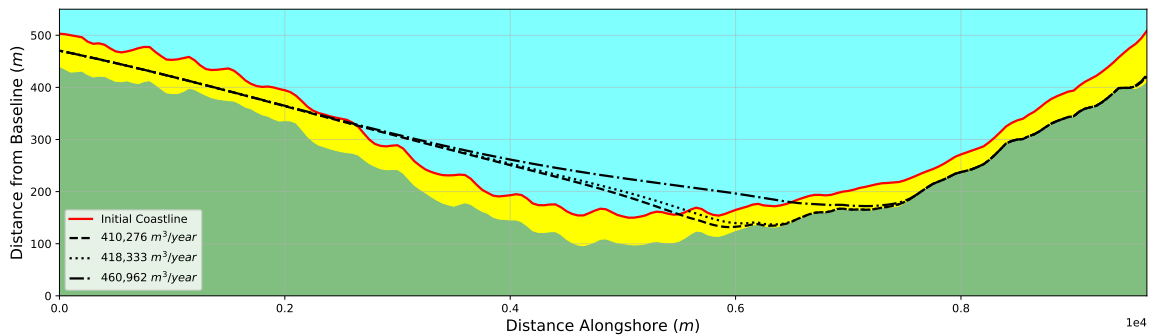
by eThekweni Municipality corresponds to a lower supply rate than that estimated by Corbella and Stretch (2012b), inferring that processes along the Bight region prevent longshore migration of sand. Although highly variable, these values are a satisfactory estimate for further analysing shoreline evolution.

### 5.4.2 Coastline Evolution

Prediction of the long term coastline position in addition to volume changes presents significant objective. Longshore supply rates estimated previously are simulated over 50 years to obtain final plan beach shapes. All supply rates were run 10 times using the same set of wave sequences for comparative purposes. The blue shaded region represents the ocean and the yellow shaded region represents the coastal region. Beach widths were interpolated using eThekweni Municipality's beach survey data. Green areas indicate the hinterland. The interface between the beach and the hinterland (*yellow and green*) was used as vertical boundary limits for erosion.



(a)



(b)

Fig. 5.9 Randomly selected 50 year simulation result with 10 year intervals shown in red (a) and average final beach positions for the labelled supply rates (b).

Figure 5.9a shows the result for a single wave sequence over a 50 year simulation period with 10 year iterations labelled. A continuous sediment influx was imposed at the uMngeni of  $460,961 \text{ m}^3/\text{year}$ . The red lines show that coastline change slows down over time due to the general orientation. Due to lack of observed wave data and coastal surveys for the same period, comparisons with historic data were not possible.

Figure 5.9b shows average final beach positions for the labelled supply rates. Expectedly, the profiles for the eThekweni (2017) and Corbella and Stretch (2012b) supply rates show very close resemblance given the small difference in supply volume. The difference in sediment supply volume appears to be concentrated towards the right side of the remaining coastline. This is due to the position of the sediment supply together with the incoming wave climate. All three profiles converge at approximately the same point for all simulations. In reality, this phenomenon occurs due to the existence of rock outcrops and headlands at the uMhlanga lighthouse which are not reflected in the model. The model does however indicate that coastline orientation plays a role in thus equilibrium state being reached.

It may be said that the coastline is generally re-orientating itself towards the dominant wave angle. This may be due to an inadequate sediment supply together with high seasonal variations in wave characteristics. Seasonal wave roses (fig. 3.4) show a high proportion of SSE incidence waves together with increased wave heights during autumn and winter. Offshore features such as rock reefs are likely to prevent these profiles from occurring, resulting in a more even distribution of sediment however these were not accounted for in the model. Generally, these results indicate that assuming a continuous sediment supply, influxes used for these simulations are adequate in conserving sediment volume in the long term, however more sediment is required to prevent severe localised erosion.

### 5.4.3 Area Conservation

Figure 5.10 shows coastline evolution for a single 50 year simulation. Although this supply rate exceeds the required equilibrium volume by approximately  $140,000 \text{ m}^3/\text{year}$ , figure 5.10 suggests additional sediment volumes are required to maintain beach width throughout the domain. The plotted shoreline positions indicate sediment buildup between approximately 2.2 and 9 kilometres alongshore while the region between 0 and 2.2 kilometres appears to experience erosion. The region immediately adjacent to the uMngeni boundary shows relatively low variability which may be attributed to the wave sequence however the general shoreline trend indicates conservation of beach width along the total coastline.

## Results & Discussion

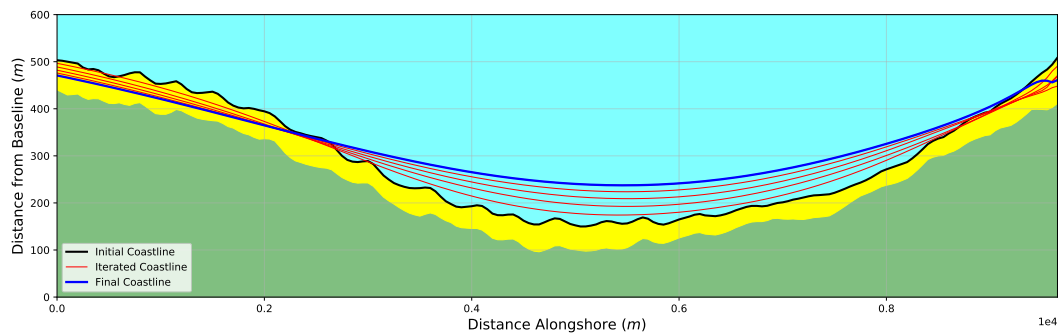


Fig. 5.10 Coastline plan evolution for a sediment supply rate of  $600,000 \text{ m}^3/\text{year}$ .

In plotting plan area change over the 2400 metres of coastline adjacent to the uMngeni boundary, a relationship can be obtained to calculate the minimum supply required to maintain beach plan area (fig. 5.11). Simulations were run using supply rates of between  $500,000$  and  $600,000 \text{ m}^3/\text{year}$  at  $20,000 \text{ m}^3/\text{year}$  intervals. The same wave sequence was used throughout. Using the trend line shown, the minimum sediment required for maintaining beach width in this region and throughout the domain is approximately  $596,183 \text{ m}^3/\text{year}$ . This value is significantly higher than the sediment supply required for volume conservation of  $460,961 \text{ m}^3/\text{year}$ , inferring that a distinction should be made between beach volume conservation and beach width maintenance.

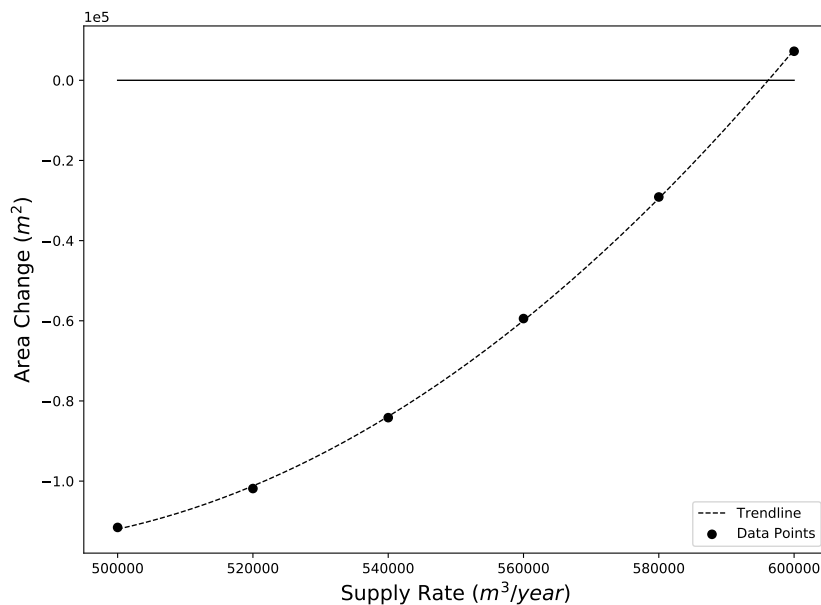


Fig. 5.11 Sediment influx versus change in area for the aforementioned 2.4 km stretch of coastline with the trend line.

### 5.4.4 Erosion & Accretion Rates

Seasonal erosion and accretion rates are summarised in table 5.6 for observed and estimated supply rates relevant to this study. Tabulated values are a mean of ten 50 year simulations using the same wave sequences for all supply rates.

Table 5.6 Annual erosion and accretion rates for various sediment inputs. The sum row represents the resultant annual erosion rate for the given supply rate.

<b>Erosion &amp; Accretion Rates (<math>m^3m^{-1}year^{-1}</math>)</b>			
Season	Longshore Supply Rate ( $m^3/year$ )		
	410,276	418,333	460,961
Summer	2.83	3.04	4.13
Autumn	-4.80	-4.45	-3.35
Winter	-5.90	-5.68	-4.67
Spring	2.45	2.66	3.78
Sum	-5.42	-4.43	-0.12

In accordance with the findings in section 5.4.2, high variations in erosion/accretion rates are experienced due to the seasonal influence on wave climates. Summer and spring appear to be recovery periods for beaches as these seasons cause accretion for all supply rates. Autumn and winter are dominated by erosion with winter yielding the greater erosive capability. These findings are in line with seasonal wave roses discussed previously where winter and autumn periods result in high prevalence of SSE waves. Relating to the 476,607  $m^3/year$  supply rate, the resultant estimated rate of accretion essentially equalled zero, which was expected.

Corbella and Stretch (2012b) estimated an erosion rate of 1.97  $m^3m^{-1}year^{-1}$  for the Durban Bight by analysing changes in measured cross shore profiles. This erosion rate translated into a net sediment change of -19010.5  $m^3/year$ . Model simulations predict that assuming a continuous sediment supply of 418,333  $m^3/year$  into the study region, the anticipated erosion will be to the order 4.43  $m^3m^{-1}year^{-1}$ , approximately double that of the Durban Bight. This may be primarily due to differing wave mechanics and the presence of coastal structures within the region. For the same angle of wave incidence, the Durban Bight will experience roughly 22.7 % more longshore sediment transport than the uMngeni-uMhlanga region.

## 5.5 Longshore Sand Wave Migration

In addition to the sand-bypassing scheme, uMngeni River constitutes the second major sediment source for the study region. River sediment discharges often form sand waves which propagate along the coastline under wave action. Anthropogenic activities along the river such as dam construction and sand mining have severely depleted river sediment deposits to the coastline. This section explores the significance of river discharges in the form of sand waves to understand the contribution of rivers to coastline evolution. Furthermore, this section aims to understand sand wave behaviour within the model domain by investigating the effects of river discharge aspect ratios on retention time within the domain. The terms sand wave, nourishment and river discharge will be used interchangeably in this section.

### 5.5.1 Advection Rate Calibration

Advection rates of sand waves assumed to be formed by river discharges were compared to observed migration rates of sand waves surveyed by the eThekweni Municipality between June and September of 2007. Observed advection rates were estimated using monthly survey data which tracked wave crest positions of sand waves. The advected distance was divided by the time between surveys to obtain an advection velocity. Two sand waves were used to calibrate and validate modelled advection rates, shown in figure 5.12. Figure 5.12a was used as the calibration sand wave. Figure 5.12b was used as the validation sand wave although this wave was tracked over a shorter period. Calibration and validation data was limited to very short periods given the erratic behaviour and physical mechanisms behind sand wave formation.

The calibration process involved estimating sand wave sizes and positions from the survey data followed by their placement at the corresponding position within the model domain. Observed wave data for the exact period was used to estimate an advection rate for the model which was thereafter compared to the observed advection velocity. A linear regression analysis was used to fit the predicted advection rates to the observed rates. The validation sand wave was thereafter used to ascertain the accuracy of the calibration. Calibration of the coastline change equation (eqn. 5.6) was done by introducing a calibration coefficient  $K_{adv}$  to equation 5.6 such that it becomes:

$$\frac{\partial y}{\partial t} + K_{adv} \frac{S_{x,0}}{(D_c + D_b)B} \frac{\partial y}{\partial x} = \frac{1}{D_c + D_b} \frac{\partial Q}{\partial x} \quad (5.6)$$

## 5.5 Longshore Sand Wave Migration

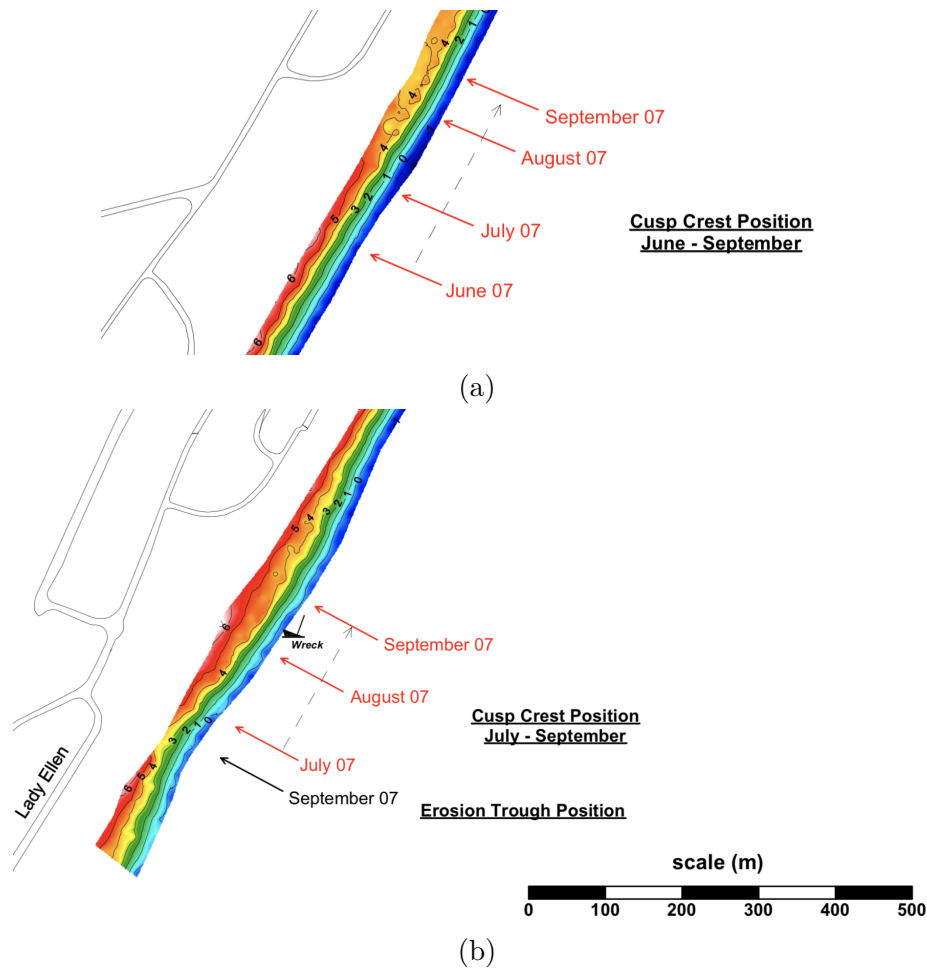


Fig. 5.12 Observed sand waves used for model calibration (a) and validation (b). Arrows indicate crest positions at monthly intervals (eThekweni Municipality, 2017).

Table 5.7 presents the results of the advection velocity calibration. The validation sand wave was not tracked over the June - July period hence the lack of data. Linear regression analysis yielded a calibration coefficient of 0.4534.

Table 5.7 Summarised advection rate calibration results. Advection rates are presented in *km/year*.

Period	Calibration Data		Validation Data	
	Observed	Simulated	Observed	Simulated
June - July	0.99	1.09	-	-
July - August	1.27	1.09	1.27	1.20
August - September	0.71	0.81	0.99	1.20

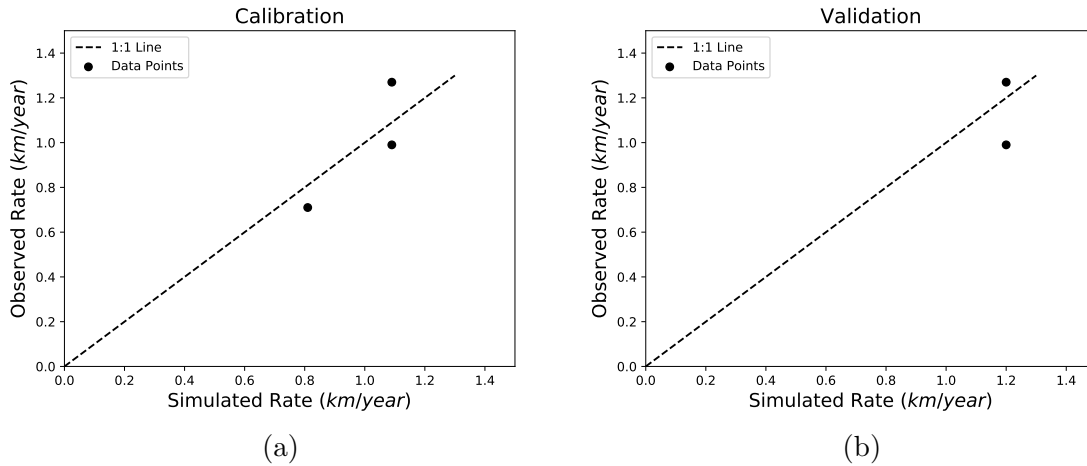


Fig. 5.13 Linear regression analysis results for calibration (a) and validation (b) datasets.

Figure 5.13 shows the results of the linear regression analysis. Figure 5.13a shows relatively good correlation to the 1:1 line shown, indicating a calibration of sufficient accuracy. Although the validation dataset contained less values than the calibration dataset, figure 5.13b indicates that the calibration was generally of a satisfactory accuracy. Discrepancies in values may be attributed to the inaccurate estimation of sand wave crest positions together with inaccurate estimation of sand wave parameters. Given the dependence of advection velocity on sand wave amplitude, incorrect estimation would significantly affect results. Furthermore, for model stability purposes, the coastline grid interval was restricted to 50 metres which greatly influenced the modelled position of the sand wave crest to factors of 50. Generally, it may be said that the advection rate calibration is sufficient for use in this study.

### 5.5.2 Sand Wave Advection

By virtue of equation 5.6, advection rates of sand waves are dependent on the amplitude of the wave together with the depth of closure and the alongshore transport rate. Understanding the effect of sand wave aspect ratios on advection rates is potentially significant in understanding how these sand waves contribute to coastline evolution as well as how long they remain in coastal systems.

In order to investigate advection rates, a constant alongshore river discharge length of 500 metres was assumed with a varying sediment discharge volume which varied the sand wave amplitude. Theron et al. (2008) stated that assuming a 10% sand load, the uMngeni River discharges approximately  $11,351 \text{ m}^3$  of sediment annually for a post-anthropogenic influence scenario. Comparatively, the pre-anthropogenic scenario

## 5.5 Longshore Sand Wave Migration

---

discharged around  $112,594 \text{ m}^3$  of sediment annually. These values were used as a range for river discharge volumes.

Plan shapes of river discharges along the Durban coastline are variable given the complex nature of the process. For application within this model, discharge shape is defined by the alongshore width and discharge volume. An internal algorithm then acts to calculate an amplitude based on these parameters. Furthermore, the plan shape is assumed to resemble a gaussian distribution, or essentially a triangular shape in plan. Simulations were run 5 times for river discharge volumes between 10,000 and 110,000  $\text{m}^3/\text{year}$  at 20,000  $\text{m}^3/\text{year}$  intervals. The same set of wave sequences were used for all river discharge volumes for comparative purposes. The simulation period used was 1 year as smaller discharges advect through the domain for greater simulation lengths. Table 5.8 details the various discharge volumes used for simulations together with their physical parameters.

Table 5.8 River discharge physical parameters.

Discharge Volume ( $\text{m}^3$ )	Amplitude ( $B$ ) ( $m$ )	Width ( $L$ ) ( $m$ )	Aspect Ratio ( $B/L$ ) ( $-$ )
10,000	2.29	500	0.00458
20,000	4.58	500	0.00916
30,000	6.87	500	0.01774
50,000	11.44	500	0.02288
70,000	16.02	500	0.03204
90,000	20.59	500	0.04118
110,000	25.17	500	0.05034

Figure 5.14 shows advection velocities for the river discharges detailed in table 5.8. Figure 5.14 exhibits the relationship presented in equation 5.6, showing a decrease in advection velocity with an increase in aspect ratio/amplitude. Significantly, the relationship does not appear to be linear as figure 5.14 indicates a decreasing rate of change of advection velocity with an increase in aspect ratio. The general coastline shape plays no role in the results presented as advection velocities are entirely dependent of the relative angle between the incoming wave and a zero-orientation coastline. Results are therefore entirely dependent on wave data and physical parameters of sand waves. In addition to advection, diffusion constitutes another dominant physical process along coastlines. Investigation of the effects of aspect ratios on sand wave diffusion presents another potentially import relationship.

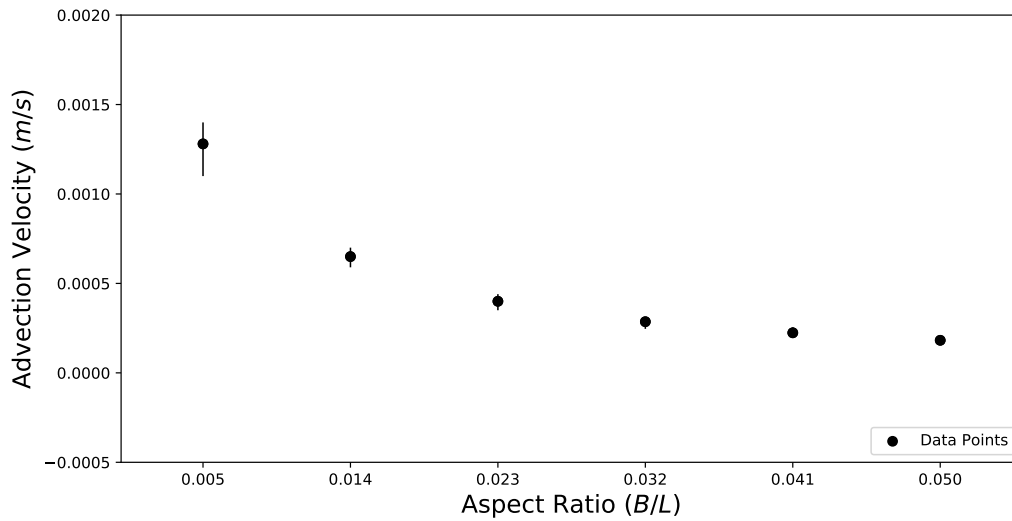


Fig. 5.14 Advection velocities for various aspect ratios with min-max ranges.

### 5.5.3 Sand Wave Diffusion

This section explores the diffusivity effects of varying aspect ratios (width:length ratio) on sand waves. As with the advection investigation, sand waves detailed in table 5.8 were used for simulations assuming a constant alongshore width of 500 metres. Similarly, simulations were carried out 5 times per discharge volume/aspect ratio. Figure 5.15 shows percentage change in sand wave amplitude after 1 year for river discharges detailed in table 5.8. Percentage changes are calculated by comparing start and end amplitudes of the sand wave over the simulation period.

Figure 5.15 indicates that the smallest aspect ratio/ river discharge ( $10,000\text{ m}^3$ ) results in the lowest amount of diffusion, with an amplitude reduction of 39.65%. Interestingly, discharge volumes corresponding to  $30,000\text{ m}^3$  and greater show highly similar diffusion amounts at the end of the simulation period, all remaining around the 70% region. This indicates that river discharges greater than  $30,000\text{ m}^3$  essentially experience the same amount of diffusion regardless of aspect ratio. Furthermore, larger river discharges are subject to greater diffusion rates than smaller discharges.

Considering the similarity of reduction values for river discharges greater than  $30,000\text{ m}^3$ , an intermediary point between the  $10,000\text{ m}^3$  and  $30,000\text{ m}^3$  discharges of  $20,000\text{ m}^3$  was simulated to ensure that the  $10,000\text{ m}^3$  point was not an outlier. Figure 5.15 confirms that diffusion rates increase with increases in aspect ratio or increases in sand wave amplitude, which may potentially define a threshold point beyond which the diffusion rate is essentially constant.

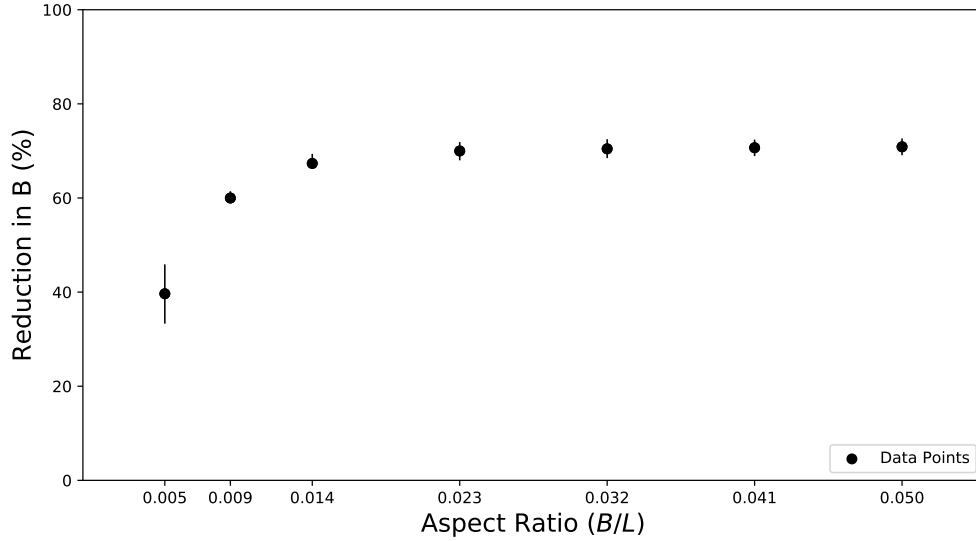


Fig. 5.15 Percentage reduction in sand wave amplitude after 1 year.

#### 5.5.4 Advection-Diffusion Relationship

Although the previous two sections highlight important relationships between river discharge parameters and physical mechanisms, the analysis integrated dimensional relationships which are not scaleable. In understanding the dimensionless relationship between diffusion and advection of varying aspect ratios, this formulation may be applied to all sand waves along the Durban coastline. To investigate this, diffusion and advection coefficients were obtained from equation 5.7:

$$\frac{\partial y}{\partial t} + \frac{S_{x,0}}{(D_c + D_b)B} \frac{\partial y}{\partial x} = \frac{s_x}{D_c + D_b} \frac{\partial^2 y}{\partial x^2} \quad (5.7)$$

where  $s_x$  is the gradient of the  $S - \phi$  curve. By introducing a time scale  $T$  together with an alongshore length scale  $L$ , equation 5.7 becomes:

$$\frac{T}{L} \frac{\partial y}{\partial t} + \frac{T}{L} \frac{S_{x,0}}{(D_c + D_b)B} \frac{\partial y}{\partial x} = \frac{T}{L} \frac{s_x}{D_c + D_b} \frac{\partial^2 y}{\partial x^2} \quad (5.8)$$

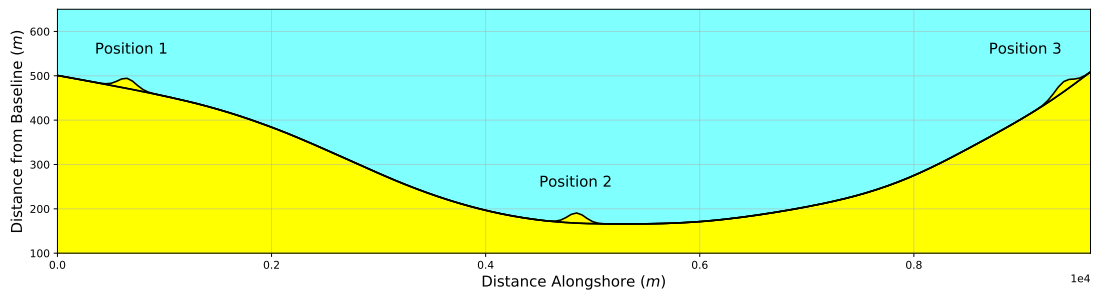
Finally, cancelling out units and extracting time scales produces:

$$T(\text{Diffusion}) = \frac{DL^2}{s_x} \quad (5.9)$$

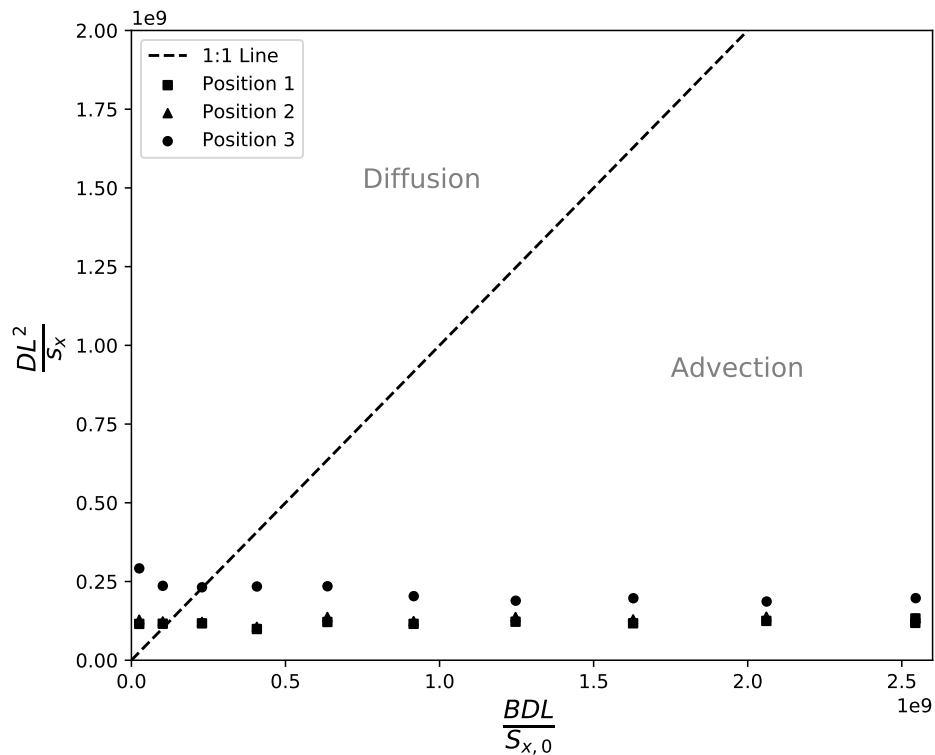
$$T(\text{Advection}) = \frac{BL(D_c + D_b)}{S_{x,0}} \quad (5.10)$$

## Results & Discussion

Figure 5.16b shows a scatter plot of diffusion versus advection coefficients for a number of discharge aspect ratios at three different positions along the coastline (see fig 5.16a). Plotted values represent the relationship between the labelled advection and diffusion coefficients, with the aspect ratio increasing from right to left. Table 5.9 details the physical parameters of river discharges used in figure 5.16b. Alongshore discharge length remained constant at 500 metres. Average wave statistics from table 5.1 were used for this section.



(a)



(b)

Fig. 5.16 Dimensionless diffusion-advection relationship for varying river discharge volumes (b) with discharge positions (a).

## 5.5 Longshore Sand Wave Migration

Table 5.9 River discharge physical parameters. Volumes in the first row are  $\times 10^3$ .

Volume	10	20	30	40	50	60	70	80	90	100
$B$ (m)	2.29	4.58	6.89	9.15	11.44	13.73	16.02	18.31	20.60	22.88
$B/L$	0.005	0.009	0.013	0.018	0.023	0.027	0.032	0.037	0.041	0.046

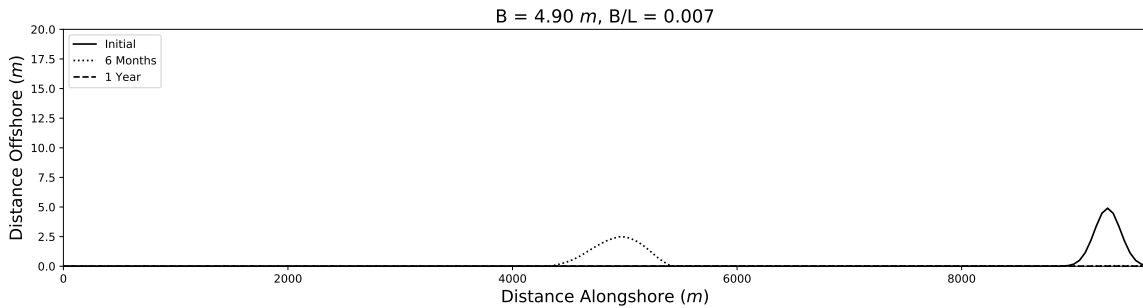
From figure 5.16b, it is evident that for the river discharge aspect ratios used, the dominant process along the Durban coastline is advection. The relationship shown indicates an increase in advection dominance with a decrease in sand wave amplitude. Apart from the 100,000  $m^3$  and 90,000  $m^3$  discharges corresponding to aspect ratios of 0.046 and 0.041 respectively for all positions, all remaining discharge volumes fall within the advection domain of the plot. Significantly, the 80,000  $m^3$  discharge for position 3 together with the 90,000  $m^3$  discharge for positions 1 and 2 essentially fall along the 1:1 line shown, indicating that an aspect ratio of between 0.037 and 0.041 is critical for balanced diffusion and advection. Furthermore, this result infers that relative positions of sand waves along the coastline impact on the diffusion-advection relationship of nourishments due to relative coastline orientations. Given that advection does not vary based on coastline position but rather based on sand wave amplitude, changes in coastline position will only affect the diffusion term.

The relationship presented in figure 5.16b is significant as it may be applied to sand waves formed by any mechanism as long as the approximate aspect ratio is known. It may therefore be applied to river discharges as well as shore nourishments operated at the Durban Harbour entrance to predict advection rates and retention times within the relevant coastal region. Considering that the primary aim of a nourishment scheme is to replenish beaches, it is evident that nourishments with aspect ratios greater than 0.037 will generally be diffusion dominated and will yield longer retention times within the coastal system due to the reduced advection rate.

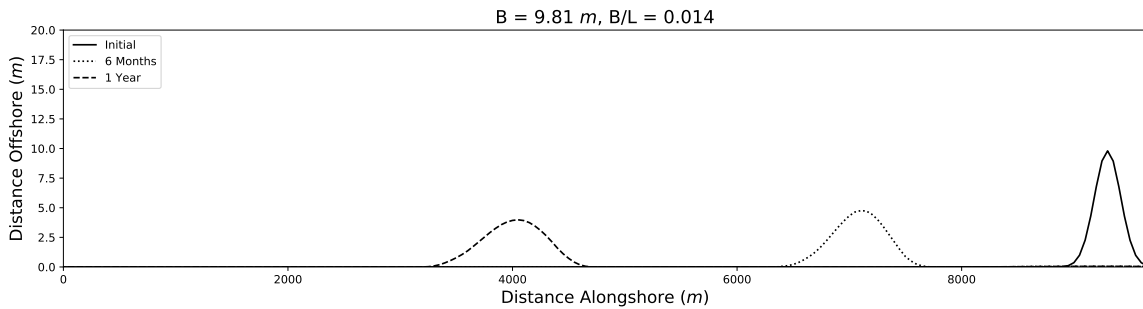
An aspect ratio of between 0.037 and 0.041 results in essentially balanced diffusion and advection of sand waves along the Durban coastline. Nourishments experience adequate diffusion while simultaneously advecting along the coast at a reasonable rate. This aspect ratio is based on the assumption that nourishments or discharges are essentially triangular in plan shape. A shortcoming of the analysis presented in figure 5.16b is the concentration of data towards the advection axis of the plot. Further studies should include a greater range of aspect ratios to obtain a greater spread of data. The next section provides visual examples of aspect ratio effects on sand wave evolution.

### 5.5.5 River Discharge Behaviour

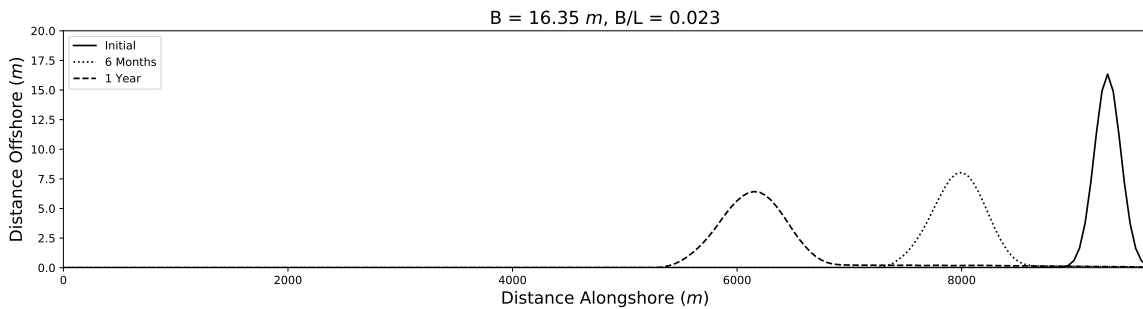
This section explores the advection and diffusion of a river sediment discharge or sand wave along the model domain for varying aspect ratios. Alongshore discharge width is constant at 700 metres with varying discharge volumes and amplitudes. For comparative purposes, three different discharge sizes were simulated once from the same starting point using the same wave sequence and simulation period of one year. Figure 5.17 shows the isolated sand wave along the duration of the simulation.



(a)



(b)



(c)

Fig. 5.17 Simulated sand wave behaviour over 1 year for a 30,000 m<sup>3</sup> (a), 60,000 m<sup>3</sup> (b) and 100,000 m<sup>3</sup> (c) river sediment discharge. Figure titles indicate amplitude of initial sand wave together with the aspect ratio.

## 5.5 Longshore Sand Wave Migration

---

Figure 5.17a corresponding to a river discharge of  $30,000 \text{ m}^3$  indicates an advection dominated sand wave with minimal diffusion over the simulation period. The sand wave position at the 1 year point has surpassed the left bound of the model domain due to the high advection velocity experienced. This size of sand wave experiences minimal diffusion as the relative orientations of coastline segments are highly similar. This results in small gradients between longshore sediment transport values, hence resulting in minimal diffusion. This phenomena also infers that small sand waves reach a point where the rate of diffusion is essentially negligible. In reality, sand waves of this size are likely to diffuse out completely relatively quickly due to the involvement of cross-shore process, inferring that small sand waves are potentially insignificant to coastline evolution.

In comparison, the  $60,000 \text{ m}^3$  discharge displayed a slightly different behaviour, exhibiting more diffusion as well as a slower advection rate. Similarly, the  $100,000 \text{ m}^3$  river discharge displays the highest amount of diffusion together with the slowest advection rate. In agreement with the findings in section 5.5.3, it is evident that river discharges of higher amplitudes are more beneficial to the coastal system given that their retention time is increased accordingly together with high amounts of diffusion. Smaller discharges are unlikely to have any significant effects on coastline behaviour unless their aspect ratios are such that the amplitudes are high.

### 5.5.6 Extreme Event Occurrence

Extreme events refer to severe floods which promote the vertical erosion of sediment along the river bed (Cooper, 1993). This eroded material is flushed out of the river mouth where it forms an ephemeral delta in the sea (Cooper, 1993). These offshore deltas are rapidly dispersed due to wave action and currents and are progressively worked onshore by the natural processes. Cooper (1993) implies that coastlines are cyclically nourished by major floods which result in large sediment discharges from rivers. This section explores the behaviour of a significantly large river discharge

In order to simulate the effects of a major flood event such as the 1987 flood in Durban (see Cooper 1993), a single nourishment was introduced into the model domain at the beginning of the simulation. The 1987 flood event was estimated to be a 1:120 year recurrence interval storm according to Cooper (1993). Furthermore, Cooper (1993) estimated that the 1987 flood discharged approximately  $1.8 \times 10^6 \text{ m}^3$  of sediment into the ocean, of which it is suggested that  $1.24 \times 10^6 \text{ m}^3$  consisted of sandy material. Swart (1987); Theron et al. (2008) suggests a slightly lower value of  $720,000 \text{ m}^3$ . According to turbidity measurements by Cooper (1993), the suspended sediment load

## Results & Discussion

---

was estimated to be around  $650,000 \text{ m}^3$ . Assuming the remaining volume is distributed between offshore deltas and onshore nourishments, a storm discharge of  $200,000 \text{ m}^3$  will be used for this study to replicate an extreme flood event. The width of the discharge was varied between 500 and 2000 metres. Table 5.10 presents the the findings relating to extreme flooding events.

Table 5.10 Extreme event discharge results. Retention time refers to the time taken for the sand wave crest to reach the left end of the model domain.

Width - L ( <i>m</i> )	Amplitude - B ( <i>m</i> )	Retention Time ( <i>years</i> )	Advection Velocity ( <i>km/year</i> )
500	45.77	3.83	2.52
1000	22.88	3.49	2.76
1500	15.26	3.17	3.04
2000	11.44	2.85	3.39

Expectedly, advection velocities increase with a decrease in sand wave amplitude which directly affects retention time within coastal systems. Large river discharges such as that shown in figure 5.18 appear to behave differently to those in the previous section in the sense that equilibrium states are reached locally as the sand wave propagates through the system. This is likely due to the relative size of the undulation which results in the discharge leaving a wake of sediment along the coastline. This sediment would act to nourish the relevant regions, with the area adjacent to the uMhlanga boundary appearing to experience the majority of sediment influx. This is due to the general coastline orientation, with the uMhlanga end being more parallel to incoming waves than the uMngeni region. Furthermore, this loss of mass within the main wave would result in an increased advection velocity towards the end of the simulation.

Corbella and Stretch (2012b) found that beaches along the Durban coastline take approximately 2 years to recover from storm damage. Taking into consideration alongshore migration of river discharges of around 2000 metres in width or greater, it is plausible to suggest that these sand waves are a potential recovery mechanism of the coastline given the similarity in time periods. Sediment left behind by the advecting sand wave may however be considered minute given the presence of cross-shore processes.

Grifoll et al. (2014) stated that short term changes following a large fluvial discharge event is large accumulation along the seabed, typically in regions shallower than 30 metres. Sediment is driven offshore by means of intense wave breaking which drive

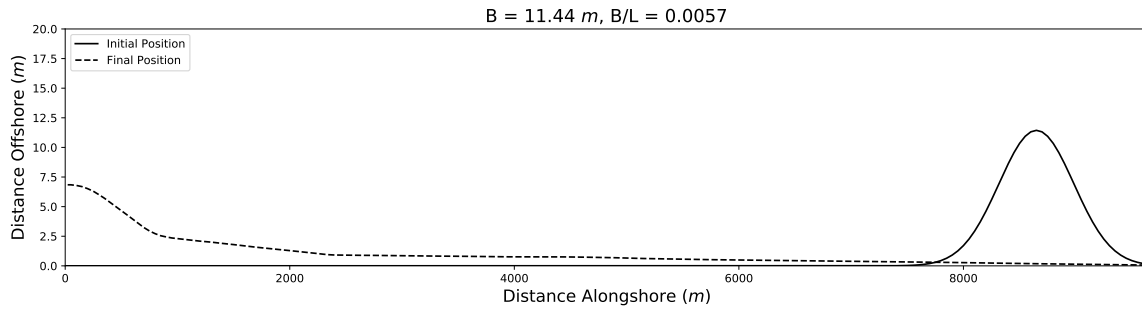


Fig. 5.18 Simulation of a  $200,000 \text{ m}^3$  sand wave with a width of 2000 metres. The plotted lines denote initial and final positions of the sand wave.

strong offshore currents (Hoefel and Elgar, 2003). Long-term changes include reworking and migration of the offshore delta together with sediment resuspension due to wave action. Quick (1991) states that a physical explanation for onshore and offshore sediment movement is yet to be given, with Hoefel and Elgar (2003) concurring in stating that the causes of shoreward sediment transport are not yet known. Quick (1991) does however state that onshore and offshore sediment movement due to calm, long-period waves and storm wave attack respectively is well documented. Cross-shore processes are therefore complex and have not been included within this study. From the results obtained, it may be said that alongshore migration of sand waves are potentially significant mechanisms behind coastline behaviour and evolution.

## 5.6 Nourishment Sand Waves

Net sediment influxes at the uMngeni River are highly variable and inherently dependent on various physical factors such as the wave climate and offshore bathymetry. Not including cross-shore processes, primary sediment sources for the study region may be identified as the uMngeni River and littoral drift from the Durban Bight region. The Durban Bight receives its sediment by means of a sand-bypassing scheme at the Durban harbour entrance. Although they play an important role in maintaining beaches, these schemes are often improperly operated and result in an erratic supply of sediment in the form of occasional, bulk nourishments. These bulk nourishments result in the formation of alongshore sand waves which propagate along the coastline. Supplied sediment may be deemed adequate for coastline maintenance however the erratic nature may result in undesirable coastline evolution. Investigation of how nourishments behave along coastlines is important in improving operation of nourishment schemes.

### 5.6.1 Nourishment Frequency Effects

Pumping frequency of nourishment schemes are variable and dependent on numerous factors such as availability of sediment and equipment capacities. Nourishments are often pumped on numerous occasions within a year, potentially resulting in the formation of numerous sand waves along the coastline. Understanding how sand waves evolve and move through the domain is essential to the effective management of nourishment schemes. This section investigates the behaviour of sand waves using the previously developed advection-diffusion relationship to emphasise the importance of aspect ratios on nourishment behaviour. The overall goal of nourishment schemes is maximum retention time. The annual sediment supply volume is kept constant at  $418,333.33 \text{ m}^3/\text{year}$  which corresponds to the estimate by Corbella and Stretch (2012b). Sand waves were assumed to follow a Gaussian distribution in plan, with the number of inflow pulses varying between 1 and 4. Sand wave parameters such as amplitude ( $B$ ) and alongshore length ( $L$ ) were varied. Figure 5.19 shows advection-diffusion relations for various nourishment sand waves.

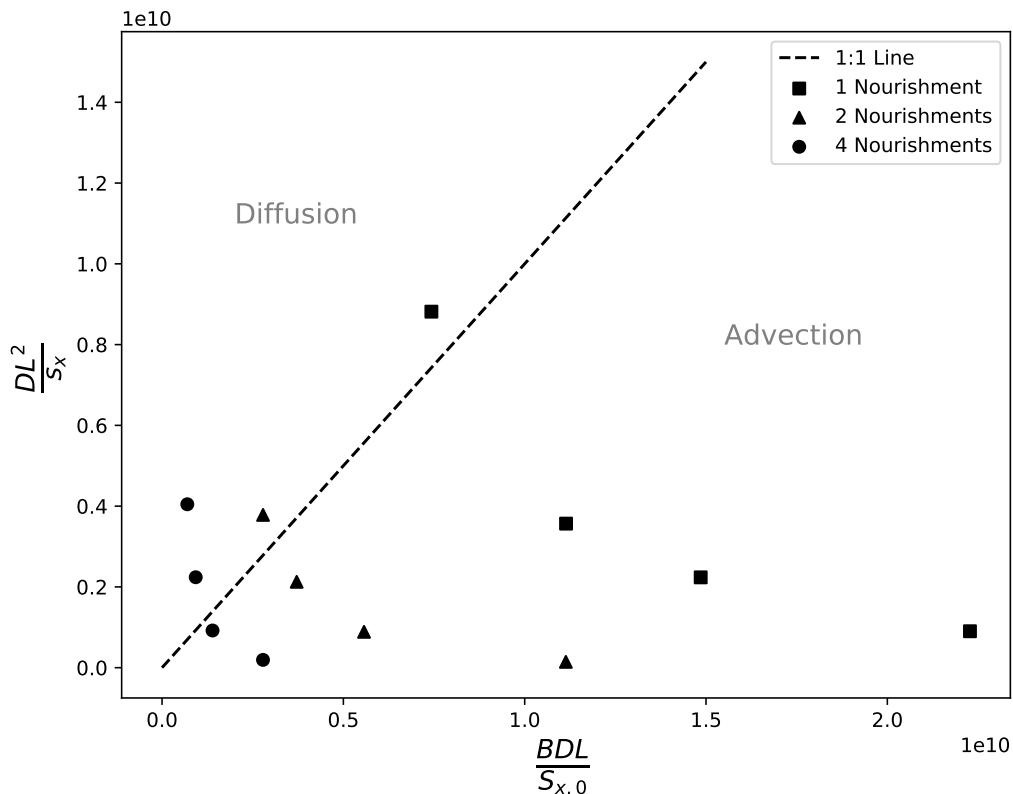


Fig. 5.19 Advection-diffusion relationship for varying aspect ratios correlating to various nourishment volumes.

## 5.6 Nourishment Sand Waves

Table 5.11 Nourishment sand wave parameters used for analysis in figure 5.19.

Nourishments	Volume ( $m^3$ )	Width - L ( $m$ )	Amplitude - B ( $m$ )	B/L	Process
1	418,333	1000	47.87	0.048	Diff
		1500	31.91	0.021	Adv
		2000	23.93	0.012	Adv
		2500	19.15	0.008	Adv
2	209,167	500	47.87	0.096	Diff
		1000	23.93	0.024	Adv
		1500	15.96	0.011	Adv
		2000	11.97	0.0067	Adv
4	104,583	500	23.93	0.048	Diff
		1000	11.97	0.012	Diff
		1500	7.98	0.005	Adv
		2000	5.98	0.003	Adv

Table 5.11 details sand wave parameters for the nourishments used in this analysis. From this data, results indicate that narrower, high-amplitude nourishments are diffusive dominant sand waves. Table 5.11 shows this observation where the highest aspect ratio per nourishment volume corresponds to a diffusive dominant state. Furthermore, table 5.11 indicates that a higher frequency of lower volume nourishments allows for a greater alongshore width while maintaining a diffusive state. This is significant as narrow, high-amplitude sand waves will diffuse rapidly which may result in an eventual change in the dominant process. Additionally, to obtain higher aspect ratios for low frequency, high volume sand waves, large sand wave amplitudes are required. For example, a single 418,333  $m^3$  nourishment requires an amplitude of 47,87 metres to maintain a diffusive state whereas a 104,583  $m^3$  nourishment of the same alongshore width requires 11.97 metres comparatively. These high amplitudes are impractical especially when considering the width of the breaker zone beyond which bed load transport is the dominant mechanism of sediment transport (Brenninkmeyer, 1974).

From figure 5.19, it is evident that multiple, smaller nourishments that divide the overall supply volume are more clustered around the 1:1 line as opposed to the single, 418,333  $m^3$  nourishment which is more spread. Additionally, an increase in nourishment frequency causes advection-diffusion values to shift towards the diffusion domain, resulting in a greater prevalence of diffusive states. Finally, it may be said that

## Results & Discussion

---

numerous nourishments are favoured over fewer, larger nourishments as they retain their diffusive state over a greater range of alongshore widths. Furthermore, required amplitudes are more realistic as compared to fewer, larger nourishments. Figure 5.19 therefore may be used as a useful planning tool when operating costly nourishment schemes to ensure that nourishment sand waves produce the desired outcome.

As mentioned previously, coastline position plays an important role in determining the advection-diffusion relationship of sand waves. This is explored in the next section.

### 5.6.2 Coastline Position Influence

Nourishment positions along coastlines may have significant implications on the advection-diffusion relationship given variations in relative coastline angles. The Durban coastline presents an interesting situation given that the uMngeni boundary region is slightly more diffusion influenced than the remaining two regions. Placement of nourishments at this position (pos. 3) will undergo significant diffusion which will increase advection velocities as the sand wave develops and propagates. Comparatively, nourishments placed at position 2 will experience less diffusion given the coastline orientation and will hence maintain a lower advection velocity.

This section explores the effects of different discharge positions along the Durban coastline on nourishment behaviour. In understanding how discharge positions affect nourishment waves, shore nourishment schemes may be operated optimally with retention times maximised. For this investigation, two points along the coastline served as nourishment points (pos. 2 and 3), as shown in figure 5.16a. From section 5.6.1, results showed that a single, large nourishment is not effective for maximising retention times within the domain, hence only nourishments assuming 2 waves or more will be considered in this section.

Table 5.12 Travel times for a  $209,167 m^3$  nourishment of varying aspect ratios between multiple points along the Durban coastline. Point of application of the nourishment is position 3.

Width - L ( <i>m</i> )	Amplitude - B ( <i>m</i> )	$B/L$ (-)	Pos. 3 → Pos. 2 ( <i>years</i> )	Pos. 2 → Pos. 1 ( <i>years</i> )	Total ( <i>years</i> )
500	47.87	0.096	2.51	1.51	4.02
1000	23.93	0.024	2.21	1.4	3.61
2000	11.97	0.0067	1.39	1.33	2.72

## 5.6 Nourishment Sand Waves

Table 5.12 shows the time taken for a 209,167  $m^3$  nourishment placed at position 3 to reach the midpoint and end of the domain. Results expectedly show that the highest aspect ratio waves have the highest retention times within the domain. Importantly, travel times between positions 3 and 2 as compared to those between positions 2 and 1 have greater differences for higher aspect ratios. A nourishment with an aspect ratio of 0.096 takes approximately one year less to reach the end of the domain from position 2 (1.51 years) in comparison to the time taken to reach position 2 from position 1 (2.51 years). Although higher aspect ratios of nourishments produce a greater retention time, consideration must be given to the time period of successive nourishments. Larger aspect ratios placed at position 3 will take longer to reach position 2 however the following period is significantly faster. Placement of a smaller aspect ratio nourishment will result in essentially even travel times between positions, resulting in a more even distribution of sediment along the coastline. This general trend may be applied to sand waves of any volume as long as the aspect ratio is known.

Table 5.13 Travel times for a 209,167  $m^3$  nourishment of varying aspect ratios between multiple points along the Durban coastline. Point of application of the nourishment is position 2 while column 5 assumes nourishment application at position 3.

Width - L ( <i>m</i> )	Amplitude - B ( <i>m</i> )	$B/L$ (-)	Pos. 2 → Pos. 1 ( <i>years</i> )	Pos. 2 → Pos. 1 ( <i>years</i> )
500	47.87	0.096	2.17	1.51
1000	23.93	0.024	1.98	1.4
2000	11.97	0.0067	1.71	1.33

Table 5.13 shows time taken for the same nourishments used in table 5.12 to travel from position 2 to position 1. It is evident that retention times for nourishments placed at position 2 exceed retention times for their counterpart placed at position 3 when considering travel time between position 2 and 1. This result infers that significant diffusion occurs between positions 2 and 3. Travel times may be increased between positions 1 and 2 should nourishments be re-nourished or applied entirely at point 2. Application of nourishments at position 2 will however starve the region between position 2 and 3 of nourished sediment given the dominant angle of wave approach hence consideration should be given to this.

Generally, the influence of coastline position may be significant however the impact of aspect ratio still governs sand wave behaviour. When applying diffusion dominant nourishments to the coastline, consideration of the diffusion rate should be done as

## Results & Discussion

---

rapid diffusion may result in a wave becoming advection dominated. Retention times of sand waves may be increased by placing nourishments in regions that experience lower diffusion rates or where the coastal orientation is closer to that of the dominant wave angle.

# Chapter 6

## Summary & Conclusions

This study comprised of five research questions with the aim of approximating the influences of varying sediment supplies on coastline evolution. A numerical one-line model was developed using existing models as a framework. This model is set apart from existing models by accounting for sand advection as well as diffusion. Calibration and validation of the longshore transport equation involved using observed wave records for the study region. Model sensitivity was also investigated. The model was then used to simulate coastline behaviour under varying sediment input circumstances to estimate sediment demands for the region. This chapter presents a summary of the results together with conclusions and recommendations.

### 6.1 One-line Model

*What is the most effective way to simulate long term coastline evolution within reasonable timeframes?*

A numerical one-line model was developed using a number of existing models as a framework. The necessary numerics of a one-line model were identified in terms of grid initialisation, wave transformations, longshore sediment transport and diffusion of sediment. Grid initialisation followed a similar method to that used by the GENESIS model developed by Hanson (1989). Longshore sediment transport was calculated using the Kamphuis (1991) formula (eqn. 2.9). Diffusion and advection were calculated using a variant of the Pelnard-Considère (1956) equation (eqn. 4.20). Fluvial sediment volumes were introduced into the model domain assuming a Gaussian distribution in plan (eqn. 4.22). Model checks involved limiting relative wave angles and the inclusion of a hard boundary in the cross-shore direction. This hard boundary ensured

adjustment of longshore transport rates based on the availability of sediment within the grid cell, developed by Hanson and Kraus (1986).

Calibration of the model involved using 18 years (reduced to 13 years) of observed wave data along the KwaZulu-Natal Coastline. The data spanned from 1992 until 2009 and was obtained from wave rider buoys situated at Durban and Richards Bay. Richards Bay data was used to supplement regions of missing data within the Durban records given their strong correlation (Corbella and Stretch, 2012b). The wave data was used in conjunction with annual estimated longshore transport rates for the Durban Bight calculated by Corbella and Stretch (2012b) to calibrate the Kamphuis (1991) longshore transport equation. The dataset was evenly split into a calibration and validation half. The one-line model was used to calculate annual longshore transport rates using a constant representative coastline angle for the region. A linear regression analysis yielded a calibration coefficient  $K$  of 0.0003078 which was found to be satisfactory when compared to the validation dataset.

## 6.2 Simulated Wave Data

### *Are statistically modelled wave climates appropriate for long-term simulations of coastline change?*

Stochastically simulated regional wave climates conditioned on synoptic scale meteorology were used as the source of wave data for this study. Simulated wave climates were compared with observed wave data for the Durban region in order to assess similarity between datasets. Comparison of the datasets required careful consideration of the respective dataset sizes given that observed data spanned 18 years while simulated data spanned over 101 years and were synthesised 101 times, resulting in a cumulative set of 10201 years of wave data. Additionally, the observed data was reduced to 13 years due to no wave period data being available for the omitted 5 years.

The comparison involved three wave characteristics; height ( $H_s$ ), period ( $T_p$ ) and direction ( $\theta$ ). Mean values for all three parameters showed close correlation, with differences falling within one standard deviation of the other for all characteristics. The observed maximum wave height (8.5 metres) was significantly lower than the simulated maximum (30.24 metres) however this was attributed to the return period of the storm event which caused the wave event given that simulated data covered a substantially longer time period. This value may also be an outlier. The probability distribution of wave occurrences by direction for both datasets showed visible similarity. A comparison of the cumulative frequencies for observed and simulated wave heights showed close

resemblance with a clear intersection point. Simulated climates exhibited more small waves ( $<1.5\text{ m}$ ) than the observed dataset with the opposite evident for waves greater than this height. Overall, the simulated wave climates using the method developed by Pringle et al. (2015) were found to closely replicate the observed wave climate for the region.

### 6.3 Long-term Coastline Change

#### *How does the coastline respond to a varying sediment supplies in the long-term?*

Simulations assuming a constant, continuous supply of sediment indicated that estimates longshore supply rates by Corbella and Stretch (2012b) of  $418,333\text{ m}^3/\text{year}$  are not adequate in maintaining a sediment balance along the uMngeni-uMhlanga region. Results yielded a minimum required sediment input of  $460,961\text{ m}^3/\text{year}$  to maintain beach volume over the long term, however this input rate did not result in beach width and area conservation throughout the domain. Further analysis inferred that a further  $135,221\text{ m}^3/\text{year}$  is required to prevent beach plan area and beach width loss along the coastline, totalling  $596,183\text{ m}^3/\text{year}$ . The aforementioned zero volume change supply rate caused coastline re-orientation towards the dominant wave angle over the long-term which in turn caused the erosion adjacent to the uMngeni boundary. This result may however be unrealistic due to hard offshore features such as rock reefs. Simulations indicated that the 5 kilometres of coastline adjacent to the uMngeni boundary experienced the most change which is consistent with the observations by the eThekweni Municipality (2017). Generally for a continuous supply, it may be said that observed longshore transport volumes are insufficient in maintaining beach volume and plan area in the study region.

#### *How do nourishment schemes behave along the coastline?*

Intermittent sediment supplies were also investigated in the form of nourishment sand waves. Results indicated that diffusive dominant sand waves may be more realistically obtained when nourishments are applied over multiple, smaller discharges. This is due to larger nourishment volumes requiring unrealistic amplitudes in order to be diffusive dominant. Furthermore, lower volume nourishments allow for more diffusion to occur while maintaining their status as diffusive dominant waves whereas larger volumes have a greater tendency to become advection dominant following rapid diffusion.

## Summary & Conclusions

---

The influence of coastline position was also investigated which indicated that retention times are somewhat reliant on the point of application of a nourishment. Coastline orientations closer to the dominant wave angle experience lower diffusion rates which maintain lower advection velocities, resulting in an increased retention time of the sand wave. Furthermore, an increase in aspect ratio results in greater discrepancies between travel times along the domain should a coastline have relatively substantial changes in orientation along its length. This presents an important relationship when planning for time between nourishment events. Lower aspect ratios yield more even travel times given changes in coastal orientation as they are less susceptible to diffusion effects. A limitation of the model was the non-inclusion of cross-shore processes which may have substantial effects on the results presented.

### ***How do river discharges behave and are they potentially significant in preventing erosion?***

River sediment discharges were investigated in terms of their role in preventing coastal erosion by looking at the diffusion-advection relationship of a discharge events. Discharges were assumed to propagate along the coastline as sand waves, hence an advection term was required in addition to diffusion to explain sand wave behaviour. A simple gaussian distribution in plan was assumed. Calibration of the advection term using observed sand waves and wave data yielded satisfactory results for further simulations.

The advection-diffusion relationship was investigated for numerous aspect ratios of sand waves. This was done for sand waves at different positions along the coastline. Results indicated that in general, sand waves along the Durban coastline are advection dominated. A critical aspect ratio of between 0.037 and 0.041 was found to be the approximate equilibrium point between advection and diffusion, with sand waves of this ratio falling along the 1:1 line. Given that the relationship identified is dimensionless, it may be applied to sand waves formed by any mechanism as long as the aspect ratio is known. Coastline position was also found to be an influential factor regarding the advection-diffusion relationship. Combining this information, it is possible that nourishments entering the uMngeni-uMhlanga domain are not remaining within the domain for long enough, which infers reconsideration of the nourishment strategy.

Extreme river discharge events depositing 200,000  $m^3$  of sediment were analysed in terms of retention time and advection velocities. Results indicated that narrower, high-amplitude sand waves with an alongshore length of 500 metres remained in the model domain for approximately 26% longer than those equalling 2000 metres in

width due to an increase in advection velocities as the sand wave amplitude decreased. Extreme discharge events were found to reach equilibrium positions as the sand wave propagated through the domain, accreting beaches by approximately 1.5 metres. This sediment may however be considered minute when taking into account cross-shore processes which were not part of this study. Extreme river discharge advection rates were comparable with beach recovery rates following storm events estimated by Corbella and Stretch (2012b). Corbella and Stretch (2012b) found that Durban's beaches took approximately 2 years to recover from storm damage, with save wave simulations indicating that narrow, high-amplitude sand waves have similar advection rates. This could be an indication that sand waves act to nourish eroded regions as they propagate along the coastline.

## 6.4 Summary

The objectives of this study were met through the development of a one-line model that was computationally efficient in running long-term coastline change simulations of up to 101 years. Although previous models have been developed for long-term simulations, this coastline model represents the first attempt at combining a numerical model with stochastically simulated regional wave climates as the input source of wave data while accounting for sand advection. The model calibration was shown to be of sufficient accuracy. Additionally, simulated wave data was shown to be appropriate for carrying out long-term coastline change simulations. The model made use of one-line theory as the fundamental mechanics behind coastline change, similar to that employed by existing models such as GENESIS.

Continuous sediment supplies indicated that current estimates of longshore sediment supply are insufficient in maintaining beach volume over the long-term. The minimum required sediment for beach volume conservation over the long term is approximately  $460,962 \text{ m}^3/\text{year}$  assuming a constant, continuous supply which exceeds the approximation by Corbella and Stretch (2012b) by around  $42,629 \text{ m}^3/\text{year}$ . This supply rate did however result in coastline re-orientation which resulted in erosion along certain sections of coastline. To ensure beach plan area and width conservation for a continuous sediment supply, the minimum volume required was calculated to be  $596,183 \text{ m}^3/\text{year}$ .

Shore nourishment behaviour were analysed in the form of alongshore sand waves. Findings showed that dividing the annual sediment supply into multiple, smaller nourishments results in more realistic sand wave amplitudes that are required for diffusive dominant waves. Furthermore, smaller nourishments may undergo more

## Summary & Conclusions

---

diffusive effects while retaining their diffusive state whereas larger nourishments tend to become advection dominant following rapid diffusion. With regards to coastline position, the effect may be substantial in regions where sand waves experience relatively large changes in coastline orientation. Results indicates that nourishment position affects diffusion and advection dominance. Diffusive waves placed within diffusion dominant regions will experience a rapid reduction in amplitude, likely changing over to an advective state which influences retention time. Lower aspect ratios which are not as susceptible to diffusion effects are able to overcome this effect, producing relative even retention times. This relationship may be useful in timing nourishment events.

The behaviour of river sediment discharges were also investigated in this study. Findings shows that discharges with aspect ratios of between 0.037 and 0.041 present a balanced scenario between diffusion and advection. Sand waves along the Durban coastline were generally found to be advection dominated. Larger aspect ratios experienced similar, larger diffusion amounts while advection rates reduced accordingly with increases in aspect ratios. Extreme flooding events were also investigated with findings indicating that these features are of a large enough scale to reach equilibrium positions as they propagate along the coastline, resulting in coastline nourishment. Rivers have potential in playing a major role in maintaining coastlines however their contribution is highly dependent on the aspect ratio of the discharge together with the point of formation.

## 6.5 Recommendations for Further Research

This study was limited by the availability of observed wave and longshore transport data for the study region. The model calibration may be improved given lengthier records of the aforementioned data which could provide results of a greater accuracy. Greater efforts are being made by the eThekweni Municipality to monitor coastline behaviour in the form of beach surveys however these records do not date back sufficiently. A greater amount of data is available for the Durban Bight region, hence a study of this type on this area may be advantageous given that this region supplies the sections of coastline northward with sediment. Greater complexities will arise however due to the presence of multiple coastal structures together with wave reflection and diffraction.

This model is also limited to regions where there are no coastal structures within the model domain. These structures may have a significant impact on coastline evolution given their impacts on longshore sediment drift and wave interactions. Inclusion of this into the model may be useful should the study region contain any structures.

## 6.5 Recommendations for Further Research

---

Furthermore, this model does not account for any solid offshore structures such as reefs which may significantly affect the extent to which coastlines change. Inclusion of these features may be useful in obtaining more accurate results.

Another limitation of the model was the non-inclusion of cross-shore processes. This made it difficult to accurately model extreme river flooding events that form offshore deltas. Inclusion of this process may provide more realistic results in regions where cross-shore transport significantly influences beach evolution or where study domains incorporate river mouths.

Corbella and Stretch (2012*b*) identified sea-level rise as a potential contributor to chronic erosion in the study region. Given that this model focused solely on sediment supply shortages as the primary cause of erosion, integration of sea-level rise may be useful in investigating the combined effect. This may help to identify the relative contributions of the phenomena to chronic erosion given the variability of sediment supply issues worldwide.

For the purpose of this study, a simple river sediment discharge technique was applied based on the assumption that storms occur during seasons of high rainfall. Furthermore, this technique assumes uniform discharge of sediment over the specified storm period. This technique does not account for any fluvial discharge physics or storm discharge dynamics, which may be of significance with respect to coastline evolution. Inclusion of these aspects will improve result accuracy and will provide a more realistic approximation of fluvial sediment discharges.



# References

- Adger, W. N. (2003), 'Social Capital, Collective Action, and Adaptation to Climate Change', *Economic Geography* **79**(4), 387–404.  
**URL:** <https://onlinelibrary.wiley.com/doi/abs/10.1111/j.1944-8287.2003.tb00220.x>
- Airoldi, L., Abbiati, M., Beck, M. W., Hawkins, S. J., Jonsson, P. R., Martin, D., Moschella, P. S., Sundelöf, A., Thompson, R. C. and Åberg, P. (2005), 'An ecological perspective on the deployment and design of low-crested and other hard coastal defence structures', *Coastal Engineering* **52**(10), 1073–1087.  
**URL:** <http://www.sciencedirect.com/science/article/pii/S0378383905001158>
- Alvarez, F. and Pan, S.-q. (2016), 'Predicting coastal morphological changes with empirical orthogonal function method', *Water Science and Engineering* **9**(1), 14–20.  
**URL:** <https://doi.org/10.1016/j.wse.2015.10.003>
- Amponsah-Dacosta, F. and Mathada, H. (2017), 'Study of Sand Mining and Related Environmental Problems along the Nzhelele River in Limpopo Province of South Africa', *Mine Water and Circular Economy* pp. 1259–1266.
- Arkema, K. K., Guannel, G., Verutes, G., Wood, S. A., Guerry, A., Ruckelshaus, M., Kareiva, P., Lacayo, M. and Silver, J. M. (2013), 'Coastal habitats shield people and property from sea-level rise and storms', *Nature Climate Change* **3**(10), 913.
- Ashton, A. D. and Murray, A. B. (2006), 'High-angle wave instability and emergent shoreline shapes: 1. Modeling of sand waves, flying spits, and capes', *Journal of Geophysical Research: Earth Surface* **111**(F4).  
**URL:** <https://agupubs.onlinelibrary.wiley.com/doi/abs/10.1029/2005JF000422>
- Ashton, A., Murray, A. B. and Arnoult, O. (2001), 'Formation of coastline features by large-scale instabilities induced by high-angle waves', *Nature* **414**(6861), 296–300.  
**URL:** <https://doi.org/10.1038/35104541>
- Baykal, C. (2014), 'Development of a numerical 2-dimensional beach evolution model', *Turkish Journal of Earth Sciences* **23**(2), 215–231.
- Bayram, A., Larson, M. and Hanson, H. (2007), 'A new formula for the total longshore sediment transport rate', *Coastal Engineering* **54**(9), 700–710.  
**URL:** <https://doi.org/10.1016/j.coastaleng.2007.04.001>
- Bernatchez, P. and Fraser, C. (2012), 'Evolution of Coastal Defence Structures and Consequences for Beach Width Trends, Québec, Canada', *Journal of Coastal Research*

## References

---

- pp. 1550–1566.  
**URL:** <https://doi.org/10.2112/JCOASTRES-D-10-00189.1>
- Besio, G., Blondeaux, P., Brocchini, M. and Vittori, G. (2004), ‘On the modeling of sand wave migration’, *Journal of Geophysical Research: Oceans* **109**(C4).  
**URL:** <https://agupubs.onlinelibrary.wiley.com/doi/abs/10.1029/2002JC001622>
- Birkemeier, W. A. (1985), ‘Field Data on Seaward Limit of Profile Change’, *Journal of Waterway, Port, Coastal, and Ocean Engineering* **111**(3), 598–602.  
**URL:** [https://doi.org/10.1061/\(asce\)0733-950x\(1985\)111:3\(598\)](https://doi.org/10.1061/(asce)0733-950x(1985)111:3(598))
- Bosboom, J. and Stive, M. J. F. (2015), *Coastal Dynamics I*, Delft Academic Press.  
**URL:** <https://books.google.co.za/books?id=b-ZirgEACAAJ>
- Bouma, T. J., Van Belzen, J., Balke, T., Zhu, Z., Airoidi, L., Blight, A. J., Davies, A. J., Galvan, C., Hawkins, S. J. and Hoggart, S. P. G. (2014), ‘Identifying knowledge gaps hampering application of intertidal habitats in coastal protection: Opportunities & steps to take’, *Coastal Engineering* **87**, 147–157.
- Breetzke, T., van Weele, G., Mather, A. and Moore, L. (2012), ‘The Establishment of Coastal Setback Lines for the Overberg District’.  
**URL:** [http://www.rhdhv.co.za/media/27-5/SSI\\_overberg\\_setback\\_final\\_report\\_compressed.pdf](http://www.rhdhv.co.za/media/27-5/SSI_overberg_setback_final_report_compressed.pdf)
- Brenninkmeyer, B. M. (1974), *Mode and Period of Sand Transport in the Surf Zone*.  
**URL:** <https://ascelibrary.org/doi/abs/10.1061/9780872621138.050>
- Brown, J. M., Phelps, J. J. C., Barkwith, A., Hurst, M. D., Ellis, M. A. and Plater, A. J. (2016), ‘The effectiveness of beach mega-nourishment, assessed over three management epochs’, *Journal of Environmental Management* **184**, 400–408.  
**URL:** <http://www.sciencedirect.com/science/article/pii/S0301479716307708>
- Bruun, P. (1954), ‘Coastal Erosion and the Development of Beach Profiles’.  
**URL:** <file://catalog.hathitrust.org/Record/101737975>  
<http://hdl.handle.net/2027/uiug.30112088627325>
- Burcharth, H. F. and Hughes, S. (2003), *Types and Functions of Coastal Structures*, Vol. 6, Coastal Engineering Research Center.
- Callaghan, D. P., Nielsen, P., Short, A. and Ranasinghe, R. (2008), ‘Statistical simulation of wave climate and extreme beach erosion’, *Coastal Engineering* **55**(5), 375–390.  
**URL:** <https://doi.org/10.1016/j.coastaleng.2007.12.003>
- Capobianco, M., Hanson, H., Larson, M., Steetzel, H., Stive, M. J. F., Chatelus, Y., Aarninkhof, S. G. J. and Karambas, T. (2002), ‘Nourishment design and evaluation: applicability of model concepts’, *Coastal engineering* **47**(2), 113–135.
- Carter, R. (1988), *Coastal Environments: An Introduction to the Physical, Ecological, and Cultural Systems of Coastlines*, Elsevier.  
**URL:** <https://doi.org/10.1016/c2009-0-21648-5>

- Castelle, B., Scott, T., Brander, R. W. and McCarroll, R. J. (2016), 'Rip current types, circulation and hazard', *Earth-Science Reviews* **163**, 1–21.  
**URL:** <https://doi.org/10.1016/j.earscirev.2016.09.008>
- CEP (1998), 'Manual for Sand Dune Management in the Wider Caribbean', *Caribbean Environment Programme* .  
**URL:** <http://www.cep.unep.org/issues/sanddunes.PDF>
- Charlier, R. H. and Meyer, C. P. D. (1995), 'Beach nourishment as efficient coastal protection', *Environmental Management and Health* **6**(5), 26–34.  
**URL:** <https://doi.org/10.1108/09566169510096511>
- Chatterjee, S. and Hadi, A. S. (1986), 'Influential Observations, High Leverage Points, and Outliers in Linear Regression', *Statist. Sci.* **1**(3), 379–393.  
**URL:** <https://doi.org/10.1214/ss/1177013622>
- Chu, X., Zhai, K., Lu, X., Liu, J., Xu, X. and Xu, H. (2009), 'A quantitative assessment of human impacts on decrease in sediment flux from major Chinese rivers entering the western Pacific Ocean', *Geophysical Research Letters* **36**(19).  
**URL:** <https://agupubs.onlinelibrary.wiley.com/doi/abs/10.1029/2009GL039513>
- Church, J. A. and McInnes, K. L. (2006), Sea-level rise around the Australian coastline and the changing frequency of extreme sea-level events.
- Church, J. A. and White, N. J. (2006), 'A 20th century acceleration in global sea-level rise', *Geophysical Research Letters* **33**(1).  
**URL:** <https://agupubs.onlinelibrary.wiley.com/doi/abs/10.1029/2005GL024826>
- Clausner, J. E. (2000), 'Sand bypassing and performance database', *Coastal and Hydraulics Laboratory Engineering Technical Note ERDC/CHL TN-II-41* pp. 53–73.
- Cooper, A. (1993), 'Sedimentation in a river dominated estuary', *Sedimentology* **40**(5), 979–1017.  
**URL:** <https://onlinelibrary.wiley.com/doi/abs/10.1111/j.1365-3091.1993.tb01372.x>
- Corbella, S. and Stretch, D. D. (2012a), 'Coastal defences on the KwaZulu-Natal coast of South Africa: a review with particular reference to geotextiles', *Journal of the South African Institution of Civil Engineering* **54**, 55–64.  
**URL:** [http://www.scielo.org.za/scielo.php?script=sci\\_arttext&pid=S1021-20192012000200006&nrm=iso](http://www.scielo.org.za/scielo.php?script=sci_arttext&pid=S1021-20192012000200006&nrm=iso)
- Corbella, S. and Stretch, D. D. (2012b), 'Decadal trends in beach morphology on the east coast of South Africa and likely causative factors', *Natural Hazards and Earth System Science* **12**(8), 2515–2527.
- Corbella, S. and Stretch, D. D. (2012c), 'Predicting coastal erosion trends using non-stationary statistics and process-based models', *Coastal Engineering* **70**, 40–49.
- Crossland, C. J., Baird, D., Ducrotoy, J.-P., Lindeboom, H., Buddemeier, R. W., Dennison, W. C., Maxwell, B. A., Smith, S. V. and Swaney, D. P. (2005), The Coastal Zone: a Domain of Global Interactions, in 'Coastal Fluxes in the Anthropocene',

## References

---

- Springer Berlin Heidelberg, pp. 1–37.  
**URL:** [https://doi.org/10.1007/3-540-27851-6\\_1](https://doi.org/10.1007/3-540-27851-6_1)
- Davis, J. D. and Macknight, S. (1990), ‘Environmental Considerations for Port and Harbor Developments’, *Transport and the Environment Series* (126), 131.
- de Vriend, H. J., Capobianco, M., Chesher, T., de Swart, H. E., Latteux, B. and Stive, M. J. F. (1993), ‘Approaches to long-term modelling of coastal morphology: A review’, *Coastal Engineering* **21**(1-3), 225–269.  
**URL:** [https://doi.org/10.1016/0378-3839\(93\)90051-9](https://doi.org/10.1016/0378-3839(93)90051-9)
- DEA (2008), A Summary Guide to South Africa’s Integrated Coastal Management Act, Technical report.  
**URL:** <http://www.ngo.grida.no/soesa/nsoer/>
- Dean, R. G. (1991), ‘Equilibrium Beach Profiles: Characteristics and Applications’, *Journal of Coastal Research* **7**(1), 53–84.  
**URL:** <http://www.jstor.org/stable/4297805>
- der Zel, D. W. (1975), ‘Umgeni River catchment analysis’, *Water SA* **1**(2), 70–75.  
**URL:** [https://journals.co.za/content/waters/1/2/AJA03784738\\_1346](https://journals.co.za/content/waters/1/2/AJA03784738_1346)
- Dugan, J., Airoidi, L., Chapman, G., Walker, S. and Schlacher, T. (2011), ‘Estuarine and coastal structures: environmental effects, a focus on shore and nearshore structures’.
- Dutykh, D. (2016), ‘How to overcome the Courant-Friedrichs-Lewy condition of explicit discretizations?’.  
**URL:** <http://rgdoi.net/10.13140/RG.2.2.12420.32642>
- Dwarakish, G. S. and Salim, A. M. (2015), ‘Review on the Role of Ports in the Development of a Nation’, *Aquatic Procedia* **4**, 295–301.  
**URL:** <http://www.sciencedirect.com/science/article/pii/S2214241X15000413>
- Ergin, A., Güler, I., Yalciner, A., Baykal, C., Artagan, S. and Şafak, I. (2006), ‘A One-Line Numerical Model for Wind Wave Induced Shoreline Changes’.
- eThekweni Municipality (2017), ‘Umgeni to Umhlanga Beach Monitoring Program: Technical Report 106 - January 2017’.
- Falqués, A. and Calvete, D. (2005), ‘Large-scale dynamics of sandy coastlines: Diffusivity and instability’, *Journal of Geophysical Research: Oceans* **110**(C3).  
**URL:** <https://agupubs.onlinelibrary.wiley.com/doi/abs/10.1029/2004JC002587>
- Falqués, A., Calvete Manrique, D. and Ribas, F. (2011), ‘Shoreline instability due to very oblique wave incidence: Some remarks on the physics’, *Journal of Coastal Research* **27**, 291–295.
- Feagin, R., Sherman, D. and Grant, W. (2005), ‘Coastal Erosion, Global Sea-level Rise, and the Loss of Sand Dune Plant Habitats’, *Frontiers in Ecology and the Environment* **3**, 359–364.

- Frey, A. (2012), 'Introduction to GenCade', *Engineer Research and Development Center*.
- Genovese, E. and Green, C. (2015), 'Assessment of storm surge damage to coastal settlements in Southeast Florida', *Journal of Risk Research* **18**(4), 407–427.  
**URL:** <https://doi.org/10.1080/13669877.2014.896400>
- Grabemann, I. and Weisse, R. (2008), 'Climate change impact on extreme wave conditions in the North Sea: an ensemble study', *Ocean Dynamics* **58**(3), 199–212.  
**URL:** <https://doi.org/10.1007/s10236-008-0141-x>
- Gravois, U., Callaghan, D., Baldock, T., Smith, K. and Martin, B. (2016), 'Review of beach profile and shoreline models applicable to the statistical modelling of beach erosion and the impacts of storm clustering'.
- Green, S. C. (2012), 'The Regulation of Sand Mining in South Africa'.
- Greene, K. (2002), 'Beach nourishment: a review of the biological and physical impacts'.
- Grifoll, M., Gracia, V., Aretxabaleta, A., Guillén, J., Espino, M. and Warner, J. C. (2014), 'Formation of fine sediment deposit from a flash flood river in the Mediterranean Sea', *Journal of Geophysical Research: Oceans* **119**(9), 5837–5853.  
**URL:** <https://agupubs.onlinelibrary.wiley.com/doi/abs/10.1002/2014JC010187>
- Hallegatte, S., Ranger, N., Mestre, O., Dumas, P., Corfee-Morlot, J., Herweijer, C. and Wood, R. M. (2010), 'Assessing climate change impacts, sea level rise and storm surge risk in port cities: a case study on Copenhagen', *Climatic Change* **104**(1), 113–137.  
**URL:** <https://doi.org/10.1007/s10584-010-9978-3>
- Hallermeier, R. J. (1980), 'A profile zonation for seasonal sand beaches from wave climate', *Coastal Engineering* **4**, 253–277.  
**URL:** <http://www.sciencedirect.com/science/article/pii/0378383980900228>
- Hamm, L., Capobianco, M., Dette, H. H., Lechuga, A., Spanhoff, R. and Stive, M. J. F. (2002), 'A summary of European experience with shore nourishment', *Coastal Engineering* **47**(2), 237–264.  
**URL:** [https://doi.org/10.1016/s0378-3839\(02\)00127-8](https://doi.org/10.1016/s0378-3839(02)00127-8)
- Hanson, J. D. (1999), The coastal geomorphology of Scotland: understanding sediment budgets for effective coastal management, in J. M. Baxter, K. Duncan, S. M. Atkins and G. Lees, eds, 'Scotland's Living Coastline', Natural Heritage of Scotland, The Stationery Office, London, pp. 34–44.  
**URL:** <http://eprints.gla.ac.uk/100006/>
- Hanson, H. (1989), 'Genesis: A Generalized Shoreline Change Numerical Model', *Journal of Coastal Research* **5**(1), 1–27.  
**URL:** <http://www.jstor.org/stable/4297483>
- Hanson, H., Brampton, A., Capobianco, M., Dette, H. H., Hamm, L., Laustrup, C., Lechuga, A. and Spanhoff, R. (2002), 'Beach nourishment projects, practices, and objectives: a European overview', *Coastal Engineering* **47**(2), 81–111.  
**URL:** [https://doi.org/10.1016/s0378-3839\(02\)00122-9](https://doi.org/10.1016/s0378-3839(02)00122-9)

## References

---

- Hanson, H. and Kraus, N. C. (1986), *Seawall boundary condition in numerical models of shoreline evolution*, Springfield, Va. :available from National Technical Information Service,.  
**URL:** <https://www.biodiversitylibrary.org/item/102716>
- Hapke, C. J., Reid, D. and Richmond, B. (2009), ‘Rates and Trends of Coastal Change in California and the Regional Behavior of the Beach and Cliff System’, *Journal of Coastal Research* pp. 603–615.  
**URL:** <https://doi.org/10.2112/08-1006.1>
- Haslett, S. K. (2016), *Coastal Systems: Third Edition*, University of Wales Press.  
**URL:** <https://www.amazon.com/Coastal-Systems-Simon-K-Haslett/dp/1783169001?SubscriptionId=AKIAIOBINVZYXZQZ2U3A&tag=chimbiori05-20&linkCode=sm2&camp=2025&creative=165953&creativeASIN=1783169001>
- Hoefel, F. and Elgar, S. (2003), ‘Wave-Induced Sediment Transport and Sandbar Migration’, *Science* **299**(5614), 1885–1887.  
**URL:** <http://science.sciencemag.org/content/299/5614/1885>
- Kamphuis, J. W. (1991), ‘Alongshore Sediment Transport Rate’, *Journal of Waterway, Port, Coastal, and Ocean Engineering* **117**(6), 624–640.  
**URL:** [https://doi.org/10.1061/\(asce\)0733-950x\(1991\)117:6\(624\)](https://doi.org/10.1061/(asce)0733-950x(1991)117:6(624))
- Kay, R. and Alder, J. (2005), *Coastal Planning and Management*, CRC Press.  
**URL:** <https://www.amazon.com/Coastal-Planning-Management-Robert-Kay/dp/0415317738?SubscriptionId=AKIAIOBINVZYXZQZ2U3A&tag=chimbiori05-20&linkCode=sm2&camp=2025&creative=165953&creativeASIN=0415317738>
- Knutson, T. R., McBride, J. L., Chan, J., Emanuel, K., Holland, G., Landsea, C., Held, I., Kossin, J. P., Srivastava, A. K. and Sugi, M. (2010), ‘Tropical cyclones and climate change’, *Nature Geoscience* **3**, 157.  
**URL:** <https://doi.org/10.1038/ngeo779> <http://10.0.4.14/ngeo779>  
<https://www.nature.com/articles/ngeo779#supplementary-information>
- Kondolf, G. (1997), ‘Hungry Water: Effects of Dams and Gravel Mining on River Channels’, *Environmental management* **21**, 533–551.
- Laubscher, W. I., Swart, D. H., Schoonees, J. S., Pfaff, W. M. and Davis, A. B. (1990), *The Durban Beach Restoration Scheme after 30 Years*.  
**URL:** <https://ascelibrary.org/doi/abs/10.1061/9780872627765.247>
- Leatherman, S. P., Zhang, K. and Douglas, B. C. (2000), ‘Sea Level Rise Shown to Drive Coastal Erosion’, *Eos, Transactions American Geophysical Union* **81**(6), 55–57.  
**URL:** <https://agupubs.onlinelibrary.wiley.com/doi/abs/10.1029/00EO00034>
- Lefèvre, J. and Aouf, L. (2012), ‘Latest developments in Wave in Data Assimilation’.
- Loza, P. (2008), ‘Sand Bypassing Systems’.
- Maharaj, B., Pillay, V. and Sucheran, R. (2008), ‘Durban - A subtropical coastal paradise? Tourism dynamics in a post-apartheid city’, *Études caribéennes* (9-10).  
**URL:** <https://doi.org/10.4000/etudescaribeennes.1192>

- Mallik, T. K., Samsuddin, M., Prakash, T. N., Vasudevan, V. and Machado, T. (1987), 'Beach erosion and accretion - An example from Kerala, Southwest Coast of India', *Environmental Geology and Water Sciences* **10**(2), 105–110.  
**URL:** <https://doi.org/10.1007/BF02574668>
- Marchesiello, P., McWilliams, J. C. and Shchepetkin, A. (2001), 'Open boundary conditions for long-term integration of regional oceanic models', *Ocean Modelling* **3**(1-2), 1–20.  
**URL:** [https://doi.org/10.1016/s1463-5003\(00\)00013-5](https://doi.org/10.1016/s1463-5003(00)00013-5)
- Mascarenhas, F. C. B., Valentini, E. and da Costa, A. L. T. (1996), 'Modelling and predicting beach evolution after groin construction in the north-east coast of Brazil', *Transactions on Ecology and the Environment* **9**, 83–92.
- Mather, A. A., Garland, G. G. and Stretch, D. D. (2009), 'Southern African sea levels: corrections, influences and trends', *African Journal of Marine Science* **31**(2), 145–156.  
**URL:** <https://doi.org/10.2989/AJMS.2009.31.2.3.875>
- Mendelsohn, R., Emanuel, K., Chonabayashi, S. and Bakkensen, L. (2012), 'The impact of climate change on global tropical cyclone damage', *Nature Climate Change* **2**, 205.  
**URL:** <https://doi.org/10.1038/nclimate1357> <http://10.0.4.14/nclimate1357>  
<https://www.nature.com/articles/nclimate1357#supplementary-information>
- Michaelides, K. and Singer, M. B. (2014), 'Impact of coarse sediment supply from hillslopes to the channel in runoff-dominated, dryland fluvial systems', *Journal of Geophysical Research: Earth Surface* **119**(6), 1205–1221.  
**URL:** <https://agupubs.onlinelibrary.wiley.com/doi/abs/10.1002/2013JF002959>
- Miche, M. (1944), *Mouvement ondulatoires de la mer en profondeur constante ou décroissante*, ANNALES DES PONTS ET CHAUSSEES, Verlag nicht ermittelbar.  
**URL:** <https://books.google.co.za/books?id=9DOGnQAACAAJ>
- Moore, B. D. (1982), *Beach Profile Evolution in Response to Changes in Water Level and Wave Height*, University of Delaware.  
**URL:** <https://books.google.co.za/books?id=0wdItwAACAAJ>
- Mori, N., Yasuda, T., Mase, H., Tom, T. and Oku, Y. (2010), 'Projection of Extreme Wave Climate Change under Global Warming', *Hydrological Research Letters* **4**(0), 15–19.  
**URL:** <https://doi.org/10.3178/hrl.4.15>
- Morton, R. and Sallenger, A. H. (2003), 'Morphological Impacts of Extreme Storms on Sandy Beaches and Barriers', *Journal of Coastal Research* **19**(3), 560–573.  
**URL:** <http://www.jstor.org/stable/4299198>
- Nicholson, J., Broker, I., Roelvink, J. A., Price, D., Tanguy, J. M. and Moreno, L. (1997), 'Intercomparison of coastal area morphodynamic models', *Coastal Engineering* **31**(1), 97–123.  
**URL:** <http://www.sciencedirect.com/science/article/pii/S0378383996000543>

## References

---

- Noble, R. (2011), ‘Coastal Structures’ Effects on Shorelines’, *Coastal Engineering Proceedings* **1**(16).  
**URL:** <https://icce-ojs-tamu.tdl.org/icce/index.php/icce/article/view/3401>
- Nordstrom, K. F. (2000), *Beaches and Dunes of Developed Coasts*, Cambridge University Press.
- Padmalal, D. and Maya, K. (2014), *Sand Mining*, Springer Netherlands.  
**URL:** <https://doi.org/10.1007/978-94-017-9144-1>
- Parsons, A. J. (2012), ‘How Useful Are Catchment Sediment Budgets?’, *Progress in Physical Geography: Earth and Environment* **36**(1), 60–71.  
**URL:** <https://doi.org/10.1177/0309133311424591>
- Pelnard-Considère, R. (1956), ‘Essai de théorie de l’évolution des formes de rivage en plages de sable et de galets’.
- Perkins, M. J., Ng, T. P. T., Dudgeon, D., Bonebrake, T. C. and Leung, K. M. Y. (2015), ‘Conserving intertidal habitats: what is the potential of ecological engineering to mitigate impacts of coastal structures?’, *Estuarine, Coastal and Shelf Science* **167**, 504–515.
- Peterson, C. H., Bishop, M. J., Anna, L. M. and Johnson, G. A. (2014), ‘Multi-year persistence of beach habitat degradation from nourishment using coarse shelly sediments’, *Science of The Total Environment* **487**, 481–492.  
**URL:** <https://doi.org/10.1016/j.scitotenv.2014.04.046>
- Phillips, M. and Jones, A. (2006), ‘Erosion and tourism infrastructure in the coastal zone: Problems, consequences and management’, *Tourism Management* **27**(3), 517–524.
- Pilkey, O. H., Neal, W. J. and Bush, D. M. (1991), ‘Coastal Erosion’, *Episodes: International Geoscience News Magazine* **14**(1), 45–51.
- Prasad, D. H. and Kumar, N. D. (2014), ‘Coastal Erosion Studies: A Review’, *International Journal of Geosciences* **05**(03), 341–345.  
**URL:** <https://doi.org/10.4236/ijg.2014.53033>
- Pringle, J. (2015), ‘On Weather and Waves: Applications to Coastal Engineering’.
- Pringle, J., Stretch, D. D. and Bárdossy, A. (2015), ‘On linking atmospheric circulation patterns to extreme wave events for coastal vulnerability assessments’, *Natural Hazards* **79**(1), 45–59.  
**URL:** <https://doi.org/10.1007/s11069-015-1825-4>
- Quick, M. C. (1991), ‘Onshore-offshore sediment transport on beaches’, *Coastal Engineering* **15**(4), 313–332.  
**URL:** <http://www.sciencedirect.com/science/article/pii/0378383991900148>

- Ranasinghe, R., Duong, T. M., Uhlenbrook, S., Roelvink, D. and Stive, M. (2012), 'Climate-change impact assessment for inlet-interrupted coastlines', *Nature Climate Change* **3**, 83.  
**URL:** <https://doi.org/10.1038/nclimate1664> <http://10.0.4.14/nclimate1664>  
<https://www.nature.com/articles/nclimate1664#supplementary-information>
- Røed, L. P. and Cooper, C. K. (1986), Open Boundary Conditions in Numerical Ocean Models, in 'Advanced Physical Oceanographic Numerical Modelling', Springer Netherlands, pp. 411–436.  
**URL:** [https://doi.org/10.1007/978-94-017-0627-8\\_23](https://doi.org/10.1007/978-94-017-0627-8_23)
- Roelvink, D. and Reniers, A. (2011), *A Guide to Modeling Coastal Morphology*, WORLD SCIENTIFIC.  
**URL:** <https://www.worldscientific.com/doi/abs/10.1142/7712>
- Rosati, J. D. (2005), 'Concepts in Sediment Budgets', *Journal of Coastal Research* pp. 307–322.  
**URL:** <https://doi.org/10.2112/02-475A.1>
- Roussow, J. (1989), 'Design Waves for the South African Coastline'.
- Ruggiero, P., Komar, P. D., McDougal, W. G., Marra, J. J. and Beach, R. A. (2001), 'Wave Runup, Extreme Water Levels and the Erosion of Properties Backing Beaches', *Journal of Coastal Research* **17**(2), 407–419.  
**URL:** <http://www.jstor.org/stable/4300192>
- Saye, S. E., van der Wal, D., Pye, K. and Blott, S. (2005), 'Beach-dune Morphological Relationships and Erosion/Accretion: An Investigation at Five Sites in England and Wales using LIDAR data', *Geomorphology* **72**, 128–155.
- Schoonees, J. S. (2000), 'Annual variation in the net longshore sediment transport rate', *Coastal Engineering* **40**(2), 141–160.  
**URL:** [https://doi.org/10.1016/s0378-3839\(00\)00009-0](https://doi.org/10.1016/s0378-3839(00)00009-0)
- Schoonees, J. S. and Theron, A. K. (1996), *Improvement of the Most Accurate Longshore Transport Formula*.  
**URL:** <https://ascelibrary.org/doi/abs/10.1061/9780784402429.282>
- Schwab, W. C., Baldwin, W. E., Hapke, C. J., Lentz, E. E., Gayes, P. T., Denny, J. F., List, J. H. and Warner, J. C. (2013), 'Geologic Evidence for Onshore Sediment Transport from the Inner Continental Shelf: Fire Island, New York', *Journal of Coastal Research* pp. 526–544.  
**URL:** <https://doi.org/10.2112/JCOASTRES-D-12-00160.1>
- Scott, T., Masselink, G., O'Hare, T., Saulter, A., Poate, T., Russell, P., Davidson, M. and Conley, D. (2016), 'The extreme 2013/2014 winter storms: Beach recovery along the southwest coast of England', *Marine Geology* **382**, 224–241.  
**URL:** <http://www.sciencedirect.com/science/article/pii/S0025322716302766>
- Seymour, R. J. (2005), *Longshore Sediment Transport*, Springer Netherlands, Dordrecht, p. 600.  
**URL:** [https://doi.org/10.1007/1-4020-3880-1\\_199](https://doi.org/10.1007/1-4020-3880-1_199)

## References

---

- Shabangu, P. E. (2015), ‘Investigation of a simplified open boundary condition for coastal and shelf sea hydrodynamic models’.
- Smith, E., Wang, P. and Zhang, J. (2003), ‘Evaluation of the CERC Formula Using Large-Scale Model Data’.
- Snoussi, M., Haïda, S. and Imassi, S. (2002), ‘Effects of the construction of dams on the water and sediment fluxes of the Moulouya and the Sebou Rivers, Morocco’, *Regional Environmental Change* **3**(1), 5–12.  
**URL:** <https://doi.org/10.1007/s10113-001-0035-7>
- Stive, M. J. F., de Schipper, M. A., Luijendijk, A. P., Aarninkhof, S. G. J., van Gelder-Maas, C., van Thiel de Vries, J. S. M., de Vries, S., Henriquez, M., Marx, S. and Ranasinghe, R. (2013), ‘A New Alternative to Saving Our Beaches from Sea-Level Rise: The Sand Engine’, *Journal of Coastal Research* pp. 1001–1008.  
**URL:** <https://doi.org/10.2112/JCOASTRES-D-13-00070.1>
- Stive, M., Roelvink, D. J. A. and de Vriend, H. (2011), ‘Large-Scale Coastal Evolution Concept’, *Twenty-Second Coastal Engineering Conference; proceedings of the International Conference July 2-6, 1990, Delft, The Netherlands 2, 1962-1974. (1990)*.
- Syvitski, J. and Saito, Y. (2007), ‘Morphodynamics of Deltas under the Influence of Humans’, *Global and Planetary Change* **57**, 261–282.
- Theron, K., de Lange, W., Nahman, A. and Hardwick, D. (2008), ‘Sand supply from Rivers within the Ethekewini Jurisdiction, implications for Coastal Sand Budgets and Resource Economics.’, *Africa* (September), 1–92.
- Thevenot, M. M. and Kraus, N. C. (1995), ‘Longshore sand waves at Southampton Beach, New York: observation and numerical simulation of their movement’, *Marine Geology* **126**(1), 249–269.  
**URL:** <http://www.sciencedirect.com/science/article/pii/0025322795000819>
- Thomas, R. C. and Frey, A. E. (2013), *Shoreline Change Modeling Using One-line Models: General Model Comparison and Literature Review*, Technical note, U.S. Army Engineer Research and Development Center [Coastal and Hydraulics Laboratory].  
**URL:** <https://books.google.co.za/books?id=fQPTnQEACAAJ>
- Thomas, R. S. (1994), ‘Breakwaters and Coast Defences. Coastal Defence Structures: Technical Note’, *Proceedings of the Institution of Civil Engineers - Water, Maritime and Energy* **106**(4), 377–380.  
**URL:** <https://doi.org/10.1680/iwtme.1994.27242>
- Tonnon, P. K., Huisman, B. J. A., Stam, G. N. and van Rijn, L. C. (2018), ‘Numerical modelling of erosion rates, life span and maintenance volumes of mega nourishments’, *Coastal Engineering* **131**, 51–69.  
**URL:** <http://www.sciencedirect.com/science/article/pii/S0378383917301825>

- Turner, R. K., Subak, S. and Adger, W. N. (1996), 'Pressures, trends, and impacts in coastal zones: Interactions between socioeconomic and natural systems', *Environmental Management* **20**(2), 159–173.  
**URL:** <https://doi.org/10.1007/BF01204001>
- USACE (1984), *Shore Protection Manual*, number 1 in 'Shore Protection Manual', Department of the Army, Waterways Experiment Station, Corps of Engineers, Coastal Engineering Research Center.  
**URL:** <https://books.google.co.za/books?id=km0YAQAIAAJ>
- Vaidya, A. M., Kori, S. K. and Kudale, M. D. (2015), 'Shoreline Response to Coastal Structures', *Aquatic Procedia* **4**, 333–340.  
**URL:** <http://www.sciencedirect.com/science/article/pii/S2214241X15000462>
- van den Berg, N., Falqués, A. and Ribas, F. (2012), 'Modeling large scale shoreline sand waves under oblique wave incidence', *Journal of Geophysical Research: Earth Surface* **117**(F3).  
**URL:** <https://agupubs.onlinelibrary.wiley.com/doi/abs/10.1029/2011JF002177>
- Van Rijn, L. C. (2011), 'Coastal Erosion and Control', *Ocean and Coastal Management* **54**(12), 867–887.  
**URL:** <http://dx.doi.org/10.1016/j.ocecoaman.2011.05.004>
- van Rijn, L. C. (2014), 'A simple general expression for longshore transport of sand, gravel and shingle', *Coastal Engineering* **90**, 23–39.  
**URL:** <http://www.sciencedirect.com/science/article/pii/S0378383914000787>
- Verhagen, H. J. (1996), 'Analysis of Beach Nourishment Schemes', *Journal of Coastal Research* **12**(1), 179–185.  
**URL:** <http://www.jstor.org/stable/4298472>
- Vidal, R. and van Oord, G. (2010), 'Environmental Impacts in Beach Nourishments: A Comparison of Options', *Terra et Aqua* **119**, 14–20.
- Vitousek, S. and Barnard, P. L. (2015), *A Nonlinear, Implicit One-Line Model to Predict Long-term Shoreline Change*.  
**URL:** [https://www.worldscientific.com/doi/abs/10.1142/9789814689977\\_0215](https://www.worldscientific.com/doi/abs/10.1142/9789814689977_0215)
- Walling, D. E. (2006), 'Human impact on land–ocean sediment transfer by the world's rivers', *Geomorphology* **79**(3), 192–216.  
**URL:** <http://www.sciencedirect.com/science/article/pii/S0169555X06002510>
- Webster, P. J., Holland, G. J., Curry, J. A. and Chang, H.-R. (2005), 'Changes in Tropical Cyclone Number, Duration, and Intensity in a Warming Environment', *Science* **309**(5742), 1844–1846.  
**URL:** <http://science.sciencemag.org/content/309/5742/1844>
- Winter, M. and Checkland, P. (2003), 'Soft systems: a fresh perspective for project management', *Proceedings of the Institution of Civil Engineers - Civil Engineering* **156**(4), 187–192.  
**URL:** <https://doi.org/10.1680/cien.2003.156.4.187>

## References

---

- Woodroffe, C. D. (2002), *Coasts: Form, Process and Evolution*, Coasts: Form, Process, and Evolution, Cambridge University Press.  
**URL:** <https://books.google.co.za/books?id=jRqW0FVwWh8C>
- Yang, H., Yang, S., Xu, K. H., Milliman, J. D., Wang, H., Yang, Z., Chen, Z. and Zhang, C. Y. (2018), 'Human impacts on sediment in the Yangtze River: A review and new perspectives', *Global and Planetary Change* **162**.
- Young, R. S., Pilkey, O. H., Bush, D. M. and Thieler, E. R. (1995), 'A Discussion of the Generalized Model for Simulating Shoreline Change (GENESIS)', *Journal of Coastal Research* **11**(3), 875–886.  
**URL:** <http://www.jstor.org/stable/4298387>
- Yuan, F. and Cox, R. (2013), 'Modelling Coastal Process for Long-term Shoreline Change'.
- Zhang, K., Douglas, B. C. and Leatherman, S. P. (2004), 'Global Warming and Coastal Erosion', *Climatic Change* **64**(1), 41.  
**URL:** <https://doi.org/10.1023/B:CLIM.0000024690.32682.48>

# Appendix A

## Beach Data

This appendix presents data relevant to the Durban coastline that was used in this study. Shown below are the coastal coordinates used for this study, obtained from the eThekweni Municipality.

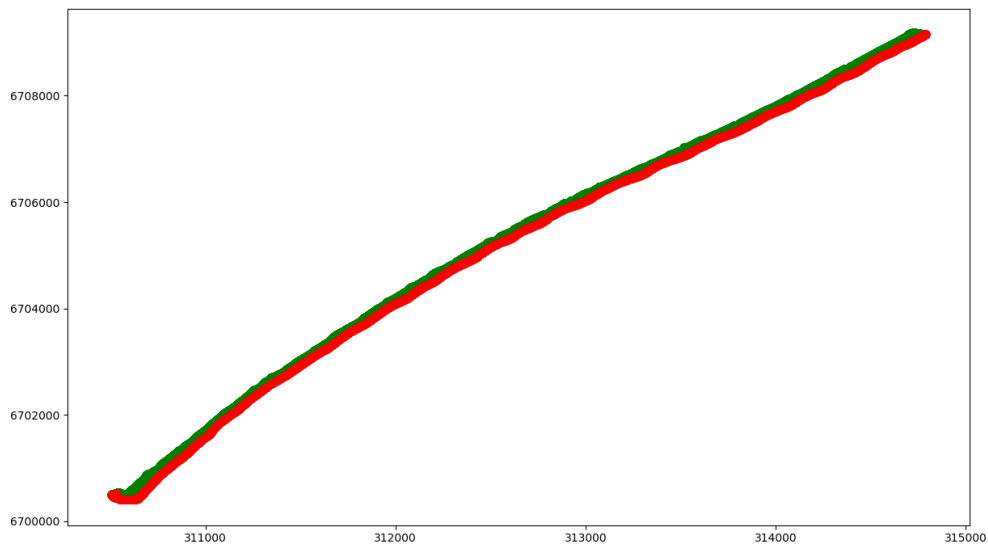


Fig. A.1 Surveyed coastline coordinates in UTM format showing regions above (*green*) and below (*red*) MSL (eThekweni Municipality, 2017).

# Beach Data

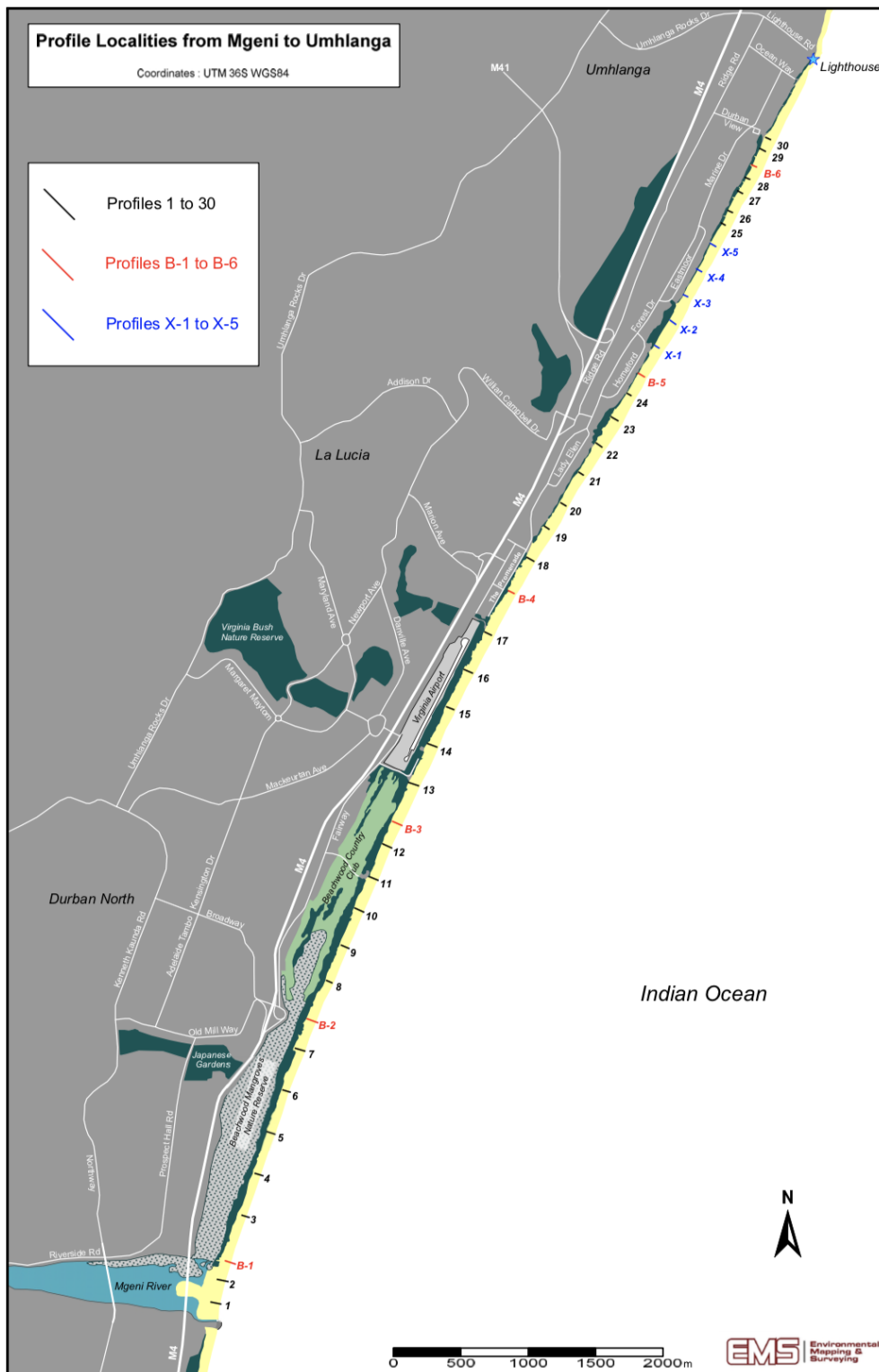


Fig. A.2 Profile localities from uMgeni to uMhlanga (eThekweni Municipality, 2017)

---

### 3. Technical Notes

**Date of Survey:**

11 January 2016  
Large swell 03 to 06 October 2016

**Survey Personnel:**

Rio Leuci  
Zane Thackeray

**Equipment Used:**

Hemisphere Vector VS 330 RTK GPS  
Sick LMS 291 Lidar  
Suzuki King Quad 4x4 ATV

**Benchmark:**

Trignet Durban Base

**Vertical Datum:**

Land Leveling Datum (LLD). 28.55m separation to Ellipsoidal Height

**Mapping Coordinates:**

UTM 36 South on WG84 spheroid

**Beach Sediment Volume:**

Volumes calculated from  $\geq 0$  LLD

**Beach Area:**

Areas calculated from  $\geq 0$  LLD

**Area below Profile:**

Area below Profile calculated from  $\geq 0$  LLD

Fig. A.3 Technical notes for eThekweni Municipalities Beach Survey - January 2017



# Appendix B

## Wave Data Statistics

### B.1 Observed Wave Data

This section show statistical data for the observed wave climates used in this study.

Table B.1 Annual wave characteristics for observed wave data.

Year	$H_s$ (m)			$T_p$ (s)			$D$ (°)		
	$\mu$	<i>Min.</i>	<i>Max.</i>	$\mu$	<i>Min.</i>	<i>Max.</i>	$\mu$	<i>Min.</i>	<i>Max.</i>
1997	1.31	0.53	2.89	10.53	3.05	18.29	139.92	65.0	211.9
1998	1.58	0.53	3.73	10.62	3.71	18.29	138.55	57.6	212.5
1999	1.35	0.42	3.39	10.43	3.24	18.29	134.59	63.3	231.8
2000	1.57	0.54	5.25	10.94	3.88	18.29	138.91	63.8	218.9
2001	1.60	0.41	4.32	10.47	3.24	18.29	138.11	1.00	212.1
2002	1.52	0.45	4.07	10.20	3.05	18.29	133.81	57.8	221.8
2003	1.60	0.05	3.89	10.44	2.50	20.00	130.25	64.0	301.0
2004	1.48	0.01	4.10	10.87	3.80	40.00	135.34	32.0	219.0
2005	1.58	0.72	4.80	11.00	4.00	20.00	139.07	61.0	221.0
2006	1.60	0.68	4.42	10.95	4.00	20.00	140.66	61.0	228.0
2007	1.63	0.70	8.50	11.33	3.80	20.00	141.06	64.0	233.0
2008	1.57	0.72	4.67	11.18	3.30	22.20	140.56	58.0	228.0
2009	1.61	0.75	4.10	11.06	4.00	18.10	139.87	62.0	226.0
<b>Full</b>	1.56	0.01	8.50	10.84	2.50	40.00	137.71	1.00	233.0

## B.2 Simulated Wave Data

Table B.2 Statistics for randomly selected 100 year wave sequences.

Sequence	$H_s$ (m)			$T_P$ (s)			$D$ (°)		
	$\mu$	<i>Min.</i>	<i>Max.</i>	$\mu$	<i>Min.</i>	<i>Max.</i>	$\mu$	<i>Min.</i>	<i>Max.</i>
2	1.71	0.1	9.03	10.39	1.31	20.0	133.74	31.13	210.0
11	1.70	0.1	9.47	10.39	1.11	20.0	133.85	30.06	210.0
18	1.70	0.1	9.26	10.40	1.10	20.0	134.06	31.26	210.0
27	1.71	0.26	10.16	10.41	1.12	20.0	134.11	30.38	210.0
38	1.70	0.1	9.01	10.37	1.10	20.0	133.76	31.62	210.0
53	1.70	0.1	9.52	10.36	1.12	20.0	133.95	30.46	210.0
62	1.70	0.1	12.09	10.38	1.12	20.0	133.54	30.78	210.0
74	1.70	0.1	19.20	10.37	1.17	20.0	133.95	30.57	210.0
81	1.71	0.1	16.22	10.40	1.14	20.0	133.92	30.23	210.0
100	1.71	0.1	25.85	10.40	1.16	20.0	134.26	31.30	210.0

Shown below are wave roses for a single wave sequence showing the variation of wave data at different time intervals.

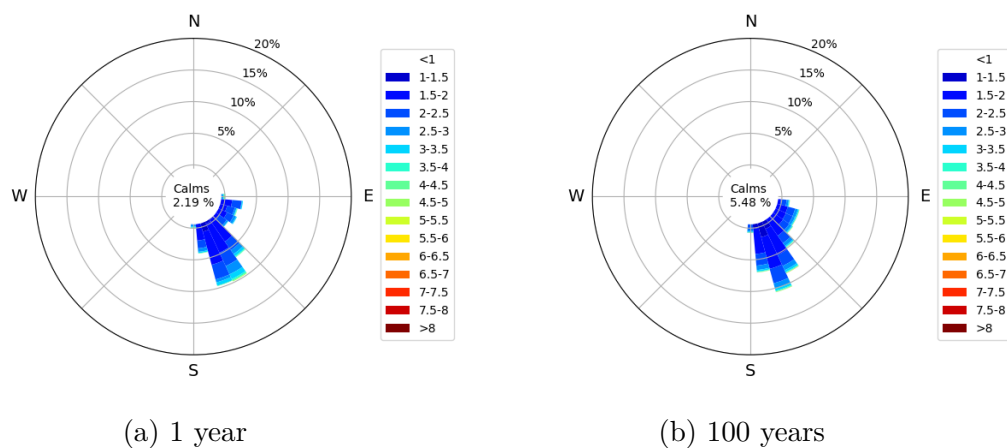


Fig. B.1 Wave roses for a single simulated wave sequence at different intervals.

# Appendix C

## Model Calibration

Table C.1 Results of model calibration using first half of observed wave data.

Year	Annual Longshore Transport ( $m^3$ )	
	Observed	Calibrated
1997	720 000	388 319
1998	440 000	542 576
1999	570 000	327 434
2000	430 000	518 204
2001	390 000	478 554
2002	220 000	386 724
Mean $\mu$	461 667	440 302
St. Dev. $\sigma$	154 641	77 786

Table C.2 Results of model validation using second half of observed wave data.

Year	Annual Longshore Transport ( $m^3$ )	
	Observed	Calibrated
2003	600 000	353 272
2004	460 000	406 921
2006	390 000	562 912
2007	440 000	639 991
2008	120 000	520 588
2009	240 000	527 776
Mean $\mu$	375 000	501 910
St. Dev. $\sigma$	155 751	95 675



# Appendix D

## Model Pseudocode

This appendix presents pseudocode for the one-line model developed for this study. As the model contains numerous functions within multiple files, only the core model pseudocode together with selected numerical functions such as wave transformations and vertical boundary limits will be presented.

---

**Algorithm 1:** Shoreline Change Model

---

**Data:** Wave Sequence File,  
Simulation Period,  
Coastline Coordinates,  
Beach Limit Coordinates,  
Storm Data,  
Constants (Calibration Coefficient ( $K$ ), Closure Depth ( $D_c$ ), Grid Interval ( $\Delta x$ ), Model Time Step ( $\Delta t$ ), Saltwater Density ( $\rho_w$ ), Porosity ( $p$ ), Sand Density ( $\rho_s$ ) etc.)

**Result:** Explicit coastline change model that calculates shoreline positions for a specified time period.

- 1 Import Python modules
  - 2 Generate interpolated coastline
  - 3 Calculate dimensionless cross-shore profile shape parameter
  - 4 **Open** wave sequence file
  - 5 Synthesise storm events (dates and volumes)
  - 6 Generate base coastline for sand waves
-

## Model Pseudocode

---

---

### Algorithm 1: Shoreline Change Model (continued)

---

```
7 while date  $\neq$  enddate do
8   Check simulation date
9   Import wave data for time stamp
10  Calculate slope and orientation for coastline segments using SLOPES
11  Calculate relative wave directions
12  Perform wave transformation using TRANSFORM
13  Calculate longshore sediment transport rates (Q) using LST
14  Apply boundary conditions
15  Calculate shoreline change and update previous coastline
16  if coastline < beach limit then
17    | Adjust Q using CORRECT
18    | Update coastline
19    | Perform volume check
20  else
21    | Perform volume check
22  if date = storm date then
23    | Calculate Gaussian distribution of discharge using STORMSED
24    | Initialise as gaussy
25  if any(gaussy > gaussbase) then
26    | Calculate inclination of tangent to nourishment
27    | Isolate nourishment plume
28    | Follow procedure from line 10 to line 21
29    | Advect nourishment using advect
30  Update time step, return to line 8
```

---

---

**Algorithm 2: SLOPES**

---

**Data:** Coastline coordinates ( $\mathbf{y}$ ), general coastline orientation ( $\psi$ ), grid interval ( $\Delta x$ )

**Result:** Individual grid orientations and slopes relative to North.

- 1 Calculate  $\Delta y$  for each grid cell:  $\Delta y = y_{i+1} - y_i$
  - 2 Calculate slope:  $slope = 2\pi - \arctan \frac{\Delta y}{\Delta x}$
  - 3 Calculate normals:  $normal = slope + \psi - \frac{3}{2}\pi$
- 

---

**Algorithm 3: TRANSFORM**

---

**Data:** Significant wave height ( $H_s$ ), relative wave angle ( $\theta_b$ ), peak period ( $T_p$ )

**Result:** Transforms deepwater waves to breaking conditions using an iterative process.

- 1 Check that wave steepness ratio does not exceed 0.142
  - 2 Calculate parameters for deepwater conditions:
  - 3     Wavelength  $L_0$ , wave number  $k_0$ , wave phase speed  $c_0$
  - 4     Check deepwater wave energy  $E_{deep} = \frac{1}{8}\rho_w g H_0^2 n c \cos \varphi$
  - 5 Make initial assumption for breaking depth  $h$ .
  - 6 **while** *True* **do**
  - 7     Calculate breaking wavelength  $L_b$  and wave number  $k_b$
  - 8     Calculate ratio between phase speed and group speed  $n$ :  
$$n = \frac{c_g}{c_{phase}} = 0.5 \left( 1 + \frac{2kh}{\sinh 2kh} \right)$$
  - 9     Calculate phase ( $c_p$ ) and group ( $c_g$ ) velocities at the breaking depth.
  - 10    Refract wave angles using Snell's Law:  $\frac{\sin \varphi_1}{c_1} = \frac{\sin \varphi_2}{c_2}$
  - 11    Use calculated parameters to calculate transformation coefficients  $K_{sh}$  and  $K_r$ :  
$$K_r = \sqrt{\frac{\cos \phi_0}{\cos \phi}}$$
$$K_{sh} = \sqrt{\frac{1}{\tanh kh} \frac{1}{2n}}$$
  - 12    Check breaking wave energy against deepwater wave energy:  
$$E_{shallow} = \frac{1}{8}\rho_w g H_b^2 n c \cos \varphi$$
  - 13    Calculate transformed wave height at breaker depth:  $H_b = H_s * K_r * K_{sh}$  **if**  
 $H_b/h \neq 0.78$  **then**
  - 14    |  $h = H_b/0.78$  (Update assumption for  $h$ )
  - 15    | Return to line 7
  - 16    **else**
  - 17    | **break**
-

## Model Pseudocode

---

---

### Algorithm 4: LST

---

**Data:** Significant wave height ( $H_s$ ), relative wave angle ( $\theta_b$ ), peak period ( $T_p$ ), transformation coefficients ( $K$ ), breaking depth ( $h$ ), median sediment diameter ( $D_{50}$ )

**Result:** Longshore sediment transport rates for individual grid cells.

1 Breaking wave height:  $H_{sb} = H_s \times K$

2 Cross-shore slope ( $m$ ):  $\tan \beta = \frac{A^{\frac{2}{3}}}{h}$

3 Longshore transport rate:

$$Q = \frac{K}{(\rho_s - \rho_w)(1-p)} \rho_w \left( \frac{g}{2\pi} \right)^{1.25} H_{sb}^2 T_p^{1.5} m^{0.75} D_{50}^{-0.25} \sin^{0.6}(2\theta_b)$$

---

---

### Algorithm 5: ADVECT

---

**Data:** Gaussian nourishment, Gaussian baseline, coastline orientation ( $\psi$ ), significant wave height ( $H_s$ ), relative wave angle ( $\theta$ ), peak period ( $T_p$ )

**Result:** Adveacts nourishment based on incoming wave conditions.

1 Isolate plume by subtracting baseline from nourishment coordinates.

2 Calculate  $\frac{\partial y}{\partial x}$  using central difference theorem:  $\frac{\partial y}{\partial x} = \frac{y_{i+1} - y_i}{2\Delta x}$

3 Calculate  $S_{x,0}$  using the **LST** function:  $S_{x,0} = \mathbf{LST}(H_s, \theta, H_s/0.78, 1, T_p)$ :

4 Calculate maximum value of plume ( $B$ )

5 Advection velocity:  $V = \frac{S_{x,0}}{B * D}$

6 Adveact plume:  $\Delta y = plume + \frac{S_{x,0}}{B * D} \frac{\partial y}{\partial x} \Delta t$

---

---

### Algorithm 6: STORMSED

---

**Data:** Date, storm index, coastline coordinates ( $\mathbf{x}$ ), discharge width

**Result:** Calculates plan Gaussian distribution of river discharges or nourishments.

1 Obtain all storm information stored in dictionaries using storm index.

2 Calculate volume required for time step:  $V = \frac{stormvolume}{stormlength} \Delta t$

3 Specify point of application  $\mu$  along coastline and standard deviation/width ( $\sigma$ )

4 Calculate area under graph for scaling:  $A = V / (D_c + D_b)$

5 Calculate plan distribution of sediment:  $P = \frac{1}{\sigma\sqrt{2\pi}} e^{-\frac{1}{2}\left(\frac{x-\mu}{\sigma}\right)^2}$

6 Scale distribution:  $y = P \times A$

---

---

**Algorithm 7: CORRECT**

---

**Data:** Longshore transport rates ( $Q$ ), coastline coordinates ( $y$ ), beach limit coordinates ( $y$ )

**Result:** Corrects longshore sediment transport rates when coastline erodes beyond beach limit coordinates.

```
1 Define start (ysbeg) and end (ysend) positions of domain.
2 Calculate denominator  $B_q$  for calculations:  $B_q = \frac{\Delta t}{(D_c + D_b)\Delta x}$ 
3  $i = ysbeg$  (define  $i$  for calculations)
4 while True do
5     if  $Q[i] > 0$  then
6         while  $Q[i+1] \geq 0$  do
7              $y_i = coasty[i] - B_q(Q[i+1] - Q[i])$ 
8              $y_{si} = beachwidths[i]$ 
9             if  $y_i < y_{si}$  then
10                  $diff = y_{si} - y_i$ 
11                  $Q[i+1] = Q[i+1] - \frac{diff}{B_q}$ 
12                  $i+ = 1$ 
13                 if  $i = ysend + 1$  then
14                     break
15                  $k = i$ 
16                  $i+ = 1$ 
17                 if  $i = ysend + 1$  then
18                      $y_i = coasty[i-1] + B_q(Q[i] - Q[i-1])$ 
19                     break
20                 if  $i = ysend$  then
21                      $i+ = 1$ 
22                     for  $i$  in range( $i-1, k, -1$ ) do
23                          $y_i = coasty[i] - B_q(Q[i+1] - Q[i])$ 
24                          $y_{si} = beachwidths[i]$ 
25                         if  $y_i < y_{si}$  then
26                              $diff = y_{si} - y_i$ 
27                              $Q[i+1] = Q[i+1] - \frac{diff}{B_q}$ 
```

---

## Model Pseudocode

---

### Algorithm 7: CORRECT (continued)

---

```

28  else
29       $k = ysbeg - 1$ 
30      if  $ysbeg = 1$  then
31           $k = 1$ 
32      while  $Q[i + 1] < 0$  do
33           $i+ = 1$ 
34          if  $i = ysend$  then
35              if  $Q[i + 1] \leq 0$  then
36                   $y_i = coasty[i] - B_q(Q[i + 1] - Q[i])$ 
37                   $y_{si} = beachwidths[i]$ 
38                  if  $y_i < y_{si}$  then
39                       $diff = y_{si} - y_i$ 
40                       $Q[i + 1] = Q[i + 1] - \frac{diff}{B_q}$ 
41                      for  $i$  in  $range(i-1, k, -1)$  do
42                           $y_i = coasty[i] - B_q(Q[i + 1] - Q[i])$ 
43                           $y_{si} = beachwidths[i]$ 
44                          if  $y_i < y_{si}$  then
45                               $diff = y_{si} - y_i$ 
46                               $Q[i + 1] = Q[i + 1] - \frac{diff}{B_q}$ 
47                           $i+ = 1$  if  $i \geq ysend + 1$  then
48                              break
49       $y_i = coasty[i] - B_q(Q[i + 1] - Q[i])$ 
50       $y_{si} = beachwidths[i]$ 
51      if  $y_i < y_{si}$  then
52           $diff = y_{si} - y_i$ 
53           $q_{diff} = Q[i + 1] - Q[i]$ 
54           $Q[i] = Q[i] - \frac{diff}{B_q} \frac{Q[i]}{q+diff}$ 
55           $Q[i + 1] = Q[i + 1] - \frac{diff}{B_q} \frac{Q[i+1]}{q+diff}$ 

```

---

---

**Algorithm 7: CORRECT (continued)**

---

```
56   for  $i$  in range( $i-1$ ,  $k$ ,  $-1$ ) do
57      $y_i = \text{coasty}[i] - B_q(Q[i+1] - Q[i])$ 
58      $y_{si} = \text{beachwidths}[i]$ 
59     if  $y_i < y_{si}$  then
60        $\text{diff} = y_{si} - y_i$ 
61        $Q[i] = Q[i] - \frac{\text{diff}}{B_q}$ 
62    $i+ = 1$  if  $i \geq \text{ysend} + 1$  then
63     break
```

---

